

**INVESTIGATIONS OF PROTON TRANSFER REACTION MASS
SPECTROMETRY FOR APPLICATIONS IN
ORGANOPHOSPHATE DETECTION AND BREATH ANALYSIS**

by

Philip Andrew Brown

**A thesis submitted to
The University of Birmingham
for the degree of
DOCTOR OF PHILOSOPHY**

School of Physics and Astronomy

The University of Birmingham

August 2012

UNIVERSITY OF
BIRMINGHAM

University of Birmingham Research Archive

e-theses repository

This unpublished thesis/dissertation is copyright of the author and/or third parties. The intellectual property rights of the author or third parties in respect of this work are as defined by The Copyright Designs and Patents Act 1988 or as modified by any successor legislation.

Any use made of information contained in this thesis/dissertation must be in accordance with that legislation and must be properly acknowledged. Further distribution or reproduction in any format is prohibited without the permission of the copyright holder.

Abstract

The reduced electric field dependence of a series of twelve saturated alcohols was investigated with a proton transfer reaction mass spectrometer, PTR-MS. Fragmentation reactions were observed for all but one compound and the dependence of this fragmentation was recorded as a function of reduced electric field. A number of common fragment ions were observed corresponding to carbocations. Effects on the branching ratios from the hollow cathode emission current were also observed and investigated.

The reaction of dimethyl methylphosphonate, DMMP in a PTR-MS was studied, along with further chemical weapon simulants. The reaction with DMMP was investigated to explain a product ion at m/z 111.

The PTR-MS has been used to demonstrate the possibilities of breath analysis in the diagnosis of liver disease. A promising marker may be limonene, observed on the breath of patients suffering from encephalopathy. Further work would be needed to understand the source of this compound before being used for diagnostic purposes. Data are also reported relevant to the repeatability of a breath sample. The sampling repeatability was calculated for isoprene, acetone, methanol, ethanol and monoterpene. The repeatability for each compound was found to be affected by the intensity of the measured ion and the compound's solubility.

Dedication

For my Granddad.

Acknowledgements

I would firstly like to thank my supervisor, Chris Mayhew for giving me the opportunity to work within his research group. He was always available to help when things did not work, or when they worked but were just plain confusing. He also allowed me the space to work when the experiments were well behaved. Thank You.

I would like to thank Peter Watts, particularly for his knowledge of chemistry and his scientific experience. His enthusiasm for understanding chemistry was often important in finalising a reaction pathway by one further measurement.

I would like to thank Dr. Tahir Shah and Dr. Andrew Holt of the Queen Elizabeth Hospital Birmingham for their help recruiting patients to the liver study. I would like to thank Andrew Palmer at the CRF for his help organising the chemotherapy trial, and I would like to thank Dr. Dan Rea for his work recruiting patients to that trial.

I would like to thank all the members of the molecular physics group: Margaret, Shane, Sarah, Dave H. Sylvia, Lyn and Dave P. I would like to thank Margaret for her help with the liver study and Shane for his help with the chemotherapy study. I would like to thank Dave H. for his electronics know-how and kind demeanour, Sylvia for her always interesting questions, and Dave P. for knowing his hydroxyl from his elbow. Thank you also to Sarah (and a further Dave), for sharing your time, your home and most importantly your cats. Thank you to Lyn, for her fabulous leadership of the molecular physics youth movement, and for being a wonderful friend.

Thanks also go to Rich and Vinder for being good and constant friends during not just my PhD, but my undergraduate course as well. Finally, I would like to thank my family, without whose support I wouldn't be a scientist.

Table of Contents

Introduction	1
1 The Proton Transfer Reaction Mass Spectrometer	3
1.1 Introduction	3
1.2 Instrumental Details.....	5
1.2.1 Ion source.....	6
1.2.2 Drift tube.....	9
1.2.3 Quadrupole mass filter and secondary electron multiplier.....	11
1.3 Preliminary Measurements	17
1.3.1 Investigation of sample humidity on the reagent ion hydrate clusters	19
1.3.2 Investigation of fragmentation via isoprene measurements	20
1.3.3 Signal stability investigation using acetone measurements	28
1.3.4 Using an aromatic compounds mix for calibration	31
1.3.5 Studying hollow cathode effects using isoprene	33
1.3.6 Back-streaming investigation using carbon tetrafluoride	35
1.4 Conclusion	39
2 Analysis of a Series of Saturated Alcohols for Characterisation and Understanding of Proton Transfer Reaction Mass Spectrometry	41
2.1 Introduction	41
2.2 Background	41
2.3 Experimental Details.....	42
2.4 Experimental Results and Mass Spectra	47
2.4.1 Reduced electric field dependence of saturated alcohols.....	47
2.4.2 Hollow cathode emission current dependence of saturated alcohols	66
2.5 Conclusions and Further Work	71
3 Proton Transfer Reaction Mass Spectrometry of Organophosphates Related to Chemical Warfare Agents and Pesticides.....	75

3.1 Introduction	75
3.2 Background	77
3.3 Experimental and Results.....	78
3.3.1 The study of DMMP, DMMP d6 and TMP to identify the product ion at m/z 111 observed from the reaction of DMMP with H_3O^+	79
3.3.2 DEMP, DIMP and DPM analysed with H_3O^+ in a PTR-MS.....	105
3.4 Conclusions and Further Work	110
4 Using a PTR-MS for Breath Analysis of Patients with Liver Disease	112
4.1 Introduction	112
4.2 Background	114
4.3 Preliminary Study of Garlic Breath	116
4.4 Experimental Methodology	119
4.4.1 A note on breathing technique.....	121
4.4.3 Measurement details	124
4.5 Results.....	126
4.5.1 Smokers	126
4.5.2 Volatile sulphurous compounds	128
4.5.3 Limonene.....	132
4.6 Consistency of Breath Samples	140
4.6.1 Purpose of the chemotherapy study	140
4.6.2 Methodology of the chemotherapy study	141
4.6.3 Results	144
4.6.4 Discussion of repeatability.....	147
4.6.5 Conclusion of the study into the repeatability of breath analysis	150
4.7 Discussion of Limonene	151
4.8 Conclusions and Further Work	152
References	154

Appendix A - Health status questionnaire for the study of liver disease.

Appendix B - A report employing mass spectrometric techniques to an initial investigation into the stack emissions from Smurfit Kappa's Birmingham site.

Appendix C - Proton transfer reaction mass spectrometry investigations on the effects of reduced electric field and reagent ion internal energy on product ion branching ratios for a series of saturated alcohols.

Appendix D - On the use of SIFT-MS and PTR-MS experiments to explore reaction mechanisms in plasmas of volatile organics: Siloxanes.

Table of Figures

Figure 1: Mass spectra of a) electron ionisation of acetone and b) proton transfer reaction of acetone.....	3
Figure 2: PTR-MS schematic design adapted from Clementschitsh and Bayer [29].	6
Figure 3: 2-D schematic interpretation of a quadrupole mass filter.....	12
Figure 4: 3-D interpretation of a mass filter showing the path travelled by two ions of different m/z	13
Figure 5: Mass spectrum of ambient room air, showing peaks a) $\text{H}_3^{18}\text{O}^+$ at m/z 21, b) NO^+ at m/z 30, c) O_2^+ at m/z 32 and d) $\text{H}_3\text{O}^+\cdot\text{H}_2\text{O}$ at m/z 37. An inlay shows the minor peaks of ambient room air.....	16
Figure 6: MID scan of a calibration mixture in nitrogen containing benzene and toluene. The moments when the gas is added and when the gas is removed are shown on the graph.	16
Figure 7: Chemical structure of isoprene, acetone and carbon tetrafluoride.....	17
Figure 8: Common introduction method for single chemical analysis using the PTR-MS.	19
Figure 9: Graphs showing the water clusters in nitrogen a) with a Drechsel bottle and b) without a Drechsel bottle as a function of reduced electric field.	20
Figure 10: Product ion branching ratio graph for isoprene in nitrogen between 91 and 138 Td.	22
Figure 11: Suggested fragmentation for protonated isoprene.	22
Figure 12: The normalised counts per second for acetone as a function of reduced electric field.....	29
Figure 13: Figure showing the sensitivity of the PTR-MS to a mix of aromatics at a) 138 Td and b) 91 Td.	32
Figure 14: Product ion branching ratio for isoprene at 138 Td as a function of hollow cathode emission current.	34
Figure 15: Diagram of the calibration rig used to produce a known concentration of carbon tetrafluoride.	36
Figure 16: Mass spectra of carbon tetrafluoride at 2.8 ppm, 22.5 ppm and at zero concentration with an emission current of 10 mA.	38
Figure 17: Product ions observed from back streaming of carbon tetrafluoride at 22.5 ppm for three emission currents, 10, 5, 2 mA.....	39

Figure 18: Structures diagram of the 12 alcohols used in this study.....	44
Figure 19: Experimental set-up for the study of a series of saturated alcohols.	45
Figure 20: Mass spectrum of dry N ₂ showing the peaks of a clean system at a reduced electric field of 138 Td.....	46
Figure 21: Product ion branching ratio for methanol as a function of reduced electric field in nitrogen.....	49
Figure 22: Figure showing a) the normalised counts per second for the four product ions from the reaction of ethanol with H ₃ O ⁺ and b) the product ion branching ratios for the same reaction.....	50
Figure 23: Fragmentation diagram for protonated ethanol, C ₂ H ₅ OH ₂ ⁺	51
Figure 24: Chemical structure of ethanol-2,2,2-d ₃	51
Figure 25: Figure showing the time progression of three product ions produced after the addition of a) ethanol-2,2,2-d ₃ and b) ethanol at 138 Td.	52
Figure 26: Figure showing the product ion branching ratios of a) 1-propanol and b) 2-propanol.....	53
Figure 27: Fragmentation reaction of C ₃ H ₇ ⁺ product ion for 1-propanol and 2-propanol.	54
Figure 28: Figure showing the product ion branching ratios of a) 1-butanol, b) 2-methyl-1-propanol, c) 1,1-dimethylethanol and d) 2-butanol.	55
Figure 29: Fragmentation of the butyl carbocation.	56
Figure 30: Plots of the product ion branching ratio of a) 1-pentanol and b) 1-hexanol...	57
Figure 31: Proposed fragmentation pattern of protonated 1-propanol in a PTR-MS.	58
Figure 32: Proposed fragmentation pattern of protonated 1-hexanol in a PTR-MS.....	59
Figure 33: Product ion branching ratios of a) cyclopentanol and b) cyclohexanol.	60
Figure 34: Proposed fragmentation scheme of cyclopentanol.....	61
Figure 35: Proposed fragmentation scheme for cyclohexanol.....	61
Figure 36: Product ion branching ratio for cyclopentanone.	63
Figure 37: Product ion branching ratio of cyclohexanone.....	64
Figure 38: Relative stability of tertiary, secondary, primary and methyl carbocations.....	65
Figure 39: Concentration dependence of the product ions of cyclohexanol at 115 Td...	66
Figure 40: Cyclohexanol product ions as a function of hollow cathode emission current at a) 138 Td and b) 91 Td.....	68

Figure 41: Proposed fragmentation mechanism of cyclohexanol, highlighting the initial losses of hydrogen and water.	68
Figure 42: Fragmentation mechanism for propanol, highlighting the initial losses of hydrogen and water.	69
Figure 43: The effect of the hollow cathode emission current on the product ion branching ratios of a) 1-propanol and b) 2-propanol at 138 Td.	70
Figure 44: Summary diagram of the initial fragmentations of each of the protonated monomers, MH^+	73
Figure 45: Chemical structures of DMMP, sarin (GB) and soman (GD).	75
Figure 46: Chemical structures of DEMP, DIMP and DPM.	77
Figure 47: Chemical structure of DMMP and DMMP d6 showing comparison of the deuterated sites. The structure of TMP is also shown.	78
Figure 48: Mass spectrum for DMMP with H_3O^+ recorded at a reduced electric field of 115 Td.	81
Figure 49: Mass spectra of clean nitrogen for H_2O and D_2O systems.....	82
Figure 50: Experimental set-up used in the analysis of DMMP and DMMP d6.	83
Figure 51: Mass spectrum of DMMP in a D_2O system.	84
Figure 52: Experimental set-up to enable monitoring of DMMP with varied levels of humidity.....	85
Figure 53: Graph showing the water clusters for a) a H_3O^+ system with D_2O and b) a D_3O^+ system with H_2O	86
Figure 54: Graph of the product ion branching ratios of DMMP as a function of flow through D_2O in a H_3O^+ system, product ions m/z 125 and m/z 126 are shown in a) and product ions m/z 111, 112 and 113 in b).	88
Figure 55: Graph showing the product ions a) at m/z 125 and 126 and b) at m/z 111, 112 and 113 observed from the reaction of DMMP in a D_3O^+ system as a function of H_2O humidity.....	89
Figure 56: Mass spectrum of DMMP d6 reacting with H_3O^+ at 115 Td.	91
Figure 57: Mass spectrum of the reaction of TMP with H_3O^+ measured at a reduced electric field of 115 Td.....	92
Figure 58: Free energy, ΔG and enthalpy, ΔH changes for complexes and reactions relative to a starting point of $DMMP + H_3O^+$	93
Figure 59: Structure of the transition state TSa.....	94

Figure 60: Structure of the transition state TSb.	95
Figure 61: The reaction of TMP with H ₃ O ⁺ showing the origin of the product ions at <i>m/z</i> 93 and 125 from the different protonation sites and subsequent isomers of TMPH ⁺	96
Figure 62: Selected ions of the reaction of DMMP and DMMP d6 with H ₃ O ⁺ as a function of time	98
Figure 63: Time evolution spectra of a) product ions due to DMMP and b) product ions due to DMMP d6.	99
Figure 64: Comparison of the fragmentation proposed in Figure 58 with data collected using DMMP and DMMP d6.	100
Figure 65: Recorded product ions for DMMPd6 in a D ₂ O system.	101
Figure 66: Reaction mechanism producing a product ion at <i>m/z</i> 111, <i>m/z</i> 111a via loss of methanol and association of water. Reaction pathway taken from Figure 58.	102
Figure 67: Product ions of a) DEMP, b) DIMP and c) DPM as a function of reduced electric field.	106
Figure 68: Proposed sequential fragmentation of protonated DEMP.	107
Figure 69: Proposed sequential fragmentation of protonated DIMP.	108
Figure 70: Water clusters observed in a drift gas of dry nitrogen.	109
Figure 71: Teflon bags used for breath sampling.	116
Figure 72: Temporary fastening strip shown in the action of fastening.	117
Figure 73: PVC fitting used for breath analysis.	118
Figure 74: Time evolution of a breath sample to test the suitability of PTFE bags to storing volatile sulphurous compounds; b) shows a zoomed in portion of a).	119
Figure 75: Summary of volunteers involved in Liver Study.	120
Figure 76: Chart showing the intensity of the signal recorded at <i>m/z</i> 42 for each volunteer in the study.	127
Figure 77: Data for each volunteer at <i>m/z</i> 63, which would correspond to the protonated monomer of dimethyl sulphide recorded at 138 Td.	129
Figure 78: Data for each volunteer at <i>m/z</i> 49, which would correspond to the protonated monomer of methanethiol recorded at 138 Td.	131
Figure 79: Chemical structure of D-limonene.	132
Figure 80: : Data for each volunteer at <i>m/z</i> 137, which would correspond to the protonated monomer of limonene recorded at 138 Td.	133

Figure 81: Product ion branching ratios for the reaction of limonene with H_3O^+ between a reduced electric field of 91-138 Td.....	135
Figure 82: Data for each volunteer at m/z 81, which would correspond to the C_6H_9^+ fragment ion of limonene recorded at 138 Td.....	136
Figure 83: Data for each volunteer at m/z 95, which would correspond to the C_5H_7^+ fragment ion of limonene recorded at 138 Td.....	137
Figure 84: Data for each volunteer at m/z 153 recorded at 138 Td.....	139

Introduction

Proton transfer reaction mass spectrometry is a technique developed for the detection of trace quantities of volatile organic compounds, VOCs in air. The technique uses an ion-molecule reaction; namely the donation of a proton from the hydronium cation, H_3O^+ to a VOC whose proton affinity is greater than water, H_2O . The source of the VOCs can be either natural or anthropogenic. Natural sources of VOC emission can be from plants or animals, including human breath.

Man-made sources of VOCs include burning fossil fuels, industrial and domestic solvent use, emissions from agriculture and escaped gases from landfill. The analysis of VOCs from these sources has obvious implications for air quality, and environmental protection; as well as helping industrial plants to better understand their procedures.

The breadth of VOC sources has led to a wide and diverse field of applications for proton transfer reaction mass spectrometry [1, 2]. The technique has been applied to atmospheric and environmental science [3-6]; as part of my research an emissions monitoring study was conducting using proton transfer reaction mass spectrometry, a copy of the report written by a colleague is provided in Appendix B. The technique is also applied to monitoring biogenic VOCs from plants [7-9], animals [10], bacteria [11] and humans [9, 12-15]. Industrial applications have also been sought for the technique including the food industry [6, 16, 17] and in defence [18-21]. As part of my research, a further industrial application was sought to examine plasma deposition techniques [22], the accompanying paper for which can be found in Appendix D.

The proton transfer reaction mass spectrometer (PTR-MS) used by me as part of the Molecular Physics Group at the University of Birmingham is a commercially available

instrument purchased from Ionicon Analytik GmbH, a spin-off company of the University of Innsbruck, Austria. The device samples air directly and produces a mass spectrum displaying the count rate of ionised molecules versus their mass to charge ratio, m/z .

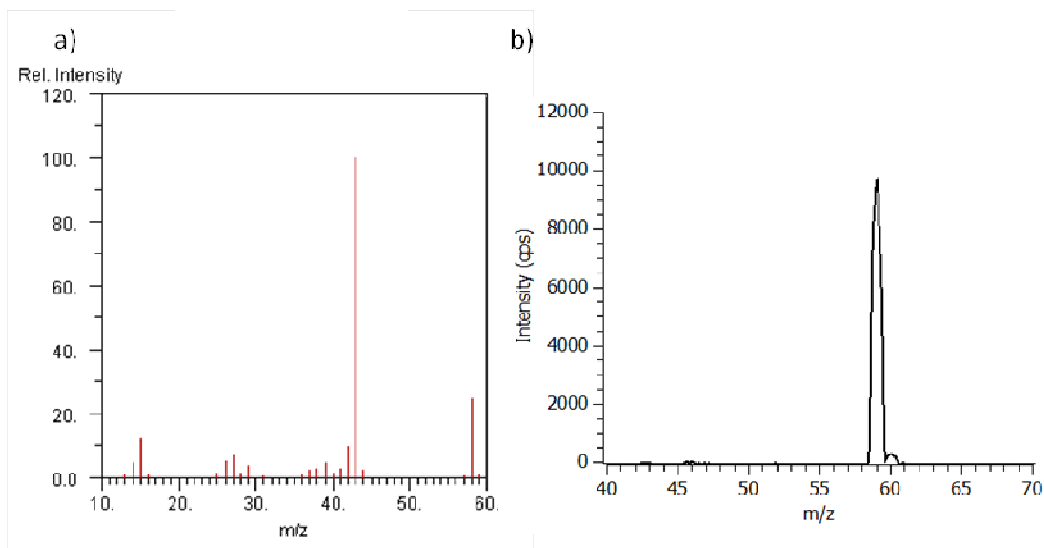
The structure of this report will be in four main segments. Firstly the PTR-MS will be introduced as a scientific instrument, with a detailed discussion about its operation and instrumentation. A further three sections will detail experimental measurements taken using the PTR-MS. Measurements of a series of alcohols will be presented, the data from which was published in an accompanying paper [23] found in Appendix C. These results allow the response of the machine to be correctly understood and characterised. Results will be presented for a series of organophosphates, including in most detail dimethyl methylphosphonate, DMMP. These will show how the PTR-MS can be used to detect chemical warfare simulants and further investigate the mechanisms at play in the PTR-MS. Results of breath samples taken from patients with liver disease at the Queen Elizabeth Hospital will be discussed along with breath samples taken from patients undergoing chemotherapy for breast cancer. The conclusions of these results will be discussed in terms of medical relevance and possible advancements in sampling technique and measurement.

I The Proton Transfer Reaction Mass Spectrometer

I.1 Introduction

Proton transfer ionisation is a type of ionisation, referred to as soft ionisation or chemical ionisation. Hard ionisation techniques may cause excessive fragmentation of product ions, particularly undesirable when a sample is composed of many unknown trace substances. Electron impact is the most commonly used hard ionisation technique, with typical electron collision energies of 70 eV [24]. Examples of electron ionisation and proton transfer reaction mass spectra are shown for acetone in Figure I. More fragmentation is observed for the electron ionisation method of mass spectrometry. Soft ionisation techniques operate at less than a few eV (few hundred kJ mol^{-1}) only. The aim of soft ionisation is to reduce product ion fragmentation.

Figure I: Mass spectra of a) electron ionisation of acetone and b) proton transfer reaction of acetone.

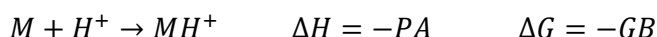


Soft, chemical ionisation methods use reagent ions that will undergo an exothermic ion-molecule reaction with the trace gas to be analysed. The reagent ion is chosen, such that the exothermicity of the reaction is low. This reduces the energy transferred to

the product ion when compared to a harder ionisation, e.g. electron impact. The lower exothermicity of the reaction should reduce the amount of product ion fragmentation.

An important parameter in proton transfer reactions is the proton affinity, PA. The proton affinity is the negative of the enthalpy change, ΔH for the protonation of a molecule, M from a free proton:

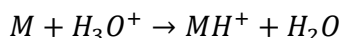
Equation 1



The proton affinity is defined for a particular molecule, at a given temperature, usually 298 K unless otherwise stated. A related parameter the gas phase basicity, GB is the negative of the change in Gibbs free energy, ΔG as shown in Equation 1 [25].

The PTR-MS uses hydronium cations, H_3O^+ as the reagent ion. The hydronium cation will transfer a proton to a molecule that has a proton affinity greater than water ($691 \pm 3 \text{ kJ mol}^{-1}$) [26]. This reaction is shown in Equation 2. ΔH is the enthalpy change of the proton transfer reaction, described in Equation 3. This value is typically only a few eV (few hundred kJ mol^{-1}) or less. Without fragmentation, the product ion referred to as the protonated monomer, MH^+ may provide identification of the molecule, M. This identification however, is not an unambiguous assignment for the molecule.

Equation 2



Equation 3

$$\Delta H = PA(H_2O) - PA(M)$$

By producing a very pure source of H_3O^+ ions, it is possible to do without reagent ion pre-selection. This improves the reagent ion signal available, allowing for higher

sensitivity when compared to a pre-selection method, e.g. with selected ion flow tube (SIFT) mass spectrometry techniques [27].

Many volatile organic compounds (VOCs) have proton affinities greater than water, allowing their detection by proton transfer reaction mass spectrometry. However, the major components of air, (nitrogen 78%, oxygen 21%, argon 1%) have lower proton affinities than water. This enables the detection of VOCs in air to be made without the sample being pre-treated. This lack of sample pre-treatment allows the PTR-MS technique to be used for the investigation of gas mixtures in real-time, i.e. with no delay for sample pre-treatment. To exemplify this, the proton affinities of some molecules of interest in proton transfer reaction mass spectrometry, along with the major constituents of air are displayed in Table I.

Table I: Table showing the main constituents of a typical gas sample to be analysed by a PTR-MS.

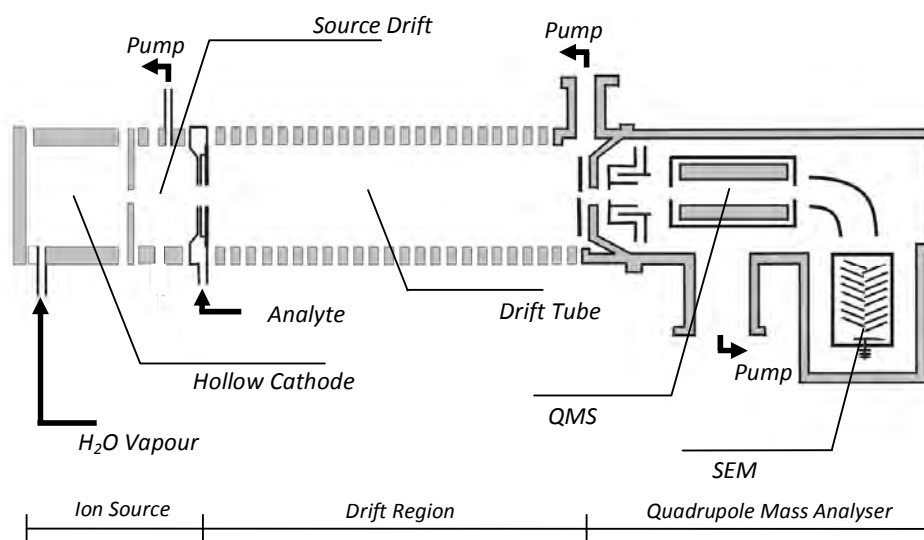
Chemical Name	Proton Affinity (kJ/mol) [26]	Supplementary Information
Molecular Oxygen	493.8	Major constituents of air and of breath
Molecular Nitrogen	421	
Carbon Dioxide	540.5	
Water	691	Source of H ₃ O ⁺ ions and constituent of air and breath
Formic Acid	742.1	Organic molecules produced by respiration pathways
Methanol	754.6	
Acetaldehyde	768.9	
Acetone	812.4	
Isoprene	826.6	

1.2 Instrumental Details

The Ionicon Analytik GmbH PTR-MS [28] used in this study consists of three main regions of operation. These regions are outlined in Figure 2. H₃O⁺ ions are created in

the ion source by ionising reactions with water vapour. The sample is introduced to the reagent ions in the drift tube; it is here that the proton transfer reactions may take place. The resultant ions from the drift tube reactions are analysed by the quadrupole mass analyser. The PTR-MS used in the investigations of this report will be explained by examining the three regions of operation sequentially from the ion source to the quadrupole mass analyser.

Figure 2: PTR-MS schematic design adapted from Clementschitsh and Bayer [29].



1.2.1 Ion source

The ion source consists of two sections, a hollow cathode discharge chamber and source ion drift region. Water vapour evaporating from liquid held in a stainless steel reservoir is introduced via 1/4 inch Teflon tubing into the hollow cathode discharge chamber. The flow of vapour is controlled by a Bronkhorst® mass flow controller. By this method a gas of mostly water vapour is created in the hollow cathode. A hollow cathode chamber consists of a cathode with a hollow structure and an arbitrarily shaped anode [30]. In the case of the PTR-MS, a cylindrical hollow cathode is used with a typical set voltage of 600 V.

The axial region of the hollow cathode, referred to as the negative glow, is a near field-free region, whose potential is close to that of the anode. Between the negative glow and the cathode, a potential difference of hundreds of volts is established, this region is known as the cathode fall. Within the cathode fall, neutral molecules are ionised by collisions with high energy electrons to produce primary ions. The primary ions may collide with neutral molecules in the negative glow region to produce secondary and tertiary ions. These ions eventually diffuse across and out of the field-free region where they are accelerated through the cathode fall, releasing secondary electrons by collision with the cathode surface. These secondary electrons become accelerated into the cathode fall region where they can ionise additional neutral molecules. This process helps to generate a plasma, which is maintained within the hollow cathode region.

The negative glow region is contained in the axial direction by the two endplates of the hollow cathode. One of these endplates has a central 1.0 mm diameter hole drilled through it [28]. This allows ions to leave the hollow cathode and enter the source drift region. While operational, the hollow cathode maintains a typical discharge current of 5 mA.

The discharge current in the hollow cathode is maintained by an electronic feedback mechanism. The feedback maintains a set discharge current by affecting the cathode voltage. Although the discharge current is typically set to 5 mA, a stable ion signal can be generated with settings from 2-10 mA. At higher discharge currents, a more stable, higher intensity ion current is produced. However, higher emission currents produce more energetic ionisation processes, this can create excessive amounts of undesirable ions and blackening of the hollow cathode by energetic reaction with carbon compounds,

which will necessitate more frequent cleaning, and may limit the hollow cathode's lifetime.

The main products of ionising water by discharge current ionisations are H_2O^+ , H^+ , H_2^+ , O^+ and OH^+ . All of these products react with neutral water molecules through a series of ion molecule reactions to form the terminal ion, H_3O^+ in the negative glow region [28]. Any ions produced by discharge current ionisation at, or just outside the orifice in the anode endplate should be converted to hydronium cations by way of collisions with neutral water molecules in the source drift region, thus further improving the purity and intensity of the reagent ion signal.

After the source drift region, the reagent ions enter the drift tube through a machined orifice. The stream of ions into the drift tube is guided by a set of ion optics, which may be tuned to allow optimisation of the reagent ion signal.

The design of the ion source is such that it can produce a signal of H_3O^+ ions with better than 99.5% purity [28]. However, in reality the purity will be lower due to impurity ions. The impurity ions are due to interactions with air molecules in the source drift region and hollow cathode. These air molecules may enter the ion source through leaks in the water inlet system, but are more likely back flow of the buffer gas from the drift tube region. Reactions involving nitrogen in the ion source may form NO^+ ions via molecular ionisation reactions. Molecular oxygen present in the source drift region will produce O_2^+ by charge transfer reactions with H_2O^+ .

The recombination energies of O_2^+ and NO^+ (12.07 eV and 9.26 eV [31], respectively) provide a value for the energy released by adding an electron to neutralise the ions. These values are less than the energy required to remove an electron from water, its ionisation energy (12.62 eV [31]), this means that charge transfer reactions from O_2^+ or

NO^+ to H_2O will not occur. NO^+ and O_2^+ ions produced in the ion source will be retained within the PTR-MS and may interfere with interpretation of the observed mass spectra.

Of these impurity ions, O_2^+ presents the most significant concern since its recombination energy could allow charge transfer reactions with many analyte molecules under investigation. To reduce this effect, the amount of O_2^+ in the system is limited to 2% of the H_3O^+ signal by adjusting the PTR-MS operating parameters. Increasing the water flow to the hollow cathode increases the pressure in the discharge source which helps to reduce back-flow of air from the drift tube into the hollow cathode region. Adjustment of the ion optics can be made to increase the intensity and purity of the reagent ion signal.

1.2.2 Drift tube

The drift tube is the reaction chamber of the PTR-MS, wherein molecules of sample analyte and reagent ion may react. The drift tube is cylindrical in shape and 9.6 cm long, with a diameter of 3 cm. Interactions between H_3O^+ ions and H_2O in the drift tube can form hydrate cluster ions, production of these ions occurs at the expense of the H_3O^+ signal; reducing its intensity.

Hydrate cluster ions are formed when H_3O^+ ions and H_2O molecules can interact to form adduct ions, these complex states can be stabilised by collision with a neutral molecule, M. The reaction is termed a three body reaction and is detailed in Equation 4. Details of the hydrate clusters are given in Table 2.

Equation 4

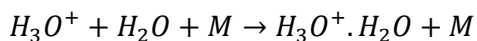


Table 2: Table showing proton affinities of water clusters $(\text{H}_2\text{O})_m\cdot\text{H}_2\text{O}$ where $m=0,1,2,3$.

Neutral species		Protonated species	
$(\text{H}_2\text{O})_m\cdot\text{H}_2\text{O}$	Proton Affinity (kJ mol^{-1}) [32]	$(\text{H}_2\text{O})_n\cdot\text{H}_3\text{O}^+$	m/z
$m = 0$	691	$n = 0$	19
1	833	1	37
2	889	2	55
3	920	3	73

The relative amount of water cluster ions can be reduced by the application of a drift electric field. The electric field is created by a series of electrodes that cause a voltage gradient along the length of the drift tube. An increase in drift field energy helps to break up the hydrate clusters by collision induced dissociation by increasing the drift velocity. An increased drift velocity also reduces the reaction time by conveying the ions through the drift tube faster; this will reduce the available time for clustering to occur. The electric field is also important in guiding ions towards the inlet for the quadrupole detector region.

The drift tube conditions are controlled by three main parameters, the electric field strength, E , temperature, T and number density, N within the drift tube. The conditions are optimised to ensure high H_3O^+ signal intensity, while keeping the drift velocity low to avoid unnecessary fragmentation of the product ions. The amount of energy that the ions have in the drift tube is dependent on the drift velocity which is in turn dependent on the ratio between the electric field and the number density, E/N . This ratio is known as the reduced electric field and has units V cm^2 , but is more conveniently expressed in Townsends (Td), (where $1\text{Td} = 10^{-17}\text{V cm}^2$).

The drift tube is normally operated at a temperature of 318 ± 1 K, and a pressure of 2.06 ± 0.01 mbar. This results in a number density of $4.69 \pm 0.04 \times 10^{16} \text{ cm}^{-3}$. A higher number density will result in more collisions in the drift tube, facilitating a greater number of collisions between reagent ions and analyte molecules, increasing the product ion signal. However, increasing the number density reduces the mean free path length (Equation 5); this reduces the energy of the collisions that help break up water clusters, hence reducing the intensity of the H_3O^+ signal by increasing the fraction of the total available signal due to water clusters.

Equation 5

$$\lambda = \frac{1}{\sqrt{2}N\pi d^2}$$

λ = mean free path m, N = number density m^{-3} , d = collision diameter of molecules m.

Equation for mean free path in a molecular gas.

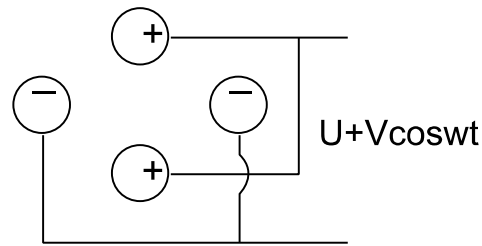
The second term important in the reduced electric field is the electric field itself. The PTR-MS used for these studies has a drift tube voltage which can be set between 400 and 600 V, giving a drift field between 41.6 and 62.5 V cm^{-1} . At a drift voltage setting of 600 V, with normal temperature and pressure parameters, the reduced electric field is at ~ 138 Td. This often provides a good balance between the ratio of reagent ion monomer and monohydrate cluster, while maintaining a high enough number density to provide sufficient reactions for good sensitivity.

1.2.3 Quadrupole mass filter and secondary electron multiplier

A fraction of the ions in the drift tube pass through a small orifice into the quadrupole mass filter region. The pressure in the quadrupole region is typically at 3.8×10^{-5} mbar, wherein ions are transferred to a quadrupole mass spectrometer via a series of ion

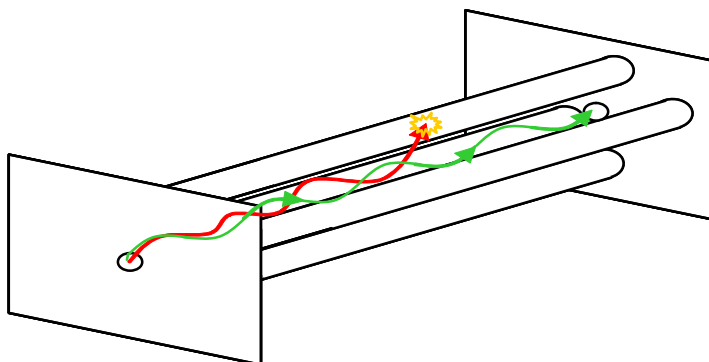
transfer optics. A schematic diagram of a mass filter is shown in Figure 3. The mass filter consists of two pairs of parallel rod shaped electrodes. The voltage across these rods is composed of a high-frequency alternating current, $V\cos(\omega t)$ and a direct voltage, U [33].

Figure 3: 2-D schematic interpretation of a quadrupole mass filter.



The positive voltage pair of electrodes act as a high mass pass filter to positive ions. The positive DC offset will repel ions toward the centre of the mass filter, while upon application of the negative half cycle of the RF voltage the ions will be attracted toward the rods. Lower mass ions will become accelerated beyond their trapping velocities and will be ejected, while higher mass ions can remain within the mass filter. The negative voltage electrodes will attract ions toward the rods using the negative DC voltage and repel them during the positive half cycle of the RF voltage. Heavier ions will be drawn toward the rods and are unable to be repelled in time to avoid ejection from the filter, whereas lower mass ions will remain in the filter. By this method the negative voltage electrodes will act as a low mass pass filter, and the quadrupole mass filter acts as band pass mass filter [34].

Figure 4: 3-D interpretation of a mass filter showing the path travelled by two ions of different m/z .



The green path ion will resonate and be detected, the red path ion fails to resonate and will not be detected.

By varying both the direct and alternating voltage, while keeping their ratio constant the quadrupole field can be tuned to allow only a given mass to charge ratio (m/z) to resonate and traverse the field region [35]. This action is illustrated in Figure 4. The quadrupole within the PTR-MS is a Balzers QMS 422. The mass filter can comfortably resolve peaks differentiated by one atomic mass unit, in an operating range up to m/z 250.

A fraction of the resonating ions will traverse the quadrupole region and be incident on the secondary electron multiplier, SEM. The SEM converts incident ions to an electrical pulse; one pulse per ion. Incident ions are converted to electrons; these electrons are accelerated toward a series of electrodes, multiplying their number. The potential difference of the SEM has an optimal voltage; too low a voltage will hinder the sensitivity, but too high a voltage causes a poorer quality signal by amplifying the 'dark count' unnecessarily.

As the counts per second incident on the SEM approach 1 million, the output signal ceases to be linearly related to the incidence of ions. For this reason, and to avoid unnecessary straining of the SEM, signals over 500,000 counts per second are avoided.

This would prohibit direct monitoring of the H_3O^+ ion, (m/z 19) as it has a typical count rate of 5 million counts per second. To indirectly measure the m/z 19 signal, the count rate of the ^{18}O isotope of H_3O^+ is measured instead. The isotopic fraction of ^{18}O is 1/487 of ^{16}O . By monitoring the m/z 21 count rate it is possible to calculate the m/z 19 signal.

The count rate of m/z 19 is an important parameter in the process of normalisation. The detected counts per second for each compound may be normalised to the total sum of reagent ion intensity, either H_3O^+ or H_3O^+ and $\text{H}_2\text{O}\cdot\text{H}_3\text{O}^+$. The product ion intensity for a given analyte will be linearly dependent on the concentration of reagent ion available for proton transfer reactions. This is shown in Equation 6. To prevent variations in the concentration of H_3O^+ ions affecting the perceived concentration of analyte, the signal intensity of product ions may be normalised. Normalisation refers the product ion signal to the intensity of the reagent ion signal; details of the normalisation procedure will be explained later.

Equation 6

Assuming proton transfer always leads to the protonated monomer, i.e. no fragmentation, the increase in concentration of protonated monomer, $\Delta[\text{MH}^+]$ produced in a time period, Δt would be:

$$\Delta[\text{MH}^+] = [\text{M}][\text{H}_3\text{O}^+]k\Delta t$$

$[\text{H}_3\text{O}^+] =$ number density of reagent ion available for proton transfer reaction, $[\text{M}] =$ number density of analyte, $k =$ reaction rate coefficient.

Reforming this equation as a differential equation:

$$d[\text{MH}^+] = [\text{M}][\text{H}_3\text{O}^+]k dt$$

Assuming that the concentration of analyte and the concentration of H_3O^+ remain constant over the reaction time, the equation can be easily integrated:

$$[MH^+] = [M][H_3O^+]kt$$

Calculation of the protonated monomer concentration.

Data acquisition from the quadrupole is controlled using the Balzers AG QUADSTAR 422 software version 6.02. The software also contains custom programs developed by Ionicon Analytik GmbH for use with the PTR-MS, allowing control over gas and water inlet flows and lens voltages, as well as handling data acquisition.

Data can be acquired in two different forms, either as a conventional mass spectrum or in 'multiple ion detection' (MID) mode. A conventional mass spectrum scans across a range of m/z values, defined by the user and outputs the data as a graph of intensity versus m/z . An example of a conventional mass spectrum is shown in Figure 5. With the quadrupole operating in MID mode, the mass filter allows ions with specific m/z values to resonate in turn. This data set is represented as a mass spectrum versus time, as shown in Figure 6.

Figure 5: Mass spectrum of ambient room air, showing peaks a) $\text{H}_3^{18}\text{O}^+$ at m/z 21, b) NO^+ at m/z 30, c) O_2^+ at m/z 32 and d) $\text{H}_3\text{O}^+\cdot\text{H}_2\text{O}$ at m/z 37. An inset shows the minor peaks of ambient room air.

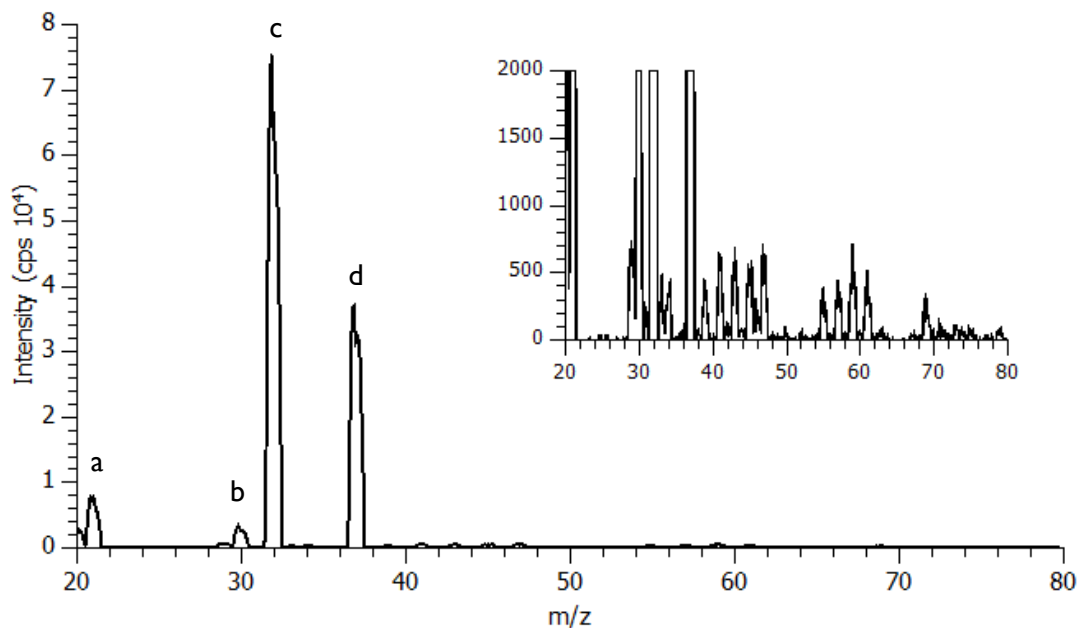
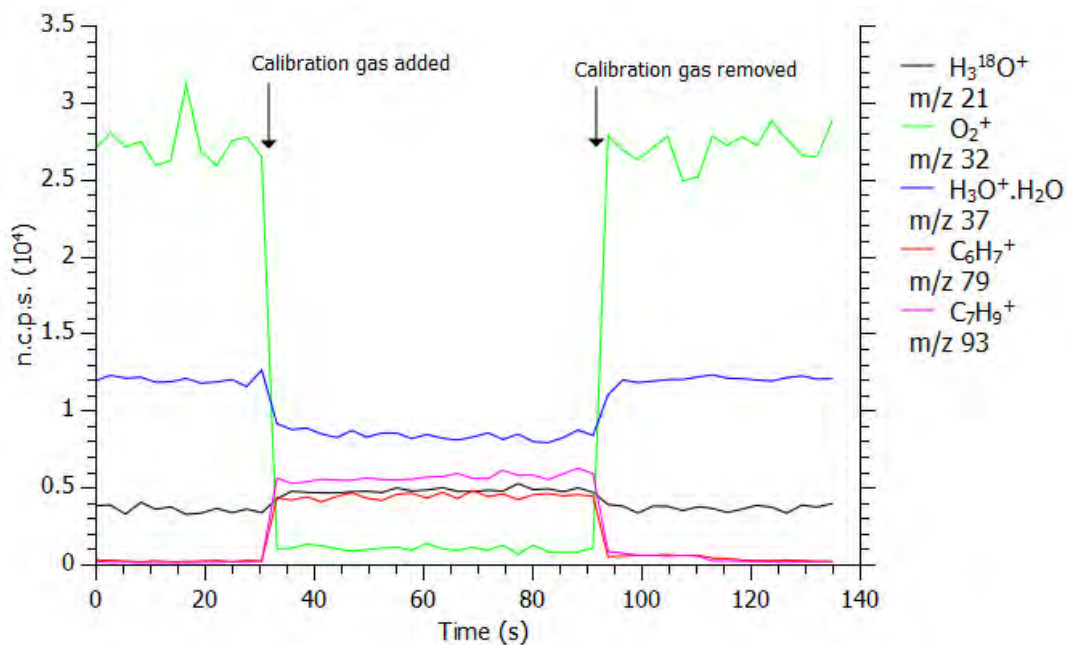


Figure 6: MID scan of a calibration mixture in nitrogen containing benzene and toluene. The moments when the gas is added and when the gas is removed are shown on the graph.



For samples of unknown chemical composition, the conventional mass spectrum can be an essential piece of data. Where a sample's chemical composition is well known, or

where temporal information on the sample is important, the MID mode spectrum may be a useful and convenient mode for data acquisition.

1.3 Preliminary Measurements

To characterise the instrument, a series of measurements were conducted to investigate the conditions and operating parameters of the PTR-MS. The measurements observed and recorded include changes to the drift tube and hollow cathode operating conditions that may affect the observed product ions produced and their behaviour. During this study, three compounds were analysed using the PTR-MS; isoprene, acetone and carbon tetrafluoride, each is shown in Table 3. In addition to these a calibrant gas was also studied, see Table 4 for details.

Table 3: Structural formulae, proton affinities and gas basicities of isoprene, acetone, carbon tetrafluoride and water.

Name	Structural Formula	Proton Affinity (kJ/mol) [26]	Gas Basicity (kJ/mol) [26]
Isoprene	$\text{CH}_2=\text{C}(\text{CH}_3)\text{CH}=\text{CH}_2$	826.4	797.6
Acetone	$(\text{CH}_3)_2\text{CO}$	812	782.1
Carbon tetrafluoride	CF_4	529.3	503.7
Water	H_2O	691	660.0

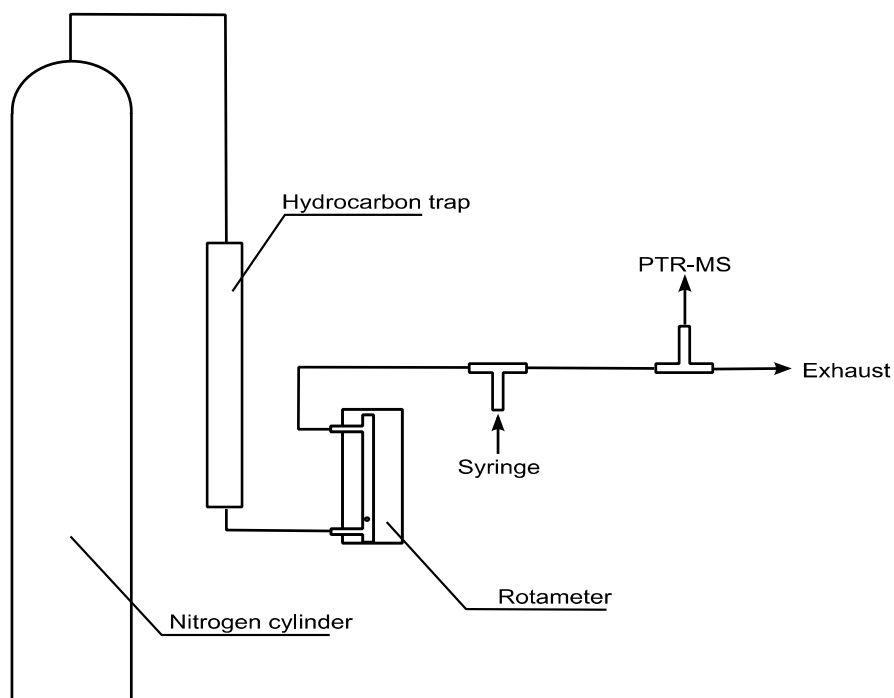
Figure 7: Chemical structure of isoprene, acetone and carbon tetrafluoride.



Each individual compound was analysed by introducing its vapour into a nitrogen mixture and injecting this into a $1000 \text{ cm}^3 \text{ min}^{-1}$ gas flow of nitrogen. The injection was performed by a syringe drive and the flow of nitrogen was provided by a white spot,

oxygen free nitrogen cylinder passed through a hydrocarbon trap (Altech). The resulting flow was sampled from a T-piece to the PTR-MS. The remaining sample mixture was exhausted outside the lab. This set-up is illustrated in Figure 8. The set-up was also used to analyse a sample of nitrogen at two extremes of humidity.

Figure 8: Common introduction method for single chemical analysis using the PTR-MS.



1.3.1 Investigation of sample humidity on the reagent ion hydrate clusters

The set-up shown in Figure 8 was used to generate two samples of different humidity. A sample was measured using the set-up as shown in Figure 8, and a second sample was produced by connecting a Drechsel bottle, containing a little distilled H₂O in line with the flow of nitrogen. This second sample was more humid than the first.

The effect that changing the reduced electric field has on the hydrate cluster ions is shown in Figure 9 for both a) the flow of nitrogen through the Drechsel bottle and b) the flow of nitrogen only. The a) sample is more representative of breath, a typical air sample would have humidity somewhere in between the a) and b) samples. The greater intensity of the hydrate cluster ion signal in the humid sample is due to the greater concentration of water molecules in the drift tube.

Figure 9: Graphs showing the water clusters in nitrogen a) with a Drechsel bottle and b) without a Drechsel bottle as a function of reduced electric field.

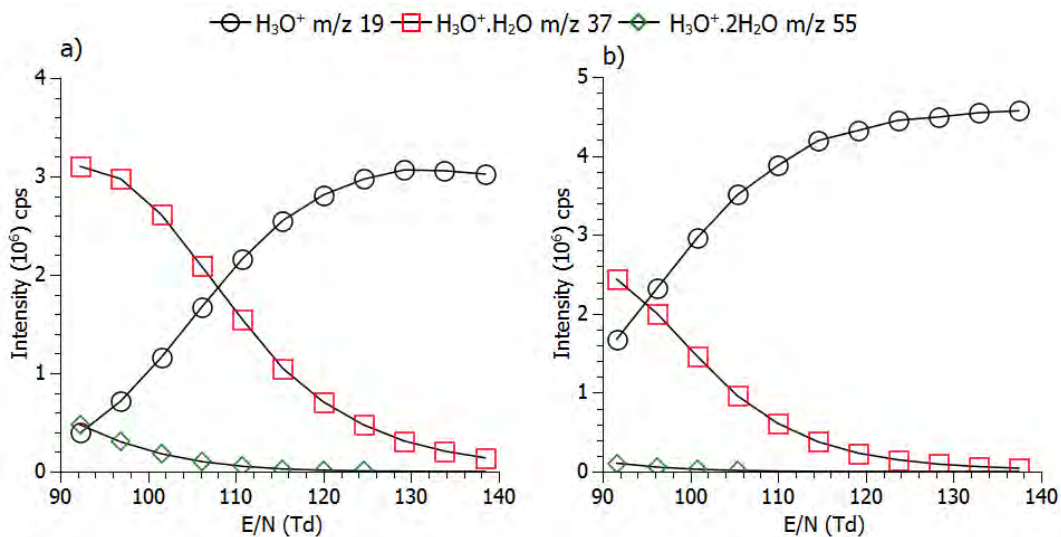


Figure 9 records the hydrate cluster ions that are present at the start of the quadrupole mass filter. This is assumed to indicate the amount of cluster ion formation in the drift tube, but it is not guaranteed to show the actual proportions of water clusters in the drift tube. Figure 9 indicates the a) sample has a greater amount of cluster formation, but it does not show the actual proportions of cluster ions in the drift tube.

The effect of the reagent ion hydrate clusters may be quite pronounced for protonated monomer detection [36, 37]. The reduced electric field is normally kept above ~120 Td for most measurement applications to avoid unnecessary complications due to water clusters.

1.3.2 Investigation of fragmentation via isoprene measurements

A syringe of nitrogen and isoprene vapour was made by using a 250 µl glass syringe to transfer a couple of drops of isoprene onto cotton wool placed inside a 10 ml plastic syringe. The high vapour pressure of isoprene (793 hPa @ 21°C) [38] can create excessive concentration of vapour. The 10 ml syringe doped with two drops of isoprene was left over night to stabilise.

A nitrogen isoprene vapour was produced by inserting the needle of the syringe, empty except for the doped cotton wool, through a septum and into the flow of nitrogen, as in Figure 8. By drawing out the syringe plunger a vapour and nitrogen mixture is created. By then injecting this vapour back into the $1000 \text{ cm}^3 \text{ min}^{-1}$ flow of nitrogen, isoprene is introduced to the PTR-MS in a stable concentration with low background interference.

After assessing a satisfactory analyte concentration by using a trial and error method looking at the protonated monomer signal, the reduced electric field was scanned by keeping the pressure ($2.06 \pm 0.01 \text{ mbar}$) and temperature ($318 \pm 1 \text{ K}$) constant and varying the drift field between 400 and 600 V in steps of 20 V. The pressure and temperature are kept constant to keep the number density fixed. The range of voltages selected provides a range of reduced electric fields between 91-138 Td. The data set recorded for isoprene is shown in Figure 10, where the behaviour of each product ion resulting from the reaction of isoprene and H_3O^+ is illustrated as a function of reduced electric field.

Figure 10: Product ion branching ratio graph for isoprene in nitrogen between 91 and 138 Td.

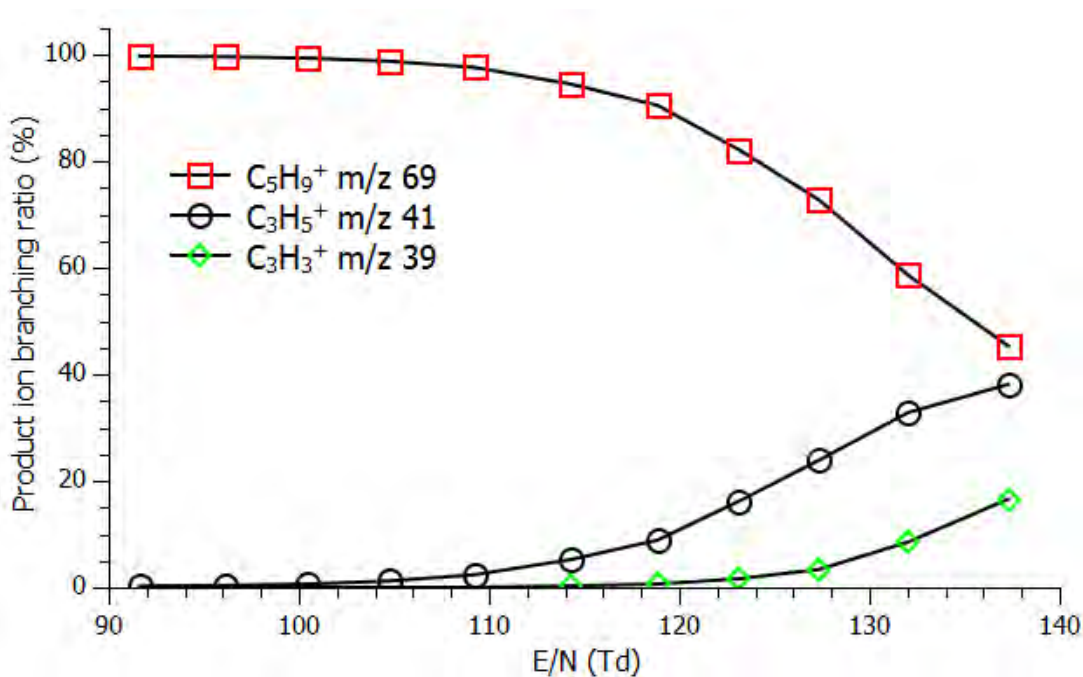
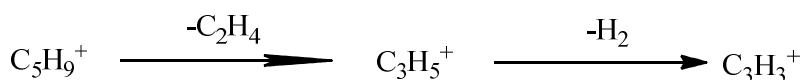


Figure 10 displays the product ion behaviour as a product ion branching ratio for the three recorded product ions from the reaction involving isoprene. A branching ratio shows each product ion as a percentage of the total product ion signal, allowing a convenient visualisation for the fragmentation profile of the ions.

C₅H₉⁺ is termed the protonated monomer of isoprene, MH⁺. At low reduced electric field the protonated monomer is the only product ion observed, but as the reduced electric field is increased the ions, C₃H₅⁺ and C₃H₃⁺ become more abundant. The fragmentation of isoprene is outlined below in Figure 11.

Figure 11: Suggested fragmentation for protonated isoprene.

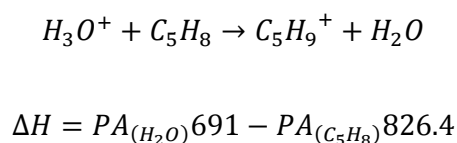


The fragmentation pattern of isoprene is expressed as a sequential loss. First, the neutral hydrocarbon, C₂H₄ is lost from the protonated parent, followed by loss of molecular hydrogen.

In the initial years of proton transfer reaction mass spectrometry, fragmentation of product ions was believed to be a minimal occurrence [28]. However, in subsequent years product ion fragmentation has been more keenly studied [23, 39-44].

The exothermicity of the reaction of isoprene with H_3O^+ , to form protonated isoprene and H_2O is equal to the difference between the proton affinities of water and isoprene, 691 kJ mol^{-1} and $826.4 \text{ kJ mol}^{-1}$, respectively [26].

Equation 7



Calculation for enthalpy change for the proton transfer reaction from a H_3O^+ ion to an isoprene molecule.

This gives an enthalpy change for the reaction of $135.4 \text{ kJ mol}^{-1}$. This energy will be distributed amongst the available degrees of freedom to translational and internal energy of the products of the ion-molecule reaction. The change in Gibbs free energy for this reaction would be $137.6 \text{ kJ mol}^{-1}$; given the gas phase basicities of water and isoprene as 660 and $797.6 \text{ kJ mol}^{-1}$, respectively [26].

At low reduced electric field no fragmentation is observed in Figure 10, suggesting the energy released in the ion-molecule reaction of the neutral analyte and H_3O^+ is not sufficient for fragmentation alone. Also at lower reduced electric fields the concentration of the $H_3O^+ \cdot H_2O$ water clusters is increased at the expense of the reagent ion monomer, H_3O^+ . Protonation from the hydrated reagent ion is a lower energy ionisation, which can also contribute to reduced fragmentation at lower reduced electric fields.

If the fragmentation were caused by excess internal energy obtained from the proton transfer reaction, occurring during the initial ionisation, the reaction is termed dissociative proton transfer. Where collisions between the product ions and the buffer gas result in sufficient increased internal energy to cause fragmentation the reaction is termed collision induced dissociation, CID.

The energy and frequency of these collisions will be altered with changes to the reduced electric field. A high reduced electric field increases the drift velocity, which increases the kinetic energy of ions in the drift tube.

The drift velocity will range between 680 and 1020 m s⁻¹ for a reduced electric field range of 91 to 138 Td. This provides a range of kinetic energy for the ion between 10.8 to 24.5 kJ mol⁻¹, equivalent to an effective temperature for the ions of between 867 and 1963 K. The method of calculation for the drift velocity and kinetic energy is outlined below.

Equation 8

At standard temperature and pressure, STP (273 K, 1 atm) the equation for the drift velocity of an ion under the influence of an electric field through a buffer gas medium is:

$$v_d = \mu E$$

v_d = drift velocity cm s⁻¹, μ = ion mobility, E = electric field strength V cm⁻¹.

For the number density in the drift tube, N this equation can be re-written:

$$v_d = \mu_0 n_0 \frac{E}{N}$$

where n_0 = number density at STP (Loschmidt constant) $2.687 \times 10^{19} \text{ cm}^{-3}$,
 μ_0 = reduced mobility = $2.76 \text{ cm}^2 \text{ s}^{-1} \text{ V}^{-1}$ for H_3O^+ in N_2 at STP [45]. Using
this equation it can be seen that the drift velocity of ions is proportional to
the ratio of electric field and number density, E/N .

The mean kinetic energy for ions in a drift field is described by McFarland et
al. [46] from work by Wannier [47, 48]. The mean kinetic energy for ions is
given by the following formula:

$$KE_{Ion} = \frac{3}{2}k_B T + \frac{1}{2}m_{Ion}v_d^2 + \frac{1}{2}m_b v_d^2$$

KE_{Ion} = kinetic energy J, k_B = Boltzmann constant = $1.381 \times 10^{-23} \text{ J K}^{-1}$, T =
temperature K, m_b = buffer gas molecular mass = $4.65 \times 10^{-26} \text{ kg}$ for N_2 ,
 m_{Ion} = ion mass = $3.16 \times 10^{-26} \text{ kg}$ for H_3O^+ .

Where the first term is concerned with the thermal energy of the ion. The
last two terms are concerned with the field energy of the ion; the second
term describes the energy from the velocity in the direction of the field.
The third term describes the energy due to velocity components arising
from collisions with the ions and the buffer gas.

Calculation of the drift velocity and kinetic energy for ions in the drift tube of a PTR-MS.

For the case where a sufficiently large electric field is placed on the ions and the
temperature is held constant the kinetic energy of ions in the drift tube will be
proportional to the square of the drift velocity.

The centre of mass kinetic energy for the collision between an ion and neutral analyte
molecule is shown in Equation 9 as calculated by McFarland et al. [46].

Equation 9

$$KE_{CM} = \frac{1}{2} \left(\frac{m_{Ion}m_n}{m_{Ion} + m_n} \right) (v_{Ion}^2 + v_n^2)$$

KE_{CM} = centre of mass kinetic energy, m_n = analyte molecule mass, v_{Ion} = ion velocity, v_n = analyte molecule velocity.

The velocity of the ion and the analyte molecule can be defined as below:

$$\frac{1}{2} m_{Ion} v_{Ion}^2 = KE_{Ion}$$

$$\frac{1}{2} m_n v_n^2 = \frac{3}{2} k_B T$$

Using these two equations in combination with the equation for the centre of mass kinetic energy above, the kinetic energy may be given by:

$$KE_{CM} = \frac{m_n}{m_n + m_{Ion}} \left(KE_{Ion} - \frac{3}{2} k_B T \right) + \frac{3}{2} k_B T$$

Calculation of the centre of mass kinetic energy, as calculated by McFarland et al. [46].

The average number of collisions undergone by a single ion in the drift tube is approximately 1,000, calculated by Equation 10. This number of collisions allows for the collision induced dissociation observed for isoprene and other molecules.

Equation 10

The calculation for the number of collisions in the drift tube will start with a calculation of the mean free path, λ .

$$\lambda = \frac{1}{\sqrt{2} N \pi d^2}$$

N = number density by volume = $4.7 \times 10^{22} \text{ m}^{-3}$, d = collision diameter of molecules $\approx 3.7 \times 10^{-10} \text{ m}$ for N_2 [49].

This gives a mean free path of 35 μm .

At a temperature, $T = 318 \text{ K}$ the thermal velocity, $v_T = 532 \text{ m s}^{-1}$.

$$v_T = \sqrt{\frac{3k_B T}{m}}$$

$k_B =$ Boltzmann constant $= 1.381 \times 10^{-23} \text{ J K}^{-1}$, $m =$ molecular mass of gas $= 4.65 \times 10^{-26} \text{ kg}$ for N_2 .

This can be used to find the frequency of thermal collisions, f_c .

$$f_c = \frac{v_T}{\lambda} = \frac{532}{5.4 \times 10^{-5}}$$

Collision frequency, $f_c = 9.98 \text{ MHz}$

With a drift velocity of 680 m s^{-1} at 91 Td, and 1020 m s^{-1} at 138 Td the residence time in the drift tube can be easily calculated from the length of the drift tube, 9.6 cm.

Residence time in drift tube = 0.137 ms at 91 Td;

= 0.091 ms at 138 Td.

By knowledge of the residence time the number of collisions can be easily calculated using the frequency of collisions.

Number of collisions = 1,360 at 91 Td;

= 910 at 138 Td.

Calculation of the number of collisions in the drift tube.

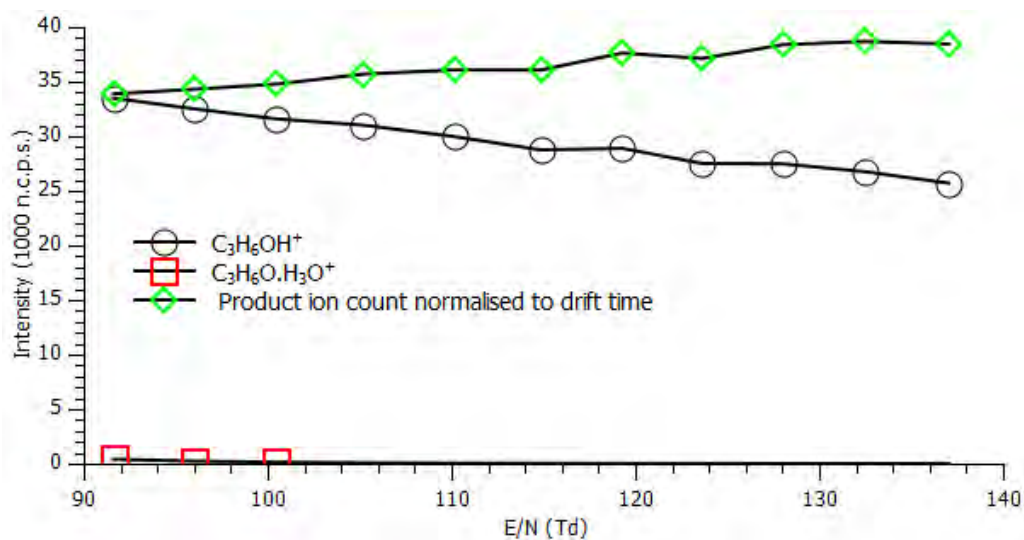
1.3.3 Signal stability investigation using acetone measurements

As for isoprene, the vapour pressure of acetone (245.3 hPa @ 20 °C) [38] proved to be problematically high for sampling. The sample for acetone was made up in a plastic 10 ml syringe in the same way as the sample of isoprene, and again left over night. The 10 ml syringe was then inserted into a 1000 cm³ min⁻¹ flow of nitrogen as outlined in Figure 8. The syringe was then filled with nitrogen to create an acetone and nitrogen vapour which was injected into the 1000 cm³ min⁻¹ flow of nitrogen.

As shown by Equation 10 the number of collisions in the drift tube is dependent on the reduced electric field. More collisions allow for a greater number of opportunities for proton transfer to occur, this leads to an increase in protonated monomer signal at lower reduced electric fields. Compensation can be made for this effect by increasing the signal in correspondence with the change in reaction time relative to the lowest reduced electric field; this is termed normalising to the drift time.

Figure 12 shows the intensity of the recorded product ions for this experiment. The signal intensity is not constant over the range of reduced electric field, whether the results are normalised to the drift time or not. The sample concentration was confirmed to be consistent by repeating the measurements across the range of reduced electric field.

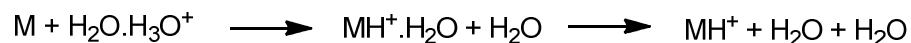
Figure 12: The normalised counts per second for acetone as a function of reduced electric field.



The observed intensity is displayed as counts per second normalised to 5 million counts per second of the sum of H_3O^+ and $\text{H}_2\text{O}.\text{H}_3\text{O}^+$. Normalisation allows the intensity to be compared between measurements where the reagent ion signal may vary. The proton affinity of the hydrate cluster $2\text{H}_2\text{O}$ is approximately 830 kJmol^{-1} [32], given this value it may seem strange to normalise to the $\text{H}_2\text{O}.\text{H}_3\text{O}^+$ signal bearing in mind the proton affinity of acetone is only 812.4 kJmol^{-1} [26].

Although acetone has a lower proton affinity than the hydrate cluster a protonated monomer may still be produced. Neutral analyte molecules, M may interact with the hydrate ion cluster, $\text{H}_3\text{O}^+.\text{H}_2\text{O}$ via a bimolecular reaction to form $\text{MH}^+.\text{H}_2\text{O}$ and H_2O . This $\text{MH}^+.\text{H}_2\text{O}$ ion may go on to lose a water molecule by collisions with the drift gas to form MH^+ .

Equation 11



Cluster ionisation reaction for $\text{H}_2\text{O}.\text{H}_3\text{O}^+$, a neutral analyte molecule, M and a neutral molecule N .

This mechanism describes how protonated monomer can be produced by the reagent ion monohydrate cluster. It should also be mentioned that quantities of $\text{MH}^+.\text{H}_2\text{O}$ may

be formed by the reverse reaction of association of H_2O with the protonated monomer. Two product ions are observed for acetone; $\text{C}_3\text{H}_6\text{OH}^+$ and $\text{C}_3\text{H}_6\text{OH}^+\cdot\text{H}_2\text{O}$ corresponding to the protonated parent and protonated monohydrate cluster respectively.

The total product ion count for acetone is shown normalised to the drift time in Figure 12. These results are closer to constancy than those un-normalised to the drift time, but still do not achieve a constant value. This is for three reasons; firstly the reaction rate between acetone and the hydrate cluster ion may be lower than the reaction rate between acetone and the hydronium ion, reducing the signal intensity at lower reduced electric field. Diffusion of ions from the drift tube may also have an effect, increasing at lower reduced electric field because of the increased residence time of ions in the drift tube; this may reduce signal intensity. Also, the quadrupole has a lower sensitivity at higher masses, this means that the $\text{C}_3\text{H}_6\text{OH}\cdot\text{H}_3\text{O}^+$ product ion is detected less efficiently by the quadrupole, which may also affect the signal intensity.

The effect of reduced electric field on the signal observed for acetone is fairly typical of the effect observed for other analyte molecules. However, analysis of certain compounds have displayed dissimilar behaviour with changes in reduced electric field, in particular the nitroaromatic compound 2,4,6 trinitrotoluene, TNT [37]. Reactions between the neutral analyte and monohydrate reagent ion cluster resulting in a protonated monomer are also commonly observed. Where normalised data is presented, it will be normalised to 5 million counts per second of the H_3O^+ and $\text{H}_3\text{O}^+\cdot\text{H}_2\text{O}$ ions, unless otherwise stated.

1.3.4 Using an aromatic compounds mix for calibration

To measure the sensitivity of the PTR-MS a calibration gas, (Restek TO-14A Aromatics Mix) was introduced to the PTR-MS. The measurements were carried out to find a general sensitivity of the PTR-MS; to understand in what approximate range of concentrations the instrument could perform. The calibration gas used is a mixture of 14 aromatic compounds at 8 separate masses, including 9 isomers, at a calibrated concentration in nitrogen. Details of the mix are shown in Table 4.

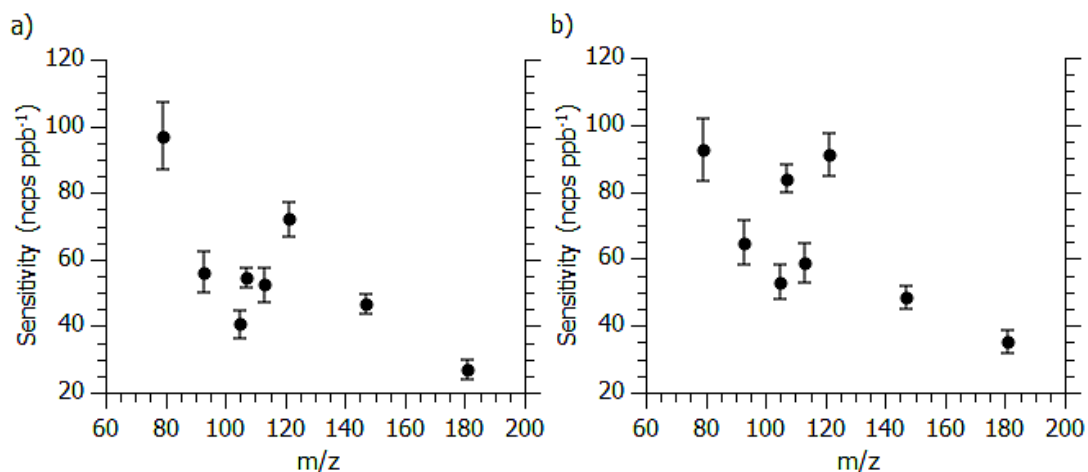
Table 4: The contents of Restek's TO-14A Aromatics Mix, showing the supplier's concentration, molecular weight and chemical formulae.

Chemical name	Chemical Formula / molecular weight	Concentration (ppb)
Benzene	C ₆ H ₆ / 78	103 ± 10
Toluene	C ₆ H ₅ CH ₃ / 92	102 ± 10
Chlorobenzene	C ₆ H ₅ Cl / 112	78 ± 8
Ethylbenzene, O-xylene, M-xylene, P-xylene	C ₈ H ₁₀ / 106	403 ± 20
Styrene	C ₈ H ₈ / 104	77 ± 8
1,2,4-Trimethylbenzene, 1,3,5-Trimethylbenzene	C ₉ H ₁₂ / 120	199 ± 14
1,2-Dichlorobenzene, 1,3-Dichlorobenzene, 1,4-Dichlorobenzene	C ₆ H ₄ Cl ₂ / 146	178 ± 13
1,2,4-Trichlorobenzene	C ₆ H ₃ Cl ₃ / 180	37 ± 4

The gas was introduced to the PTR-MS inlet via heated 1/8 inch Teflon tubing from a lecture bottle. The 1/8 inch tubing was connected across the PTR-MS inlet via a stainless steel T-piece connector, any excess calibrant gas was removed to outside the lab. Scans were taken at two drift tube settings, (E/N = 91 Td, E/N = 138 Td). The

resulting sensitivity results are shown in Figure 13. Error bars in Figure 13 are calculated from the stated error in the concentration of the calibrant mix.

Figure 13: Figure showing the sensitivity of the PTR-MS to a mix of aromatics at a) 138 Td and b) 91 Td.



Each compound, or group of isobaric compounds was monitored at the m/z of its protonated monomer. The measured counts were normalised to 5 million counts per second of the sum of H_3O^+ and $H_3O^+.H_2O$, except benzene which was normalised to 5 million counts per second of the H_3O^+ signal. Molecules with weak dipole moments will be less likely to undergo clustering reactions with $H_3O^+.H_2O$ [50]; as outlined in Equation 11. Benzene does not react with $H_3O^+.H_2O$, due to its zero dipole moment and prohibitively low proton affinity (750.4 kJ mol⁻¹ [26]).

The sensitivity was then calculated by dividing the normalised counts per second by the concentration in ppb. The reduction in sensitivity shown in Figure 13 as mass increases is a feature of quadrupole detection systems. The sensitivity at the two reduced electric fields shows good similarity. Differences in sensitivity are to be expected with different reduced electric fields, as discussed in Section 1.3.3. That these differences seem to have a greater effect on different molecules is also to be expected, different molecules

will have different tendencies to diffuse, and different reactivities with the hydrate cluster ion [36]. Fragmentation effects may also affect the recorded sensitivity. The observed sensitivity for these aromatic compounds ranges approximately from 100 to 30 ncps ppb⁻¹. This is believed to give a good indication of the instrument's sensitivity for many compounds over this mass range.

1.3.5 Studying hollow cathode effects using isoprene

A sample of isoprene vapour mixed with nitrogen was introduced to the PTR-MS using a 10 ml plastic syringe in the same method as outlined in Section 1.3.2. However, in this case the flow of nitrogen was an arbitrary but constant value, instead of the 1000 cm³ min⁻¹ used in Section 1.3.2.

As mentioned in Section 1.2.1, it is possible to adjust the operating parameters of the hollow cathode ion source. For a constant start-up voltage of 600 V the ion current may be varied between 2 and 10 mA, whilst still maintaining a good reagent ion signal.

By selecting an increased emission current, a greater accelerating cathode potential is applied, which may cause more energetic electron collisions. The higher energy collisions result in increasing the effective temperature within the hollow cathode, this will cause an increased pressure in the hollow cathode region, resulting in a measured increase in the drift tube pressure.

The location of the plasma may be extended for higher emission currents. Within the hollow cathode region, the plasma may move closer to the orifice and may extend beyond the hollow cathode region into the drift tube.

Data for the product ion branching ratio of isoprene was collected at 138 Td with a range of emission currents between 2 to 10 mA at a start-up voltage of 600 V. The results are shown in Figure 14, where the $C_3H_3^+$ product ion is not included.

Figure 14: Product ion branching ratio for isoprene at 138 Td as a function of hollow cathode emission current.

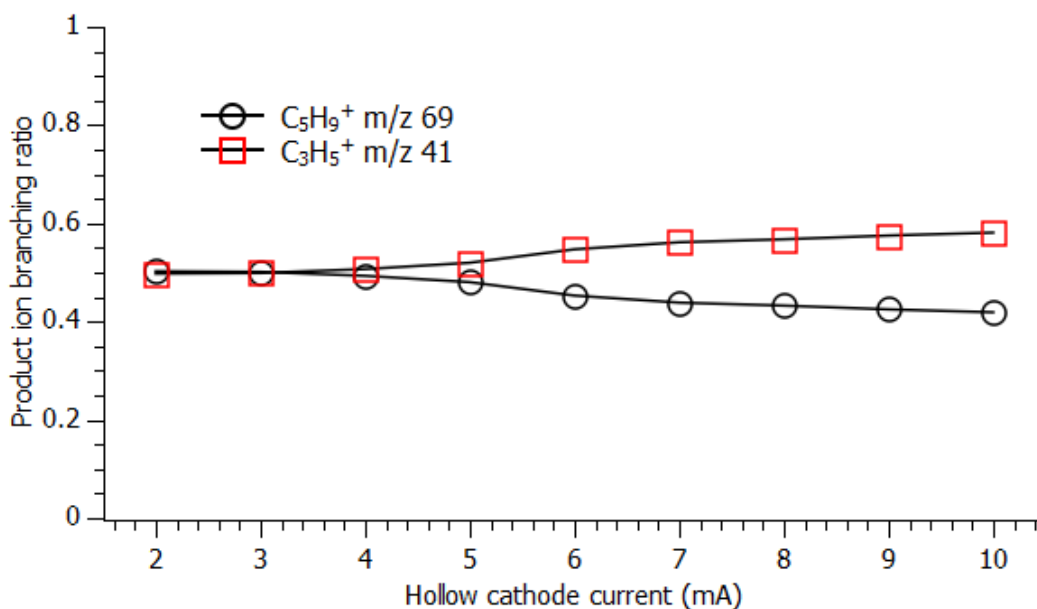


Figure 14 shows an increase in fragmentation of isoprene as the emission current is increased. This indicates that greater energy is being transferred to the protonated monomer. It may be assumed that the increased energy is derived from increased activity in the hollow cathode discharge source. There are possibly three effects that could arise from the hollow cathode, where they might impact the observed branching ratios. Increased translational energy of H_3O^+ , increased internal energy of H_3O^+ , and interactions between the analyte molecules and the ionising plasma; resulting from either back-streaming of the analyte or extension of the plasma into the drift tube.

Hydronium ions with increased energy may lose this energy by collisions with the buffer gas. The collision of hydronium ions with molecular nitrogen may produce such a collision process to dissipate any extra translational energy. Any increase in translational

energy should be dissipated efficiently, such that it is unfavoured to explain the effect on the product ion branching ratios.

Any extra internal energy of the hydronium ions may remain within the system for long enough to affect the proton transfer reaction to analyte molecules. Internally excited hydronium ions may be the source of the observed dependence of the product ion branching ratios on the hollow cathode emission current.

The glow discharge region of the hollow cathode may move closer to the inlet of the drift tube at higher emission currents. A degree of back-streaming occurs from the drift tube, as shown by the presence of impurity ions; O_2^+ and NO^+ . With closer proximity of the glow discharge, the back-streaming may become more influential. It may also be possible for some portion of the plasma to extend beyond the ion source region and affect analyte ionisations in the drift tube. Ionisations caused by the glow discharge are at considerably higher energies than those ionisations found in the drift tube. To determine the level of analyte sample concentration necessary to produce back-streaming, a series of investigations were conducted using carbon tetrafluoride as the analyte.

1.3.6 Back-streaming investigation using carbon tetrafluoride

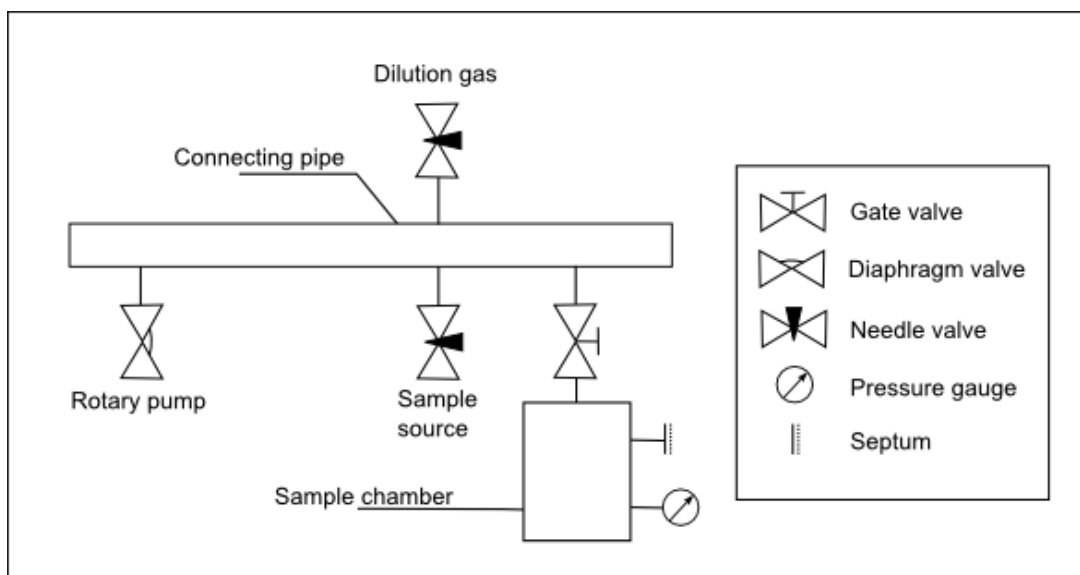
The occurrence of back-streaming in the PTR-MS is evidenced by the production of NO^+ and O_2^+ ions which appear as peaks in the mass spectra at m/z 30 and 32, respectively. The debate is whether analyte back-streaming is significant and has an effect on VOC detection. To investigate this, the compound carbon tetrafluoride, CF_4 was analysed using the PTR-MS.

Carbon tetrafluoride has a proton affinity significantly less than water (529.3 kJ mol⁻¹ for CF_4 , 691 kJ mol⁻¹ for water [26]), such that proton transfer from H_3O^+ should not occur.

The ionisation energy of carbon tetrafluoride is 14.7 eV [31], which is greater than the recombination energy of both the O_2^+ and NO^+ ions. In order for CF_4 to become ionised, it must back-stream into the hollow cathode discharge source and become ionised by electron impact. Carbon tetrafluoride was used to investigate the required concentration to produce sufficient back-streaming to be effecting.

A known concentration of carbon tetrafluoride was produced using the calibration rig detailed in Figure 15. The sample source and dilution gas used for this study included gas bottles of carbon tetrafluoride (BOC) and white spot nitrogen. A sample concentration was made up by evacuating the sample chamber with a rotary pump; the pressure gauge reading was noted as 4 mbar. The needle valve controlling the sample source was opened, allowing the chamber to fill to a pressure of 28 mbar with carbon tetrafluoride, the needle valve was then shut off. This pressure was then increased to 1659 mbar by opening the needle valve to the diluting nitrogen gas. This procedure produced an arbitrary dilution ratio for carbon tetrafluoride to nitrogen of 1:60.

Figure 15: Diagram of the calibration rig used to produce a known concentration of carbon tetrafluoride.

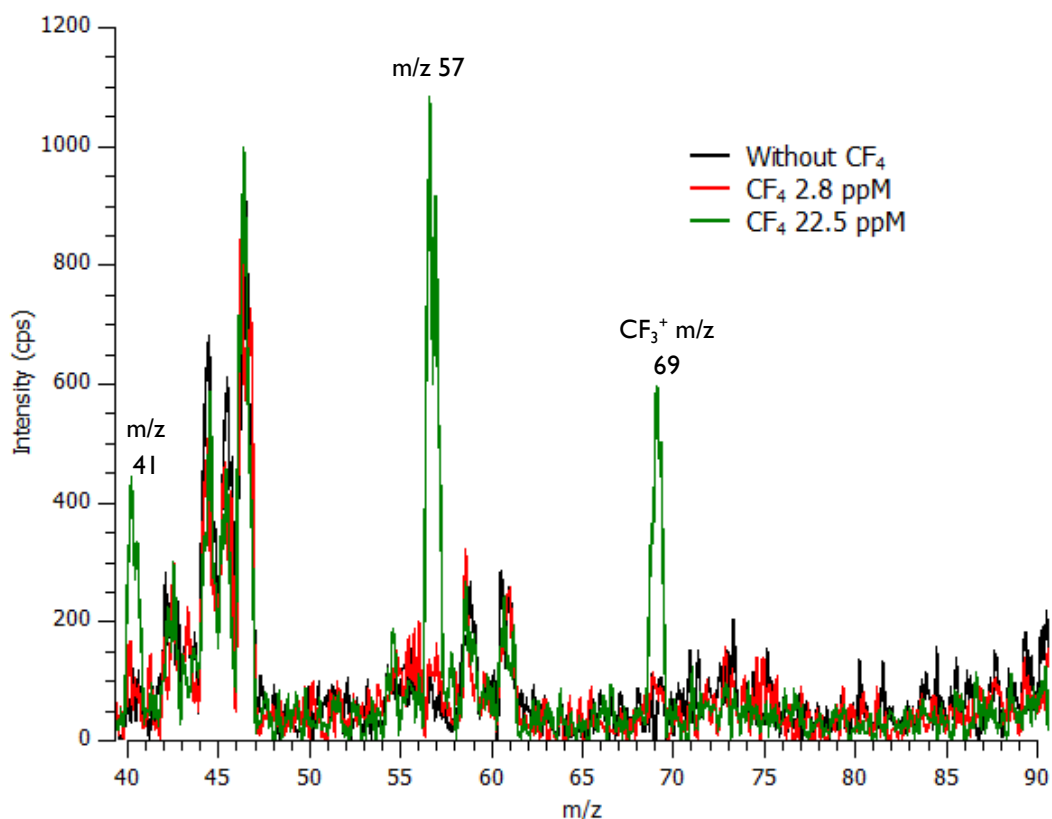


The sample mixture (dilution 1:60) of CF_4 and nitrogen was then removed from the sample chamber, through the septum, using a 10 ml plastic syringe. The carbon tetrafluoride and nitrogen mixture was injected into a $1000 \text{ cm}^3 \text{ min}^{-1}$ flow of nitrogen at flow rates of 10 and $80 \text{ cm}^3 \text{ hr}^{-1}$. This was calculated to create concentrations of carbon tetrafluoride in nitrogen of 2.8 and 22.5 ppm respectively; allowed to flow into the inlet of the PTR-MS, as illustrated in Figure 8.

The results for this experiment are shown in Figure 16 and Figure 17. With the PTR-MS set to a reduced electric field of 138 Td and an emission current of 10 mA, no product ions were observed for carbon tetrafluoride at a concentration of 2.8 ppm. However, at 22.5 ppm product ions were observed at mass spectra peaks m/z 41, 57 and 69. This implies that the concentration range for detected ions produced by back-streaming of CF_4 is between 2.8 and 22.5 ppm.

The concentration range for the detection of ions produced by back streaming may differ for other molecules beyond that reported for CF_4 . Ionisation caused by back-streaming will depend on the analyte's ionisation properties. The ionisation requirements of VOCs typically observed with a PTR-MS may be lower energy than the hard ionisation required for CF_4 .

Figure 16: Mass spectra of carbon tetrafluoride at 2.8 ppm, 22.5 ppm and at zero concentration with an emission current of 10 mA.

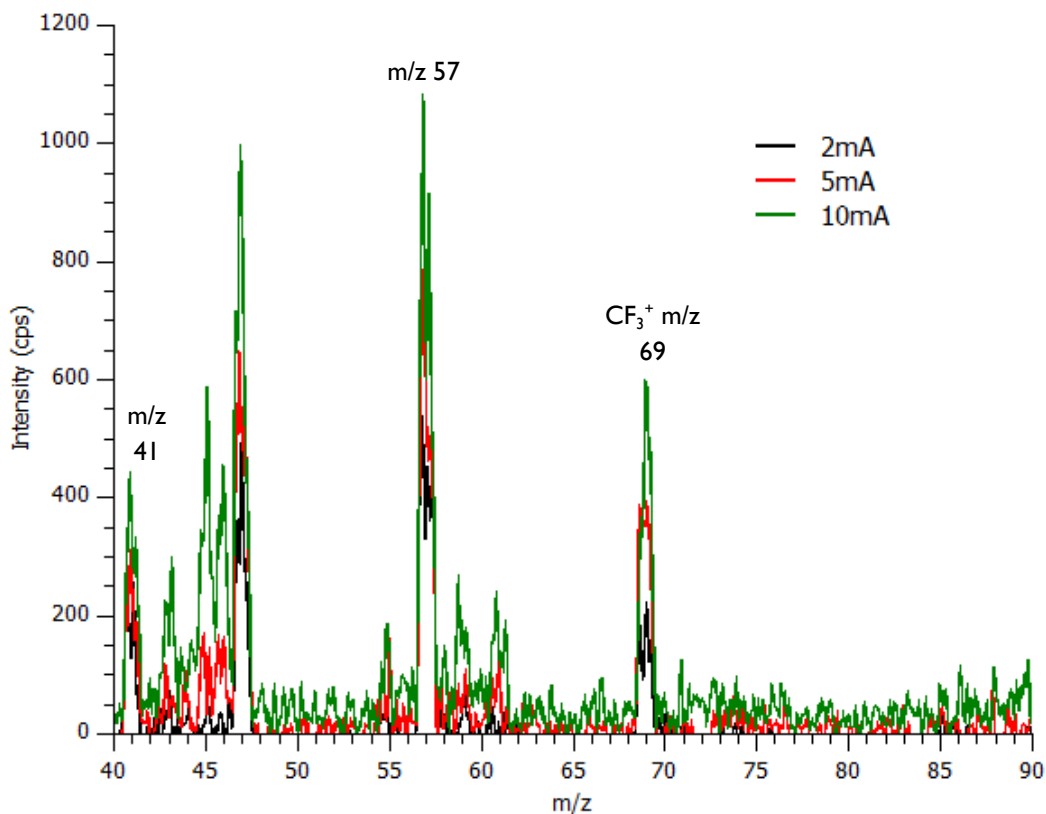


The product ion at m/z 69 has been observed where CF_4 was used in a selected ion flow tube (SIFT) study. Carbon tetrafluoride was used as a neutral gas source to generate ions of CF_3^+ [51] using a high pressure electron impact source. The SIFT study also produced F^+ , CF^+ and CF_2^+ ions, but these ions were not observed in this study. The discrepancy found in product ions generated by the SIFT-MS and PTR-MS ionisation sources should be expected in view of the very different compositions of gases being ionised. The CF_4 is ionised in a high concentration of water in the PTR-MS ionisation source, which was not so for the SIFT experiment.

Further to this, Figure 17 shows that at higher emission currents a greater product ion signal is observed by ionisation of carbon tetrafluoride. This increase in signal suggests that back-streaming becomes more important at higher emission currents. For higher

emission currents the glow discharge is moved closer to the orifice linking the ion source and drift tube regions. With the glow discharge closer to this orifice a greater fraction of any back-streaming analyte will be ionised, corroborating the expansion of the plasma towards the drift tube at higher emission currents.

Figure 17: Product ions observed from back streaming of carbon tetrafluoride at 22.5 ppm for three emission currents, 10, 5, 2 mA.



1.4 Conclusion

The PTR-MS is a versatile instrument for real time and high sensitivity mass spectrometry. However, it is important to make efforts toward rigorous characterisation of the instrument, of which little so far has been done, to develop and contribute to this diverse and emerging field of technology. Part of this chapter has dealt with the testing of the instrument with regard to its fragmentation effects, in terms of the drift tube and hollow cathode function, and also the instruments response to the

detection of samples at a given concentration. The chapter has also introduced the main components of the PTR-MS, and explained how the conditions of these components can affect the PTR-MS's functional operation.

The following chapter will examine the PTR-MS further through an investigation involving a series of saturated alcohols.

2 Analysis of a Series of Saturated Alcohols for Characterisation and Understanding of Proton Transfer Reaction Mass Spectrometry

2.1 Introduction

Before any scientific instrument can be utilised for analysis of a real world scenario it should be tested and characterised. In gas analysis and monitoring, this characterisation is often done by selecting a series of chemicals with the same functional group and/or similar hydrocarbon structure and analysing each chemical in that series individually. From these measurements further knowledge about the instrument can be built-up to aid in the analysis and monitoring of a gas sample where many chemicals are present.

To characterise the PTR-MS, a series of organic saturated alcohols were chosen. The series, shown in Table 5, ranged from single to six carbon molecules, covering a range of structural alcohol types; primary, secondary, tertiary and cyclic. Each alcohol was analysed for a range of reduced electric field values between 90 and 140 Td. Further to this, branching ratios for 1-propanol, 2-propanol and cyclohexanol were recorded as a function of the emission current of the hollow cathode.

2.2 Background

In recent years, many researchers using proton transfer reaction mass spectrometry have studied how the operating conditions of their instruments affect the observed product ions of a variety of chemical compounds [39-44]. These investigations have examined the effects that the humidity in the drift tube [36, 40] and the reduced electric field [39, 42-44] have on the observed product ions. No research papers previous to

this study have discussed the effect that changing the operating conditions of the hollow cathode can have on the observed product ions.

The observed product ions from saturated alcohols had not previously been studied as a function of reduced electric field with a PTR-MS. Buhr et al. published a paper in 2002 [52] quoting branching ratios for a range of compounds, including many saturated alcohols, but the results were measured at a single, unspecified reduced electric field that was not recorded in the paper.

There appears to be some confusion in the literature concerning the proton transfer reaction of ethanol. In a recent review by Blake in 2006 [53], when comparing the product ion branching ratios of Warneke [54] with their own they found a discrepancy which they described as anomalous. Warneke found a 50:50 branching ratio for product ions at m/z 47 and 29, whereas Blake found a 93:7 branching ratio for the same product ions at a similar reduced electric field. The dissimilarity may be explained as the loss of H_3O^+ from the protonated ethanol structure. The H_3O^+ product will not be observed because of interference from the reagent ion, confusing interpretation of branching ratios. This process has been known about in the literature for some years [55-58], but was confirmed experimentally to occur in a PTR-MS by Inomata and Tanimoto in 2010, by studying a samples of ethanol labelled with deuterium [59].

Results taken as part of this study, along with accompanying discussion have been presented in a 2010 paper published in the International Journal of Mass Spectrometry [23], attached in Appendix C.

2.3 Experimental Details

Saturated alcohols are a commonly occurring class of chemicals in the study of VOCs. The alcohols selected for this study are shown in Table 5, with their structure illustrated

in Figure 18. From the list some chemicals, such as ethanol, methanol and propanol are common, routinely found in air sampling investigations [10, 50, 60-62]. Other alcohols, particularly the cyclic compounds, although they are less common in air sampling investigations, have been chosen to extend the range of structures to be examined.

Table 5: Table showing the twelve saturated alcohols. Organised in order of molecular weight, and then by their proton affinity, where it is known [26].

Chemical Name (proton affinity/kj mol⁻¹)	Chemical Formula (mw/amu)
Methanol (754.3)	CH ₃ OH (32)
Ethanol (776.4)	C ₂ H ₅ OH (46)
1-Propanol (786.5)	C ₃ H ₇ OH (60)
2-Propanol (793.0)	C ₃ H ₇ OH (60)
1-Butanol (789.2)	C ₄ H ₉ OH (74)
2-Methyl-1-propanol (793.7)	C ₄ H ₉ OH (74)
1,1-Dimethylethanol (802.6)	C ₄ H ₉ OH (74)
2-Butanol (815)	C ₄ H ₉ OH (74)
Cyclopentanol	C ₅ H ₁₀ O (86)
1-Pentanol	C ₅ H ₁₁ OH (88)
Cyclohexanol	C ₆ H ₁₂ O (100)
1-Hexanol	C ₆ H ₁₃ OH (102)

Each of the alcohols was purchased from Sigma-Aldrich, each with a purity > 99 %. The proton affinity of water is 691 kJ mol⁻¹.

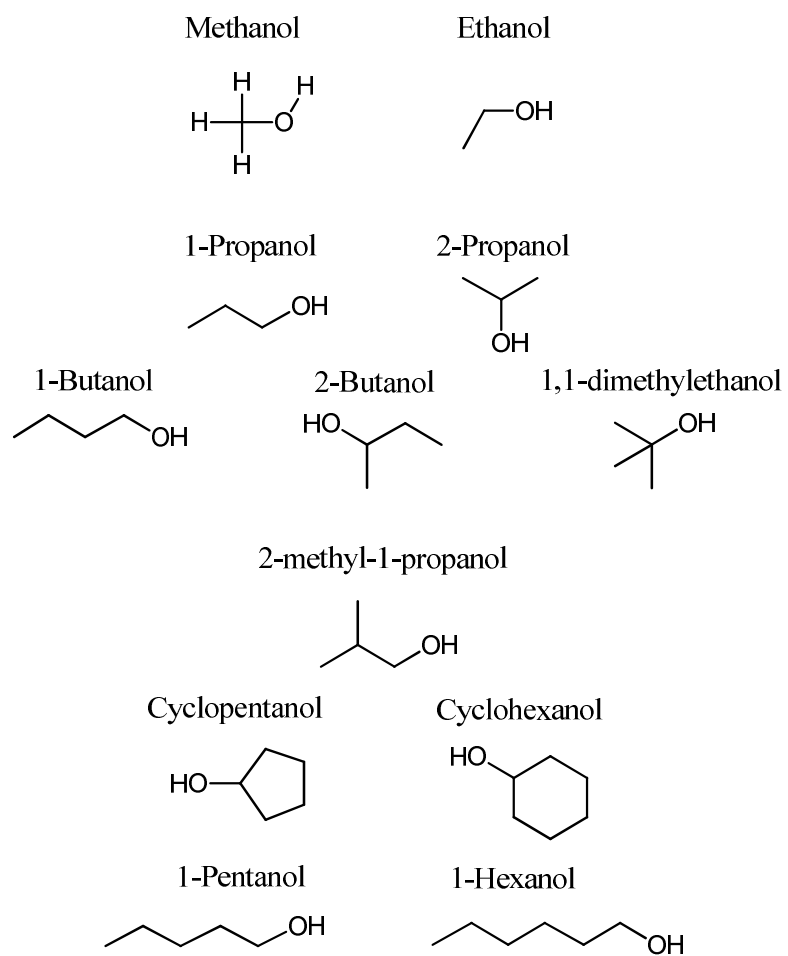
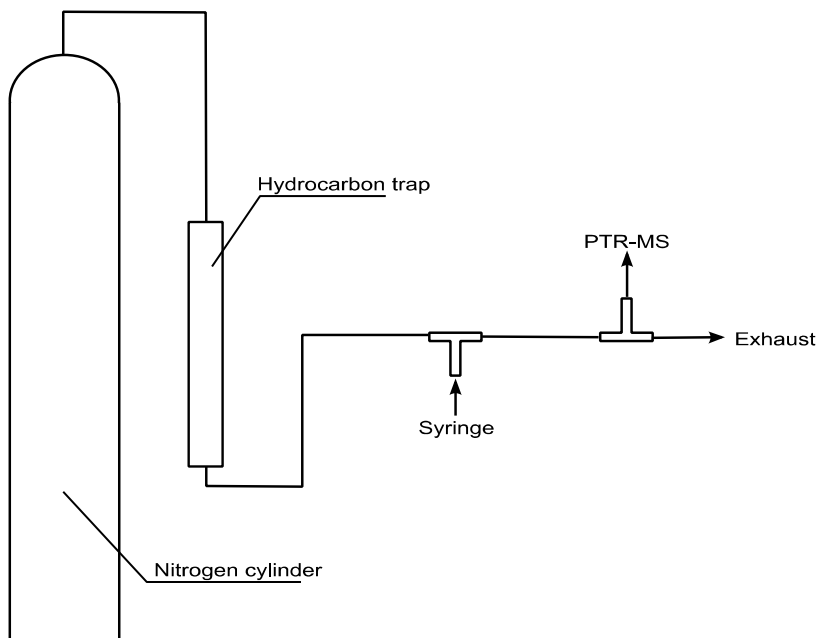


Figure 18: Structures diagram of the 12 alcohols used in this study.

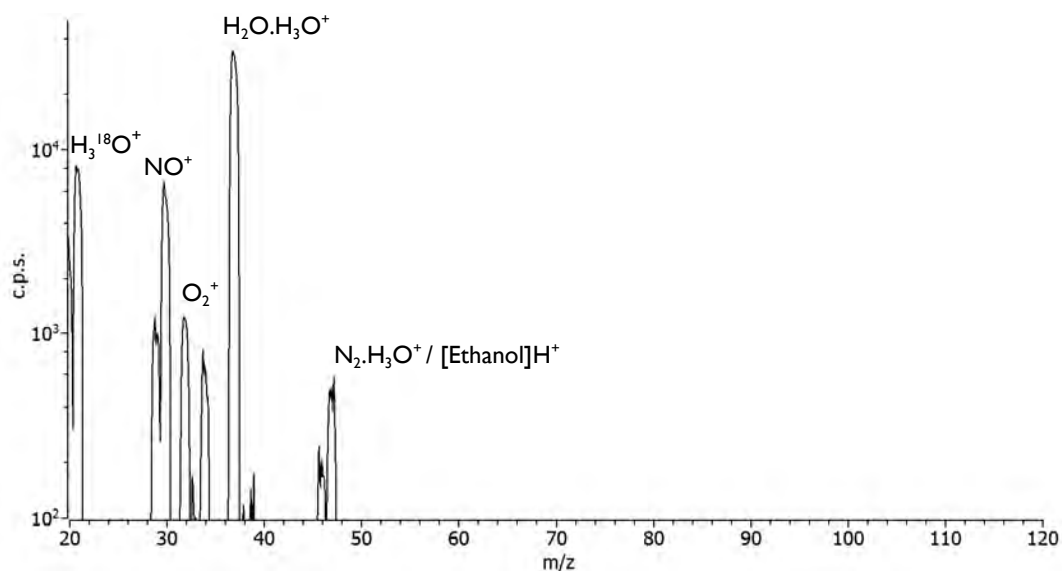
The design of this experiment was similar to that described in the previous chapter, Section 1.3 and is outlined in Figure 19.

Figure 19: Experimental set-up for the study of a series of saturated alcohols.



Samples of the respective alcohol vapour were produced by transferring a couple of drops of the alcohol liquid onto a piece of cotton wool, placed in a 10 ml plastic syringe barrel. The transfer was performed using a 250 μ l glass syringe. The 10 ml syringe was inserted; empty except for the cotton wool, into a nitrogen gas stream. The plunger of the syringe could be retracted, thereby filling the syringe with a nitrogen and alcohol vapour mixture. By injecting this vapour into the flow of nitrogen, it was possible to produce a very pure nitrogen and alcohol vapour mixture. An example mass spectrum showing the cleanliness of the signal recorded using nitrogen as a background is shown in Figure 20. The good reliability of the sample allowed low intensity ions to be identified with a high degree of confidence.

Figure 20: Mass spectrum of dry N₂ showing the peaks of a clean system at a reduced electric field of 138 Td.



By using a carrier gas of nitrogen, the amount of oxygen in the drift tube is reduced, which effectively limits the amount of oxygen available to back-stream in to the hollow cathode. This reduces the O₂⁺ signal to <0.1 % of the total reagent ion signal, which improves confidence in product ion assignment confined to proton transfer reactions only.

The flow rate of the nitrogen carrier gas was arbitrary but fixed for each alcohol in the study. Varying the flow rate from the syringe drive, thus varied the concentration of the alcohol by a given amount. This allowed any observed concentration dependence to be analysed.

Where branching ratios exhibit a concentration dependence, it is often assumed to be caused by secondary reactions. Secondary reactions occur at higher analyte concentrations. Where the primary reagent ion becomes depleted, product ions may become sufficient in number to act as secondary reagent ions. This leads to unwanted complications in the interpretation of mass spectra. By extrapolating branching ratios to

zero concentration, only the ions produced by the reaction between the primary reagent ion and analyte may be measured.

2.4 Experimental Results and Mass Spectra

The results are presented and discussed in two sections, Section 2.4.1 and Section 2.4.2. Section 2.4.1 discusses the product ion branching ratios as a function of reduced electric field with a fixed hollow cathode emission current of 5 mA. Data for each alcohol is displayed in this section. In Section 2.4.2 the product ion branching ratios are discussed at a fixed reduced electric field with varying hollow cathode emission current. This includes three of the saturated alcohols, 1-propanol, 2-propanol and cyclohexanol.

2.4.1 Reduced electric field dependence of saturated alcohols

The branching ratios for each alcohol are summarised in Table 6 for three values of reduced electric field, E/N . With the exception of methanol and ethanol, no amount of the protonated monomer, MH^+ was detected with a branching ratio greater than a few percent. This suggests that in the application of proton transfer reaction mass spectrometry, although a soft ionisation technique used, fragmentation is far from removed as a complicating factor in the interpretation of mass spectra. Methanol shows no product ion fragmentation, but the number of product ions and hence the complexity of any spectrum increases as the mass of the saturated alcohol is increased. This is shown in Table 6 and will be further discussed as the measurements of each alcohol are examined.

Table 6: Table showing the product ion branching ratio as a percentage for a series of saturated, aliphatic alcohols in dry nitrogen.

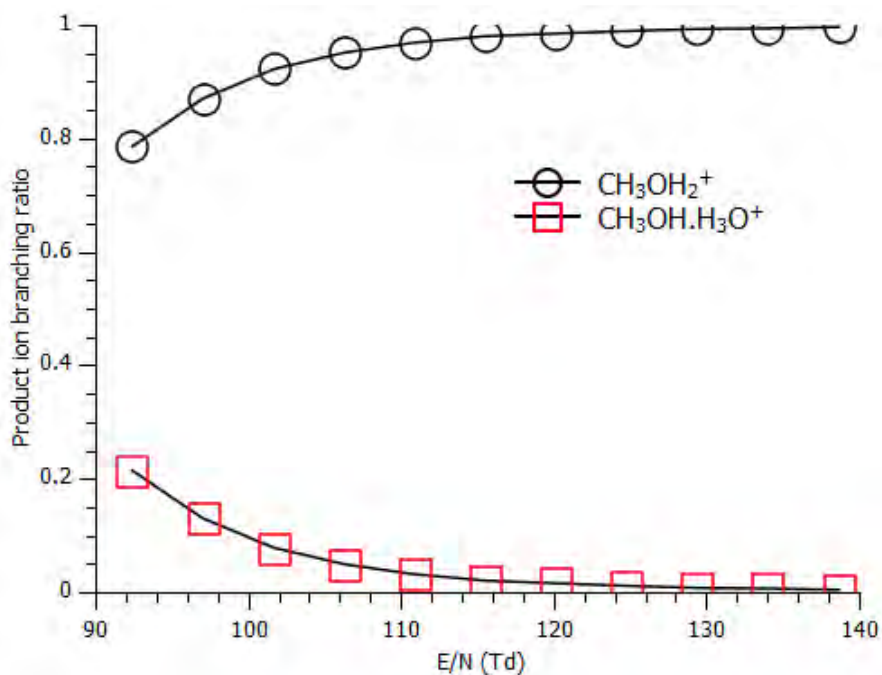
Name (PA/kJ mol ⁻¹) [26]	Formula (mw)	Product Ions and Ion Branching Ratios (%)					
		E/N = 92 ± 1 Td		E/N = 115 ± 1 Td		E/N = 138 ± 1 Td	
Methanol (754.3)	CH ₃ OH (32)	51 (21) 33 (79)	M.H ₃ O ⁺ MH ⁺	51 (2) 33 (98)	M.H ₃ O ⁺ MH ⁺	33 (100)	MH ⁺
Ethanol (776.4)	C ₂ H ₅ OH (46)	19 (?) 65 (20) 47 (75) 45 (4) 29 (1)	H ₃ O ⁺ M.H ₃ O ⁺ MH ⁺ [M-H ₂]H ⁺ [M-H ₂ O] ⁺	19 (?) 65 (1) 47 (69) 45 (15) 29 (15)	H ₃ O ⁺ M.H ₃ O ⁺ MH ⁺ [M-H ₂]H ⁺ [M-H ₂ O] ⁺	19 (?) 47 (43) 45 (17) 29 (40)	H ₃ O ⁺ MH ⁺ [M-H ₂]H ⁺ [M-H ₂ O] ⁺
1-Propanol (786.5)	C ₃ H ₇ OH (60)	79 (4) 61 (3) 43 (93)	M.H ₃ O ⁺ MH ⁺ [M-H ₂ O] ⁺	43 (83) 41 (17)	[M-H ₂ O] ⁺ [M-H ₂ O-H ₂] ⁺	43 (29) 41 (52) 39 (19)	[M-H ₂ O] ⁺ [M-H ₂ O-H ₂] ⁺ [M-H ₂ O-2H ₂] ⁺
2-Propanol (793.0)	C ₃ H ₇ OH (60)	79 (3) 61 (5) 59 (1) 43 (91)	M.H ₃ O ⁺ MH ⁺ [M-H ₂]H ⁺ [M-H ₂ O] ⁺	59 (1) 43 (85) 41 (14)	[M-H ₂]H ⁺ [M-H ₂ O] ⁺ [M-H ₂ O-H ₂] ⁺	59 (1) 43 (31) 41 (52) 39 (16)	[M-H ₂]H ⁺ [M-H ₂ O] ⁺ [M-H ₂ O-H ₂] ⁺ [M-H ₂ O-2H ₂] ⁺
1-Butanol (789.2)	C ₄ H ₉ OH (74)	93 (3) 75 (1) 73 (5) 57 (91)	M.H ₃ O ⁺ MH ⁺ [M-H ₂]H ⁺ [M-H ₂ O] ⁺	73 (2) 57 (95) 41 (3)	[M-H ₂]H ⁺ [M-H ₂ O] ⁺ [M-H ₂ O-CH ₄] ⁺	57 (55) 55 (7) 41 (26) 39 (12)	[M-H ₂ O] ⁺ [M-H ₂ O-H ₂] ⁺ [M-H ₂ O-CH ₄] ⁺ [M-H ₂ O-CH ₄ -H ₂] ⁺
2-Methyl-1-propanol (793.7)	C ₄ H ₉ OH (74)	93 (3) 73 (5) 57 (92)	M.H ₃ O ⁺ [M-H ₂]H ⁺ [M-H ₂ O] ⁺	73 (7) 57 (90) 41 (3)	[M-H ₂] ⁺ [M-H ₂ O] ⁺ [M-H ₂ O-CH ₄] ⁺	73 (8) 57 (58) 41 (26) 39 (8)	[M-H ₂]H ⁺ [M-H ₂ O] ⁺ [M-H ₂ O-CH ₄] ⁺ [M-H ₂ O-CH ₄ -H ₂] ⁺
1,1-Dimethyl-ethanol (802.6)	C ₄ H ₉ OH (74)	93 (1) 75 (1) 57 (98)	M.H ₃ O ⁺ MH ⁺ [M-H ₂ O] ⁺	57 (98) 41 (2)	[M-H ₂ O] ⁺ [M-H ₂ O-CH ₄] ⁺	57 (68) 41 (24) 39 (8)	[M-H ₂ O] ⁺ [M-H ₂ O-CH ₄] ⁺ [M-H ₂ O-CH ₄ -H ₂] ⁺
2-Butanol (815)	C ₄ H ₉ OH (74)	93 (2) 75 (1) 57 (97)	M.H ₃ O ⁺ MH ⁺ [M-H ₂ O] ⁺	57 (96) 41 (4)	[M-H ₂ O] ⁺ [M-H ₂ O-CH ₄] ⁺	57 (63) 41 (28) 39 (9)	[M-H ₂ O] ⁺ [M-H ₂ O-CH ₄] ⁺ [M-H ₂ O-CH ₄ -H ₂] ⁺
Cyclopentanol	C ₅ H ₁₀ O (86)	105 (3) 85 (16) 69 (80) 67 (1)	M.H ₃ O ⁺ [M-H ₂]H ⁺ [M-H ₂ O] ⁺ [M-H ₂ O-H ₂] ⁺	85 (17) 69 (78) 67 (1) 41 (4)	[M-H ₂] ⁺ [M-H ₂ O] ⁺ [M-H ₂ O-H ₂] ⁺ [M-H ₂ O-C ₂ H ₄] ⁺	85 (15) 69 (35) 67 (5) 41 (32) 39 (13)	[M-H ₂]H ⁺ [M-H ₂ O] ⁺ [M-H ₂ O-H ₂] ⁺ [M-H ₂ O-C ₂ H ₄] ⁺ [M-H ₂ O-C ₂ H ₄ -H ₂] ⁺
1-Pentanol	C ₅ H ₁₁ OH (88)	107 (3) 87 (10) 71 (80) 69 (6) 43 (1)	M.H ₃ O ⁺ [M-H ₂]H ⁺ [M-H ₂ O] ⁺ [M-H ₂ O-H ₂] ⁺ [M-H ₂ O-C ₂ H ₄] ⁺	87 (4) 71 (49) 69 (12) 43 (30) 41 (5)	[M-H ₂]H ⁺ [M-H ₂ O] ⁺ [M-H ₂ O-H ₂] ⁺ [M-H ₂ O-C ₂ H ₄] ⁺ [M-H ₂ O-C ₂ H ₄ -H ₂] ⁺	71 (9) 69 (16) 43 (17) 41 (44) 39 (14)	[M-H ₂ O] ⁺ [M-H ₂ O] ⁺ [M-H ₂ O-H ₂] ⁺ [M-H ₂ O-C ₂ H ₄] ⁺ [M-H ₂ O-C ₂ H ₄ -H ₂] ⁺
Cyclohexanol	C ₆ H ₁₂ O (100)	119 (2) 99 (21) 83 (77)	M.H ₃ O ⁺ [M-H ₂]H ⁺ [M-H ₂ O] ⁺	99 (21) 83 (76) 55 (3)	[M-H ₂]H ⁺ [M-H ₂ O] ⁺ [M-H ₂ O-C ₂ H ₄] ⁺	99 (23) 83 (35) 55 (42)	[M-H ₂]H ⁺ [M-H ₂ O] ⁺ [M-H ₂ O-C ₂ H ₄] ⁺
1-Hexanol	C ₆ H ₁₃ OH (102)	121 (1) 101 (20) 85 (71) 83 (7) 43 (1)	M.H ₃ O ⁺ [M-H ₂]H ⁺ [M-H ₂ O] ⁺ [M-H ₂ O-H ₂] ⁺ [M-H ₂ O-C ₃ H ₆] ⁺	101 (7) 85 (19) 83 (21) 57 (16) 43 (32) 41 (5)	[M-H ₂]H ⁺ [M-H ₂ O] ⁺ [M-H ₂ O-H ₂] ⁺ [M-H ₂ O-C ₃ H ₆] ⁺ [M-H ₂ O-C ₃ H ₆] ⁺ [M-H ₂ O-C ₃ H ₆ -H ₂] ⁺	101 (2) 85 (1) 83 (12) 57 (10) 55 (12) 43 (12) 41 (35) 39 (16)	[M-H ₂]H ⁺ [M-H ₂ O] ⁺ [M-H ₂ O-H ₂] ⁺ [M-H ₂ O-C ₃ H ₆] ⁺ [M-H ₂ O-C ₃ H ₆ -H ₂] ⁺ [M-H ₂ O-C ₃ H ₆ -H ₂] ⁺ [M-H ₂ O-C ₃ H ₆ -2H ₂] ⁺

The data has been extrapolated to zero concentration where concentration dependence was observed, the emission current of the hollow cathode has been kept constant at 5 mA.

2.4.1.1 Methanol

Methanol is a ubiquitous compound found in the atmosphere and in biological samples [10, 61, 63]. The compound is the simplest structure in the series of aliphatic, saturated alcohols and has been studied before by researches using proton transfer reaction mass spectrometry [28, 64]. To date, no other group has reported fragmentation of methanol, in agreement with the results of this study. Figure 21 shows the protonated monomer, CH_3OH_2^+ at m/z 33. At low reduced electric field the protonated monomer is seen to associate with water to produce a monohydrate cluster ion, $\text{CH}_3\text{OH}\cdot\text{H}_3\text{O}^+$ at m/z 51. The production of this ion may be attributed to either a complex of H_3O^+ and methanol by reaction with $\text{H}_3\text{O}^+\cdot\text{H}_2\text{O}$, or an association of the protonated monomer with water.

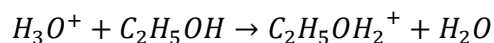
Figure 21: Product ion branching ratio for methanol as a function of reduced electric field in nitrogen.



2.4.1.2 Ethanol

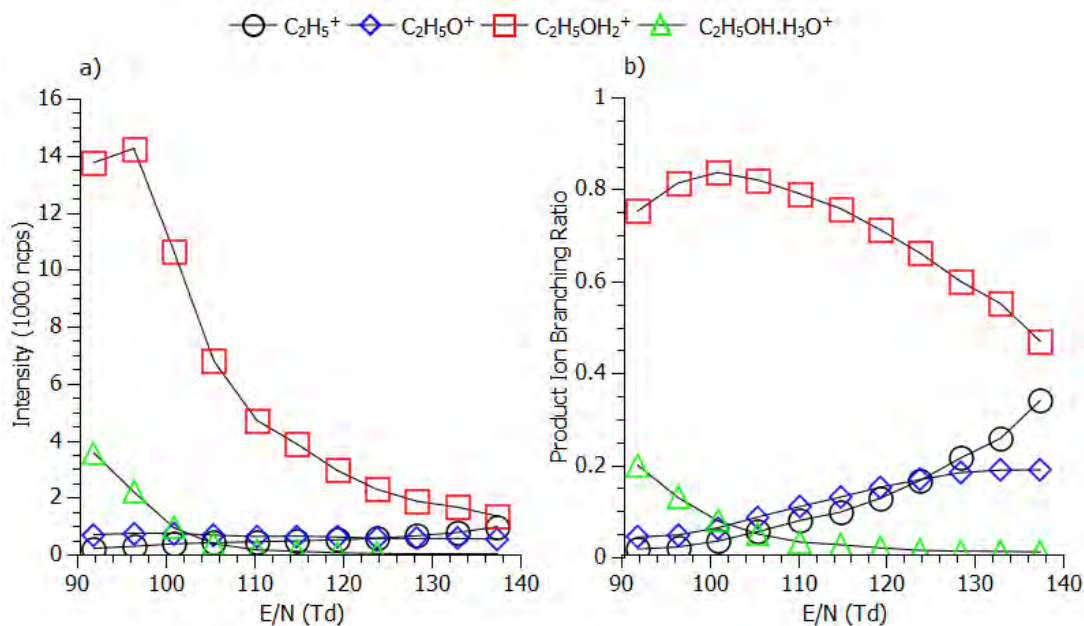
The proton transfer reaction between H_3O^+ and ethanol is shown in Equation 12. The change in enthalpy is 85.4 kJ mol^{-1} ; equal to the difference in the proton affinities of water and ethanol.

Equation 12



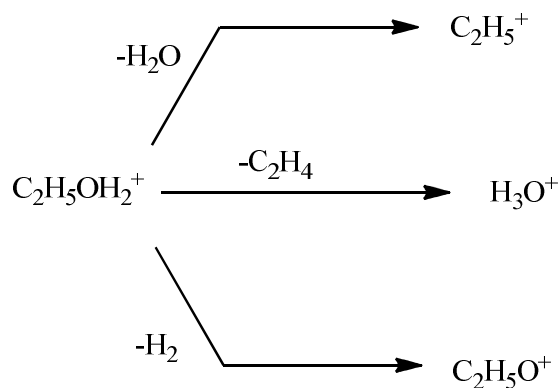
As mentioned before, the proton transfer reaction to ethanol has been described as anomalous by Blake et al. [53]. This is due to the sharply depleting signal intensity of the observed product ions at higher reduced electric field. This is shown in Figure 22, along with the product ion branching ratio. The fragmentation reaction of protonated ethanol is shown in Figure 23.

Figure 22: Figure showing a) the normalised counts per second for the four product ions from the reaction of ethanol with H_3O^+ and b) the product ion branching ratios for the same reaction.



Counts are normalised to 5 million counts per second of the sum of H_3O^+ and $\text{H}_2\text{O}\cdot\text{H}_3\text{O}^+$ signals.

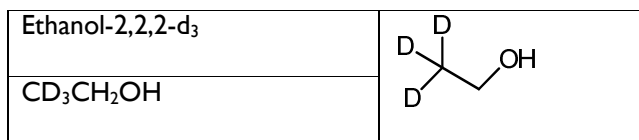
Figure 23: Fragmentation diagram for protonated ethanol, $C_2H_5OH_2^+$.



The observed loss in signal of MH^+ ion is due to the fragmentation of protonated ethanol to produce H_3O^+ and a neutral ethene molecule, C_2H_4 . H_3O^+ , as the reagent ion of the PTR-MS is not detected at m/z 19 as a product ion. This fragmentation behaviour has been observed and commented on in previous studies [55-58].

In 2009, Inomata and Tanimoto undertook a deuterium labelling study to determine the fragmentation behaviour of ethanol in a PTR-MS [59]. This study identified the H_3O^+ fragmentation pathway by measuring the product ions of ethanol, ethanol-1,1-d₂ (CH_3CD_2OH) and ethanol-2,2,2-d₃ (CD_3CH_2OH).

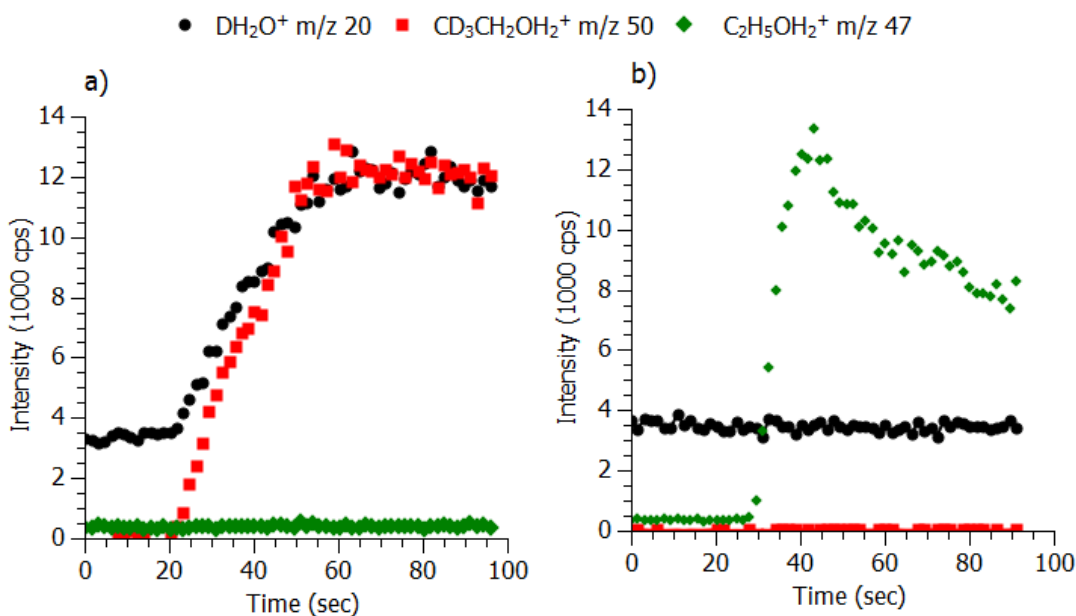
Figure 24: Chemical structure of ethanol-2,2,2-d₃.



To independently confirm the presence of a product ion at m/z 19, ethanol-2,2,2-d₃ was measured in our PTR-MS to provide a comparison with undeuterated ethanol. The chemical structure of ethanol-2,2,2-d₃ is shown in Figure 24. By studying the deuterated alcohol the product ion of H_3O^+ should be shifted to DH_2O^+ at m/z 20, allowing identification. Samples of ethanol and ethanol-2,2,2-d₃ were analysed using the same method used to record the product ions of ethanol. The same three product ions were

analysed for both samples as a function of time. The three ion signals monitored were at m/z 20, 50 and 47; corresponding to DH_2O^+ , $\text{CD}_3\text{CH}_2\text{OH}_2^+$ and $\text{C}_2\text{H}_5\text{OH}_2^+$ respectively. Figure 25 shows the results obtained from this experiment; showing a) the deuterated ethanol, and b) the corresponding undeuterated compound, shown for comparison.

Figure 25: Figure showing the time progression of three product ions produced after the addition of a) ethanol-2,2,2- d_3 and b) ethanol at 138 Td.

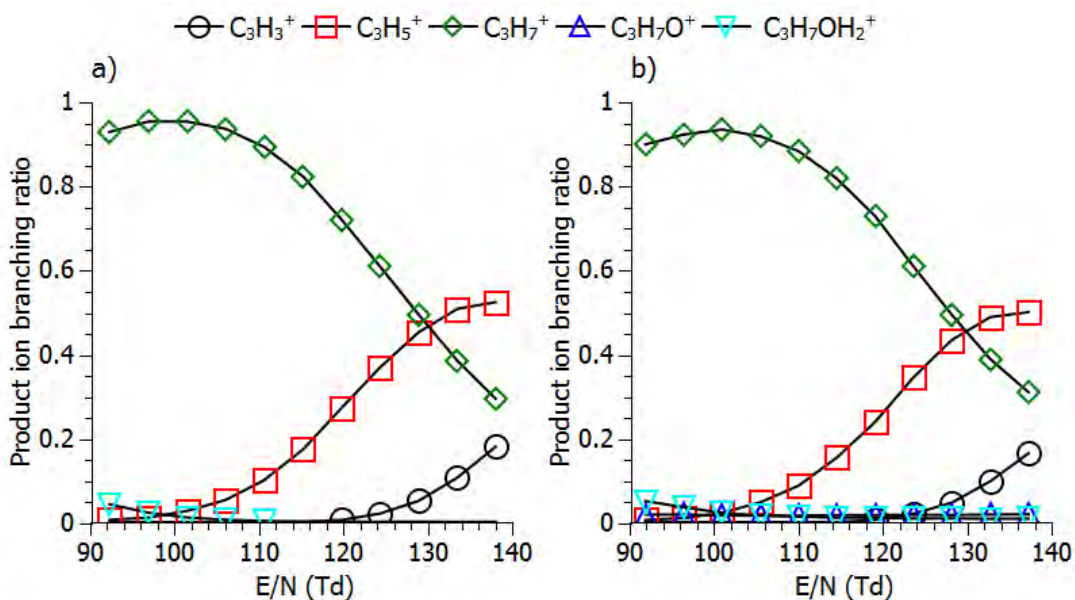


For both compounds the sample was added after approximately 20 seconds. A corresponding increase in intensity of the DH_2O^+ and $\text{CD}_3\text{CH}_2\text{OH}_2^+$ ions was observed for the ethanol-2,2,2- d_3 compound. This is analogous to the H_3O^+ and $\text{C}_2\text{H}_5\text{OH}_2^+$ product ions related to ethanol, where these results are also shown in Figure 25. The observation of the DH_2O^+ product ion confirms that a H_3O^+ product ion is formed from protonated ethanol.

2.4.1.3 1-Propanol and 2-propanol

Both 1-propanol and 2-propanol exhibit similar behaviour to each other. Their product ion branching ratios are shown in Figure 26. At low reduced electric a protonated monomer, $C_3H_7OH_2^+$ signal is detected with branching ratio of less than 5 % for both. For 2-propanol, a product ion, $C_3H_7O^+$ at m/z 59 is detected, attributed to the loss of neutral H_2 . This product ion was not observed for 1-propanol at standard, 5 mA emission current operating conditions of the hollow cathode.

Figure 26: Figure showing the product ion branching ratios of a) 1-propanol and b) 2-propanol.



The dominant reaction for both propyl alcohols is the loss of neutral H_2O from the protonated monomer resulting in formation of the m/z 43 carbocation, $C_3H_7^+$. The loss of water occurs as a result of dissociative proton transfer. Both propyl alcohols exhibit sequential loss of hydrogen molecules from the $C_3H_7^+$ product ion to form $C_3H_5^+$ and $C_3H_3^+$ product ions at m/z 41 and 39 respectively. This is shown in Figure 27. The identical nature of the fragmentation of both $C_3H_7^+$ carbocations indicates that the

product ion is identical for each propyl alcohol. This implies that the $C_3H_7^+$ carbocation of 1-propanol is quickly isomerising to the more stable secondary propyl carbocation.

Figure 27: Fragmentation reaction of $C_3H_7^+$ product ion for 1-propanol and 2-propanol.



Buhr et al. [52] observed two product ions for 1-propanol and 2-propanol at m/z 43 and 41, with branching ratios of 73 % and 27 %, respectively for both isomers; no product ion was reported at m/z 39. The data was reported at a single value of reduced electric field, corresponding to an applied electric field of 600 V. These results would appear to agree with those of this study, providing the measurements of Buhr et al. were carried out at a reduced electric field of approximately 120 Td.

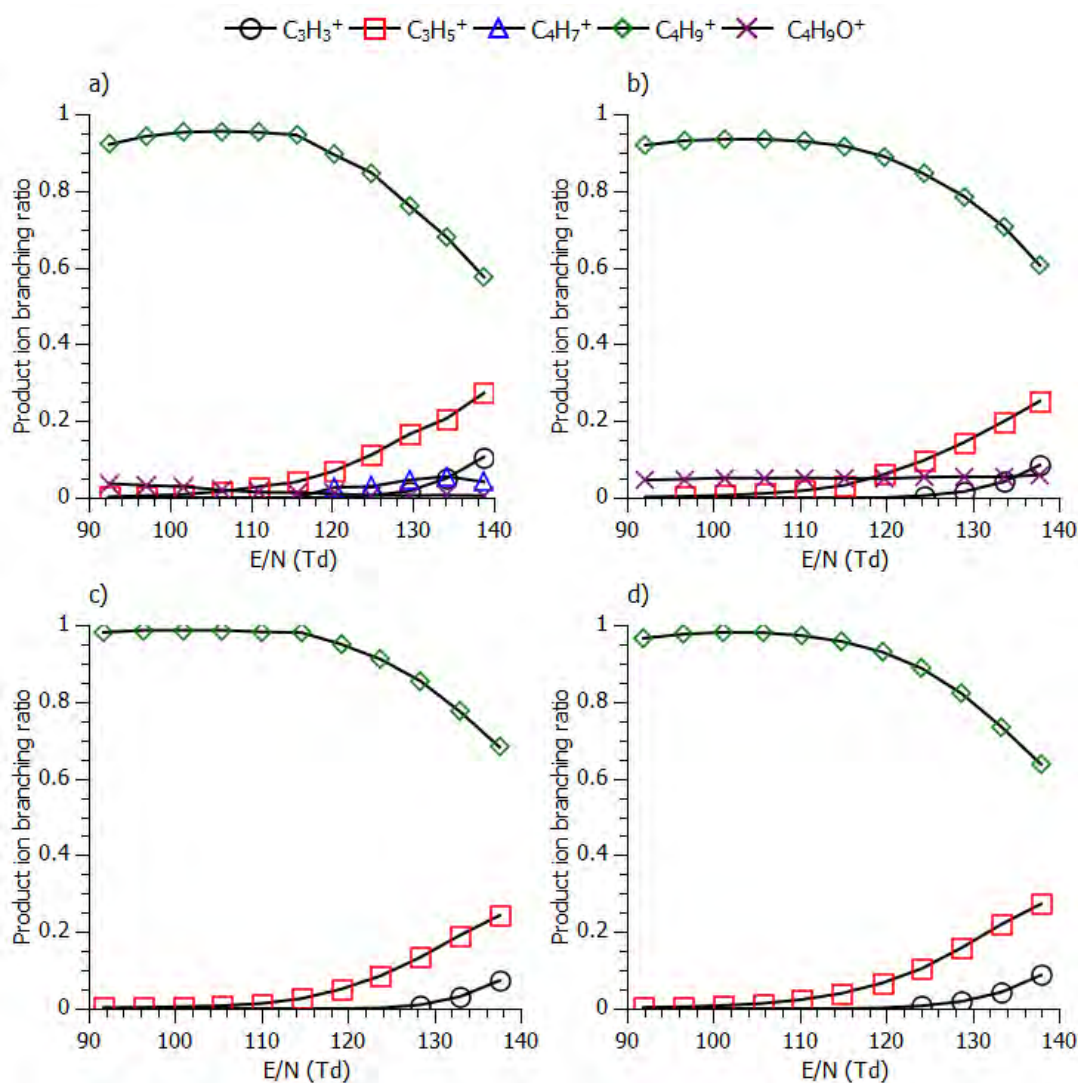
A study by Lindinger et al.[1] shows good agreement with the fragmentation profile of 1-propanol obtained in Figure 26. The m/z 39, 41 and 43 product ions are all present with similar branching ratios. Lindinger et al. also observed a product ion at m/z 27 which this study did not observe.

Wang et al. [65] observed 1-propanol and 2-propanol in a SIFT apparatus reacting with H_3O^+ at 300 K and 0.7 Torr. They observed the same three product ions for both propyl alcohols; namely $C_3H_7^+$, $C_3H_8O.H^+$ and $C_3H_8O.H_3O^+$. The most abundant species was $C_3H_7^+$ (75 % for 1-propanol, 60 % for 2-propanol). The observed dominance of this product ion indicates that the dehydration fragmentation of both propyl alcohols in the PTR-MS occurs via dissociative proton transfer reactions.

2.4.1.4 The butyl alcohols

The four isomeric butyl alcohols were examined with the PTR-MS; 1-butanol, 2-methyl-1-propanol, 1,1-dimethylethanol and 2-butanol. The dominant product ion produced by reacting each butyl alcohol with H_3O^+ was found to be the butyl carbocation C_4H_9^+ at m/z 57. The data for each reaction are shown in Figure 28.

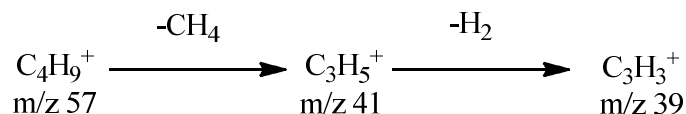
Figure 28: Figure showing the product ion branching ratios of a) 1-butanol, b) 2-methyl-1-propanol, c) 1,1-dimethylethanol and d) 2-butanol.



The production of the C_4H_9^+ ion proceeds via loss of H_2O from the protonated monomer, MH^+ . Similar to the propyl alcohols the carbocation further fragments in an identical manner for each butyl alcohol, suggesting rapid rearrangement from primary or

secondary carbocations to the tertiary isomer of $C_4H_9^+$ is occurring. The fragmentation of $C_4H_9^+$ occurs via an initial loss of methane (CH_4) followed by a loss of molecular hydrogen, and is outlined in Figure 29.

Figure 29: Fragmentation of the butyl carbocation.



The only signal of protonated monomer, MH^+ detected, was at the lowest reduced electric field of 91 Td and at very low signal intensity (1%). This indicates that the initial loss of H_2O is caused by dissociative proton transfer. This belief is supported by SIFT data collected by Spanel et al. [66], where they observed $C_4H_9^+$ as the most abundant product ion from the reaction between H_3O^+ and each of the four butyl alcohol isomers.

Both primary butyl isomers, 1-butanol and 2-methyl-1-propanol exhibit a product ion, $C_4H_9O^+$ at m/z 73 attributed to loss of neutral H_2 from the protonated monomer. For the case of 1-butanol, this product ion is seen to further fragment to form $C_4H_7^+$ by loss of water. The presence of a $C_4H_7^+$ product ion could be attributed to loss of H_2 from $C_4H_9^+$, but as this product ion is not observed for any of the other butyl alcohols it may be assumed that no loss of H_2 from $C_4H_9^+$ is occurring in this case. $C_4H_9O^+$ fragments only in the analysis of 1-butanol which indicates that this product ion has a different structure between the cases of 1-butanol and 2-methyl-1-propanol.

Buhr et al. [52] measured the branching ratios of each butyl alcohol, except 2-methyl-1-propanol. When compared to the results presented in this study their data are in agreement, providing they are assumed to have been measured at 120 Td. Buhr et al. observed product ions at m/z 57, m/z 41 and m/z 58, because of its relative intensity to

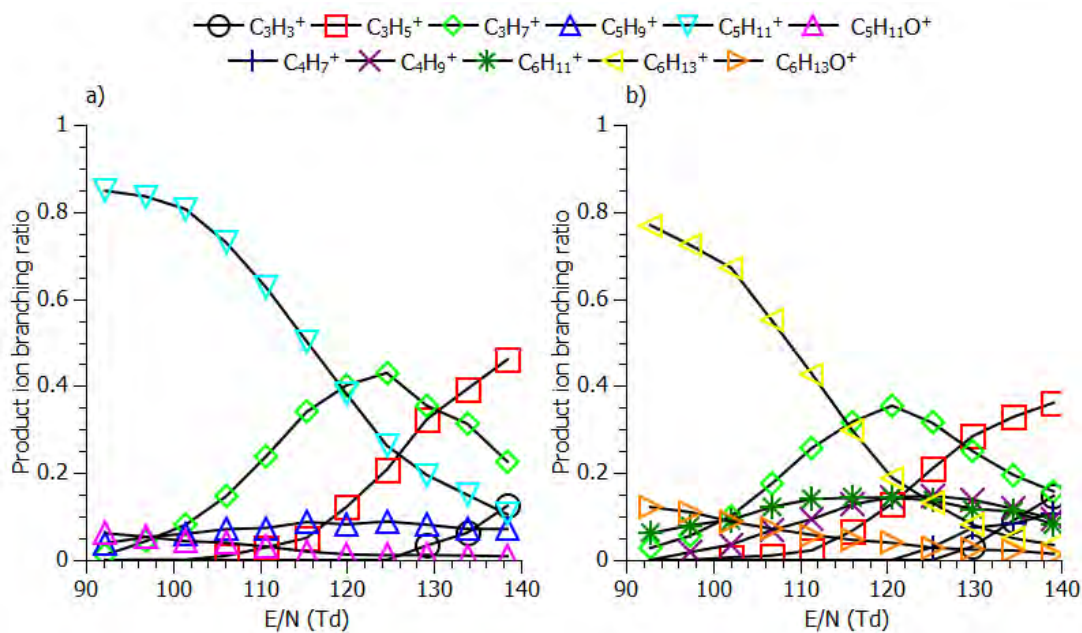
the m/z 57 ion the m/z 58 ion may be assumed to be the ^{13}C isomer for each butyl alcohol.

The proton transfer reaction involving 1,1-dimethylethanol and H_3O^+ has been studied in detail in both an ion mobility spectrometer, IMS [67] and a Fourier transform mass spectrometer FTMS [68] by Bell et al. Both studies observed fragmentation only to the C_4H_9^+ product ion. This indicates that the operating conditions of the PTR-MS may allow for higher energy fragmentations than the conditions of either an IMS or a FTMS.

2.4.1.5 1-Pentanol and 1-Hexanol

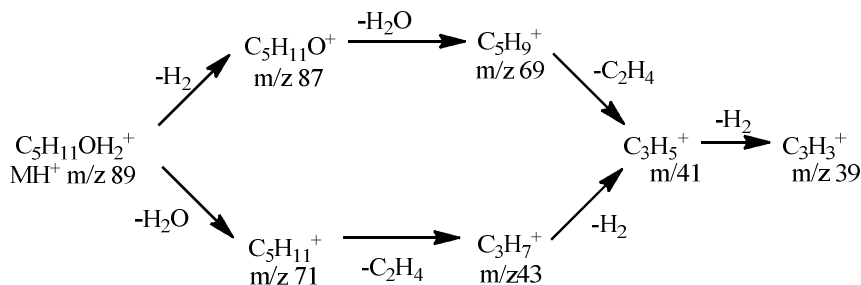
At first glance, the reaction of H_3O^+ with both 1-pentanol and 1-hexanol seems too complex to analyse sensibly. However, by building on the fragmentation reactions seen earlier with the butyl and propyl alcohols, the analysis may be simplified. The product ion branching ratios for 1-pentanol and 1-hexanol are shown in Figure 30.

Figure 30: Plots of the product ion branching ratio of a) 1-pentanol and b) 1-hexanol.



The reaction involving 1-pentanol will be discussed first; a reaction scheme is outlined in Figure 31. The initial loss of water from the protonated monomer which was observed with the propyl and butyl alcohols is also observed. In this case, the loss of water forms a $C_5H_{11}^+$ product ion at m/z 71. The subsequent fragmentation of the m/z 43 product ion, $C_3H_7^+$ proceeds via a sequential loss of molecular hydrogen as seen with the fragmentation of the propyl alcohols. This indicates that the $C_3H_7^+$ ions have a common structure for 1-pentanol and both propyl alcohols, namely an isopropyl structure.

Figure 31: Proposed fragmentation pattern of protonated 1-propanol in a PTR-MS.



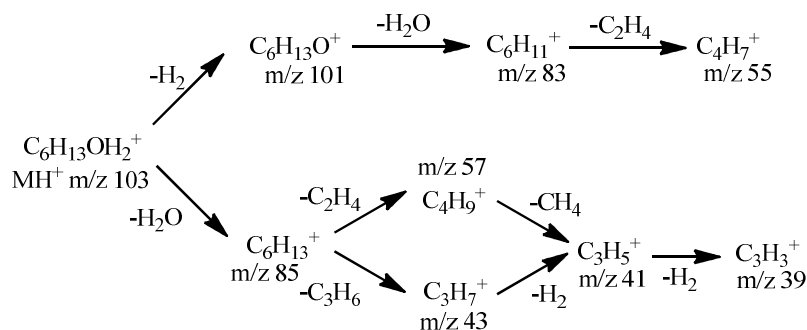
The isopropyl carbocation, $C_3H_7^+$ is produced via initial loss of water from the protonated monomer, $C_5H_{11}OH_2^+$ followed by subsequent loss of C_2H_4 . The loss of ethene, C_2H_4 as a neutral fragment is also observed for the protonated monomer of ethanol.

A second fragmentation pathway is observed from $C_5H_{11}OH_2^+$ involving an initial loss of H_2 , as seen with many of the other saturated alcohols, to form $C_5H_{11}O^+$. This reaction pathway proceeds to lose water, forming an m/z 69 product ion, $C_5H_9^+$, followed by loss of C_2H_4 to form the $C_3H_5^+$ product ion at m/z 41.

Buhr et al. [52] have also studied the fragmentation of 1-pentanol and their published results do not resemble those displayed in this investigation.

For 1-hexanol, a reaction scheme is outlined in Figure 32. The initial fragmentation of water to form the product ion, $C_6H_{13}^+$ at m/z 85 is in keeping with the fragmentation schemes of the butyl and propyl alcohols as described earlier. From the reaction scheme it can be seen that common ions; $C_4H_9^+$, $C_3H_5^+$ and $C_3H_3^+$ are produced for the fragmentation of 1-hexanol and the butyl alcohols.

Figure 32: Proposed fragmentation pattern of protonated 1-hexanol in a PTR-MS.



The tertiary butyl carbocation, $C_4H_9^+$ is formed by loss of C_2H_4 from the $C_6H_{13}^+$ product ion. A $C_3H_7^+$ isopropyl carbocation is also observed as a fragment from the $C_6H_{13}^+$ product ion, via loss of propene, C_3H_6 . The neutral alkene, C_3H_6 was not observed for any other alcohols in the study, but is suggested as a sensible neutral fragment, based on the appearance, in other fragmentation reactions of the similar ethene molecule, C_2H_4 .

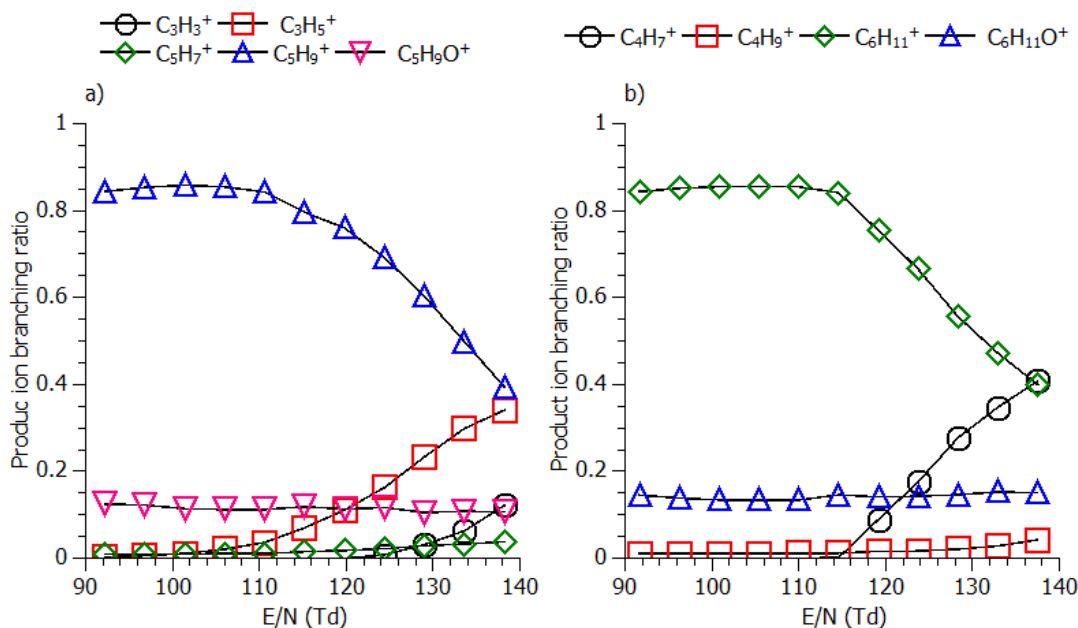
Initial loss of molecular hydrogen is also observed from the protonated monomer, resulting in a $C_6H_{13}O^+$ product ion at m/z 101. This ion then fragments further by loss of water followed by loss of C_2H_4 , eventually resulting in a $C_4H_7^+$ product ion. This product ion shows no evidence of further fragmentation; this is similar to the $C_4H_7^+$ fragment ion observed with 1-butanol.

The product ions and their branching ratios appear to be in good agreement with those observed by Buhr et al. [52], assuming their experiment has been carried out at approximately 120 Td.

2.4.1.5 Cyclopentanol and Cyclohexanol

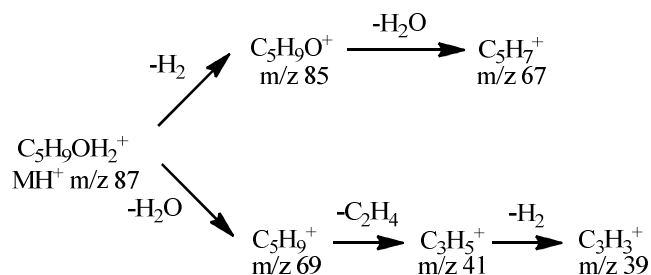
The fragmentation of cyclohexanol and cyclopentanol follow a similar pattern to the fragmentation of the acyclic alcohols in the study, despite their different structures. The product ion branching ratios for cyclopentanol and cyclohexanol are shown in Figure 33.

Figure 33: Product ion branching ratios of a) cyclopentanol and b) cyclohexanol.



The protonated monomers of cyclopentanol and cyclohexanol are $C_5H_9OH_2^+$ and $C_6H_{11}OH_2^+$, respectively. For both cyclohexanol and cyclopentanol, no protonated monomer is observed; this is similar to the previous, higher carbon number acyclic alcohols. The proposed fragmentation mechanism for cyclopentanol is described in Figure 34.

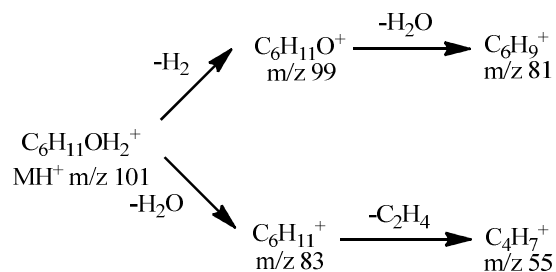
Figure 34: Proposed fragmentation scheme of cyclopentanol.



The dissociative proton transfer reaction via the loss of H₂O from the protonated monomer is observed for many of the other alcohols, an initial fragment ion corresponding to loss of H₂ is also observed. In cyclopentanol, these initial fragmentations produce C₅H₉⁺ at *m/z* 69 and C₅H₉O⁺ at *m/z* 85, respectively. The C₅H₉⁺ product ion further fragments by loss of C₂H₄ to form C₃H₅⁺ at *m/z* 41, followed by loss of H₂ to form C₃H₃⁺ at *m/z* 39. Once again, the investigations show the presence of common carbocation product ions.

A fragmentation scheme for cyclohexanol is proposed in Figure 35. No protonated monomer is observed for any value of reduced electric field. The product ion C₆H₁₁⁺ at *m/z* 83 is formed by facile loss of water from the protonated monomer. The production of the *m/z* 55 C₄H₇⁺ product ion is attributed to a loss of C₂H₄ from the C₆H₁₁⁺ product ion.

Figure 35: Proposed fragmentation scheme for cyclohexanol.



From the study of cyclohexanol, the initial loss of molecular hydrogen from the protonated monomer, $C_6H_{11}OH_2^+$ was further analysed by studying the complimentary reaction of cyclohexanone with H_3O^+ . The results are reported in Section 2.4.1.6.

2.4.1.6 Cyclopentanone and cyclohexanone

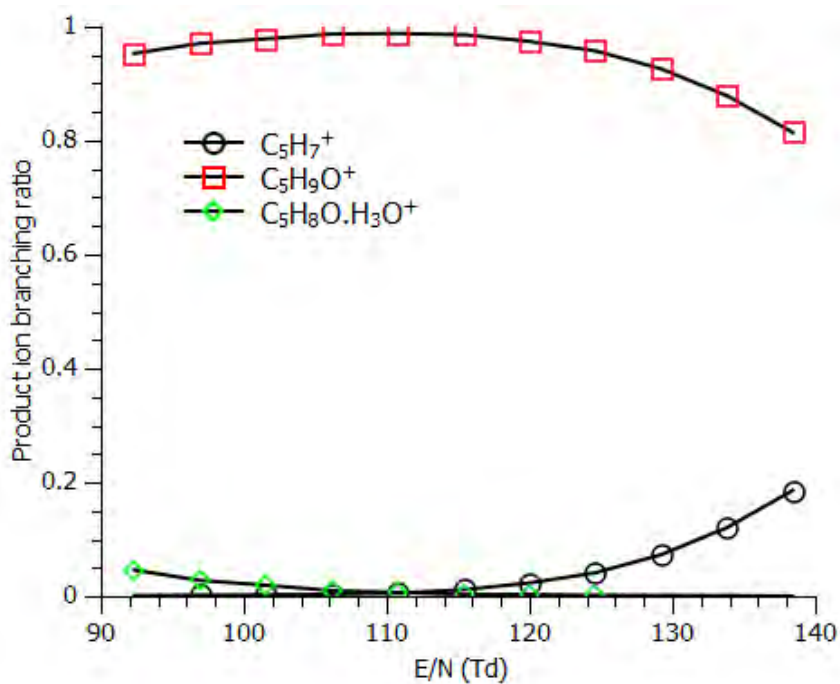
A comparative study of cyclopentanone and cyclohexanone with the corresponding alcohols, cyclopentanol and cyclohexanol was made. The study aimed to identify structural information about the product ions resulting from the formal loss of H_2 from the protonated monomers of cyclopentanol and cyclohexanol ($C_5H_9O^+$ and $C_6H_{11}O^+$ product ions, respectively) by examining at cyclopentanone and cyclohexanone. The relevant chemical information for cyclopentanone and cyclohexanone is shown in Table 7.

Table 7: Information for cyclopentanone and cyclohexanone.

Name	Formula	Proton Affinity (kJmol ⁻¹)[26]
Cyclopentanone	C_5H_8O	823.7
Cyclohexanone	$C_6H_{10}O$	841.0

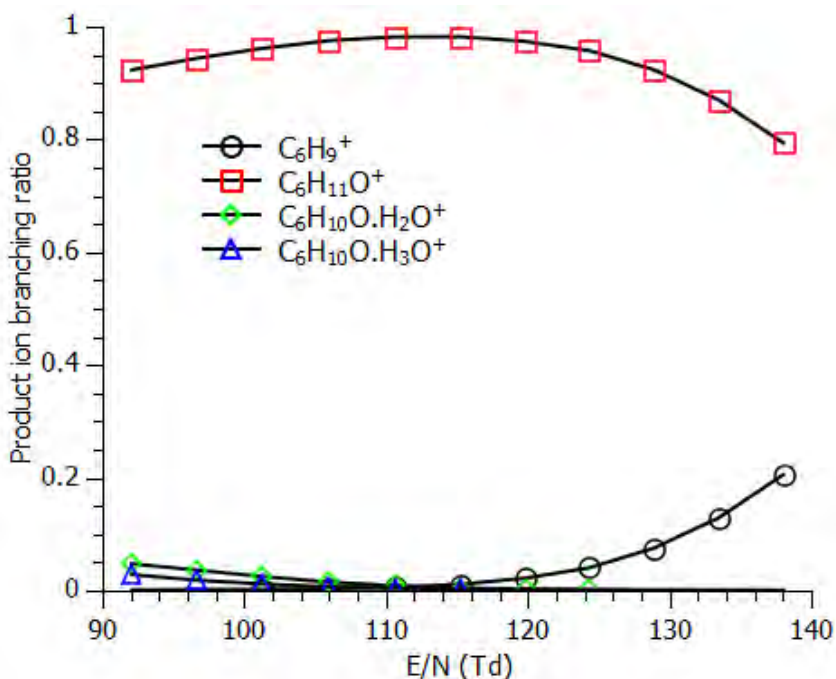
Similar fragmentation was observed from the $C_5H_9O^+$ product ions of cyclopentanone and cyclopentanol, indicating a common $C_5H_9O^+$ product ion. The cyclic structure of the molecules may be maintained in the $C_5H_9O^+$ product ion and later fragments to a non-cyclic product ion, $C_5H_7^+$. Cyclopentanone was studied using the same experimental set-up as used for the saturated alcohols, detailed in Section 2.3.2. The observed product ion branching ratios are shown in Figure 36.

Figure 36: Product ion branching ratio for cyclopentanone.



The study of cyclohexanone revealed common fragmentation of the $C_6H_{11}O^+$ product ion compared to cyclohexanol. The experiment performed was identical to that of the saturated alcohols, where the branching ratios for the ketone are shown in Figure 37. The observed loss of water from the protonated monomer of cyclohexanone, $C_6H_{11}O^+$ is similar to the observed loss of water from the $C_6H_{11}O^+$ product ion of cyclohexanol. This indicates that the two product ions have the same structure and are analogous to the $C_5H_9O^+$ product ions of cyclopentanol and cyclopentanone.

Figure 37: Product ion branching ratio of cyclohexanone.



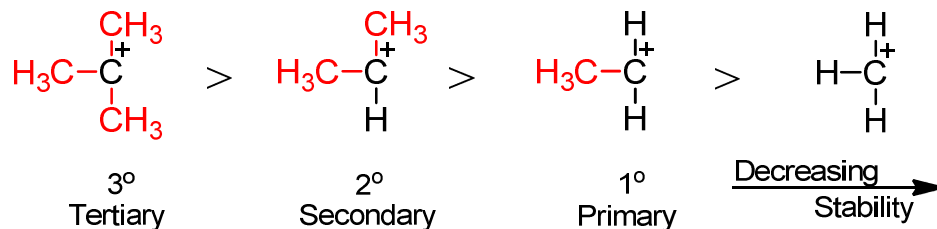
2.4.1.7 Discussion of fragmentation

At the higher reduced electric fields, many common product ions were observed between the alcohols studied. $C_3H_5^+$ and $C_3H_3^+$ product ions were commonly found for each acyclic alcohol between the propyl to hexyl carbon number. The $C_3H_5^+$ ion was found to fragment to $C_3H_3^+$ in a similar ratio for each compound, suggesting the structure of the $C_3H_5^+$ ion is common for each alcohol. Further to these two product ions, 1-pentanol, 1-hexanol and each propyl alcohol produce $C_3H_7^+$ product ions, which again are thought to have a common structure. Similarly, 1-hexanol and each butyl alcohol produced fragment ions at $C_4H_9^+$, which are again deemed to have the same structures because of their identical fragmentation via the loss of a neutral CH_4 molecule.

The fact that these common, stable product ions are observed in the fragmentation patterns through the alcohol series is not unexpected. After the initial loss of H_2O from the protonated monomer, an alkyl carbocation is formed. Alkyl carbocations will form

their most stable configurations where the greatest clustering of methyl (alkyl) groups can occur [69-71]. The effect is illustrated in Figure 38.

Figure 38: Relative stability of tertiary, secondary, primary and methyl carbocations.



The stabilisation effect of clustering methyl groups also explains why no fragmentation is observed from methanol where the formation of a methyl carbocation would require comparatively more energy, compared to a higher carbon alkyl carbocation.

Where fragmentation has been observed, it has initially involved the facile loss of water from the protonated alcohol ion. Many other common neutral molecules are also lost in fragmentation, such as: H₂, CH₄ and C₂H₄. Each of these is lost from more than one alcohol, not including isomers.

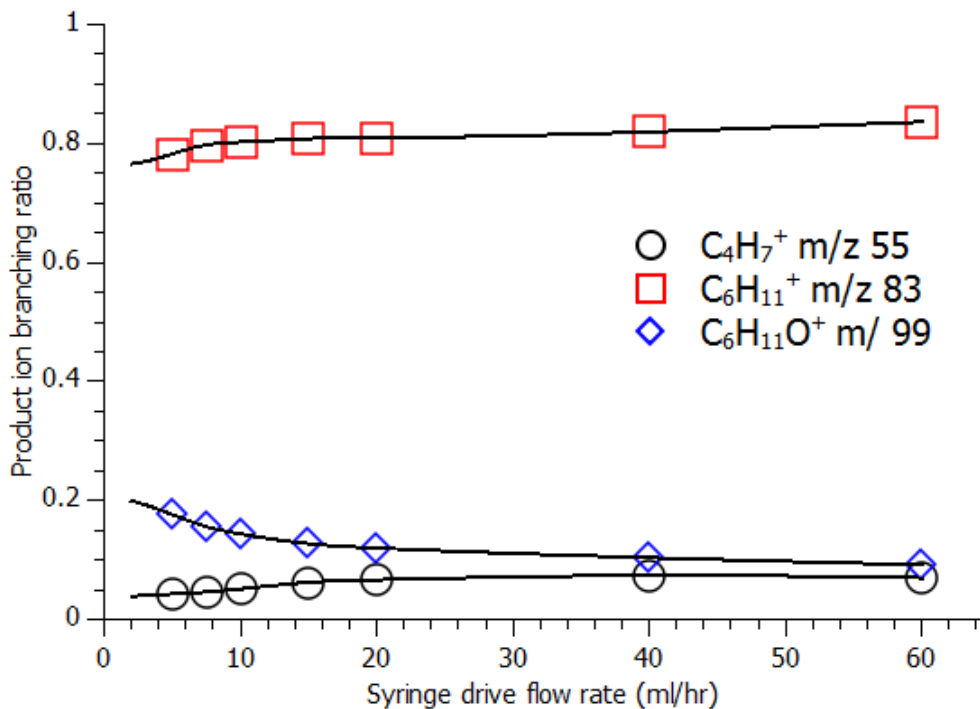
The fragmentation via initial loss of H₂ from the protonated monomer, MH⁺ has not been observed previously with other PTR-MS instruments. The loss is observed with the primary butyl alcohol structures, (1-butanol, 2-methyl-1-propanol) but not the secondary or tertiary butyl structures (2-butanol, 1,1-dimethylethanol). In contrast, the loss is not observed for the primary alcohol structure of propanol, but is observed for the secondary propyl structure.

For each alcohol exhibiting initial loss of H₂ from its protonated monomer, the corresponding product ion produced was seen to have a concentration dependence. The product ion increased in relative abundance compared to the total product ion signal, while the concentration of alcohol was decreased. Furthermore, only alcohols

showing initial loss of H₂ exhibited a concentration dependence effect in this study.

Figure 39 shows an example of this for cyclohexanol.

Figure 39: Concentration dependence of the product ions of cyclohexanol at 115 Td.



The concentration was varied in Figure 39 by changing the injection rate of the syringe, while keeping the flow rate of the nitrogen carrier gas constant. The injection rate is shown on the x-axis of Figure 39. Figure 35 shows the fragmentation mechanism for cyclohexanol. The ion at *m/z* 99, C₆H₁₁O⁺ corresponds to the initial loss of H₂ from the protonated parent. Figure 39 shows C₆H₁₁O⁺ increasing as a fraction of the total product ions at the lower analyte concentration.

2.4.2 Hollow cathode emission current dependence of saturated alcohols

The initial fragmentation of H₂ from the protonated alcohol was found to be independent of reduced electric field but was considered to be dependent on the analyte concentration. To further understand this fragmentation pathway a further operating

parameter of the PTR-MS was investigated which could add to the explanation of this fragmentation mechanism. To this end, the branching ratios of cyclohexanol and 1- and 2-propanol were analysed by varying the hollow cathode emission current. The results are presented in this section.

2.4.2.1 Cyclohexanol

Cyclohexanol vapour in nitrogen was introduced to the PTR-MS in an identical manner to that which was used for the reduced electric field study described in Section 2.3.2. The hollow cathode emission current may be varied between 2 and 10 mA, while maintaining a good reagent ion signal. Within this range, the emission current was varied in steps of 0.5 mA and the branching ratios for cyclohexanol recorded at reduced electric fields of 91 and 138 Td, the results are shown in Figure 40.

Increased evidence of fragmentation was observed for higher hollow cathode emission currents. The $C_6H_{11}O^+$ product ion is thought to correspond to the initial loss of H_2 from the protonated monomer. This ion appears in negligible quantities at lower emission currents but becomes more significant as the current is increased. As comparison, the typical operating emission current is 5 mA.

Figure 40: Cyclohexanol product ions as a function of hollow cathode emission current at a) 138 Td and b) 91 Td.

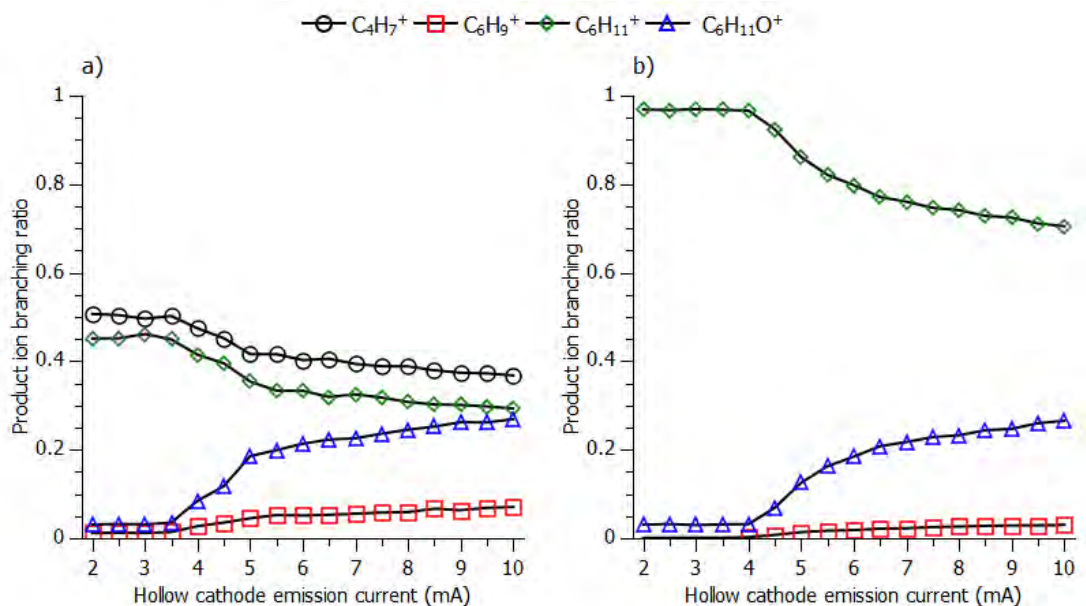
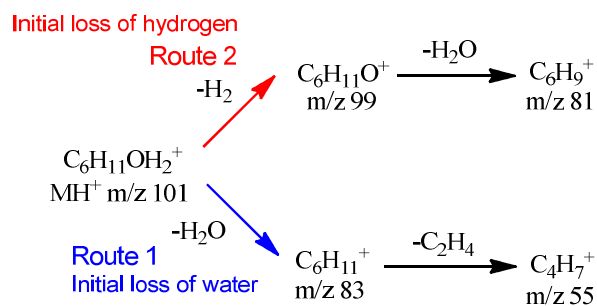


Figure 41: Proposed fragmentation mechanism of cyclohexanol, highlighting the initial losses of hydrogen and water.



Both the product ions, C_4H_7^+ and $\text{C}_6\text{H}_{11}^+$ resulting from the route 1 fragmentation mechanism shown in Figure 41, decrease their branching ratios as the hollow cathode emission current increased. Both $\text{C}_6\text{H}_{11}\text{O}^+$ and C_6H_9^+ , the product ions resulting from the route 2 fragmentation mechanism, increase their branching ratios as the emission current in increased. These relationships indicate that the hollow cathode operating conditions may be significantly involved in the production of product ions via the loss of H_2 from the protonated monomer.

The observed hollow cathode dependence of the branching ratios has not been studied by other research groups to date. The data complements the results taken with isoprene in Section 1.3.5, where an increase in product ion fragmentation was observed with increasing emission current.

2.4.2.2 1-Propanol and 2-propanol

Section 2.4.1.3 shows the reduced electric field dependence of 1-propanol and 2-propanol. For 2-Propanol a $C_3H_7O^+$ product is produced at m/z 59, corresponding to the loss of H_2 from the protonated monomer. However, no such product ion was observed for 1-propanol. To investigate this isomeric effect the behaviour of 1-Propanol and 2-propanol were analysed as a function of hollow cathode emission current.

Figure 43 shows the branching ratios for 1-propanol and 2-propanol as a function of emission current at a reduced electric field of 138 Td. The recorded branching ratios are different for each propyl alcohol, suggesting that the alcohols are stabilised in their separate isomeric forms after ionisation. At some stage later their molecular ion structures become identical as both propyl alcohols exhibit common evidence for the fragmentation of an identical $C_3H_7^+$ product ion.

Figure 42: Fragmentation mechanism for propanol, highlighting the initial losses of hydrogen and water.

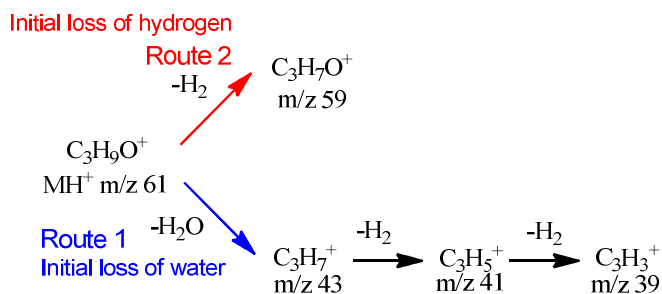
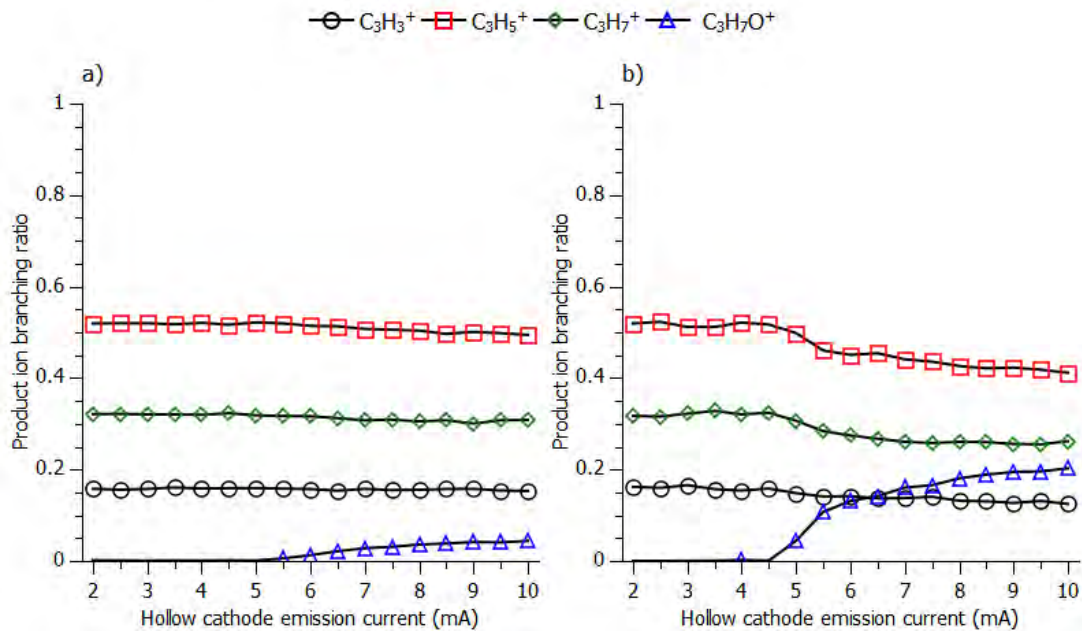


Figure 43: The effect of the hollow cathode emission current on the product ion branching ratios of a) 1-propanol and b) 2-propanol at 138 Td.



The fragmentation mechanism for both propyl alcohols is illustrated in Figure 42. The $C_3H_3^+$, $C_3H_5^+$ and $C_3H_7^+$ product ions all result from the route 1 fragmentation pathway via initial loss of water. Each of these ions decreases its branching ratio as the emission current is increased, and the $C_3H_7O^+$ ion increases its branching ratio.

2.4.2.3 Comment on hollow cathode induced fragmentation

The appearance of the product ion formed by the initial loss of H_2 was shown to be mildly dependent on the concentration and the emission current. It is suggested that two effects may occur when changing the emission current that may affect the observed branching ratios, particularly the route 2, initial loss of H_2 fragmentation pathway. Either, H_3O^+ ions may be produced with increased internal energy or the plasma of the ion source may extend beyond the ion source region and interact with analyte in the drift tube. The observed concentration dependence of the branching ratios, as illustrated in Figure 39 is not consistent with back-streaming affecting the observed branching ratios and causing the initial loss of H_2 for the alcohols in this study.

Further, more detailed study into the possible excited states of H_3O^+ , or plasma modelling is required to understand and characterise the observed effects involving the initial loss of H_2 and the effect that the hollow cathode conditions have on the observed branching ratios.

2.5 Conclusions and Further Work

By studying these saturated, aliphatic alcohols, a further useful addition has been made to the characterisation of proton transfer reaction mass spectrometry. The results have revealed the common nature of the carbocation product ions that can complicate mass spectra. Stability and rearrangement properties of the product ions have been shown to occur for a majority of the alcohols studied.

A summary illustration of the fragmentation mechanisms for each alcohol included in this study is shown in Figure 44. No appreciable differences were observed between either the propyl alcohol or butyl alcohol isomers studied, except in their responses to the initial loss of H_2 . The secondary propyl alcohol (2-propanol) showed initial loss of H_2 from its protonated monomer at a standard emission current of 5 mA. 1-Propanol showed no such evidence. Neither the secondary (2-butanol) nor the tertiary (1,1-dimethylethanol) butyl alcohol fragmented via an initial loss of H_2 , but for both primary butyl alcohols (1-butanol, 2-methyl-1-propanol) such a fragmentation was observed.

In a 1999 review, Uggerud et al. highlighted the importance of '1, 2 hydrogen eliminations' from cations [72]. In such cases a hydrogen molecule is lost from between adjacent atoms, with each adjacent atom contributing a single hydrogen atom to the molecular hydrogen.

Assuming one hydrogen atom originates from the oxygen, this 1, 2 loss mechanism would be unfavoured for 1,1 dimethyl-ethanol due to the lack of a hydrogenated atom

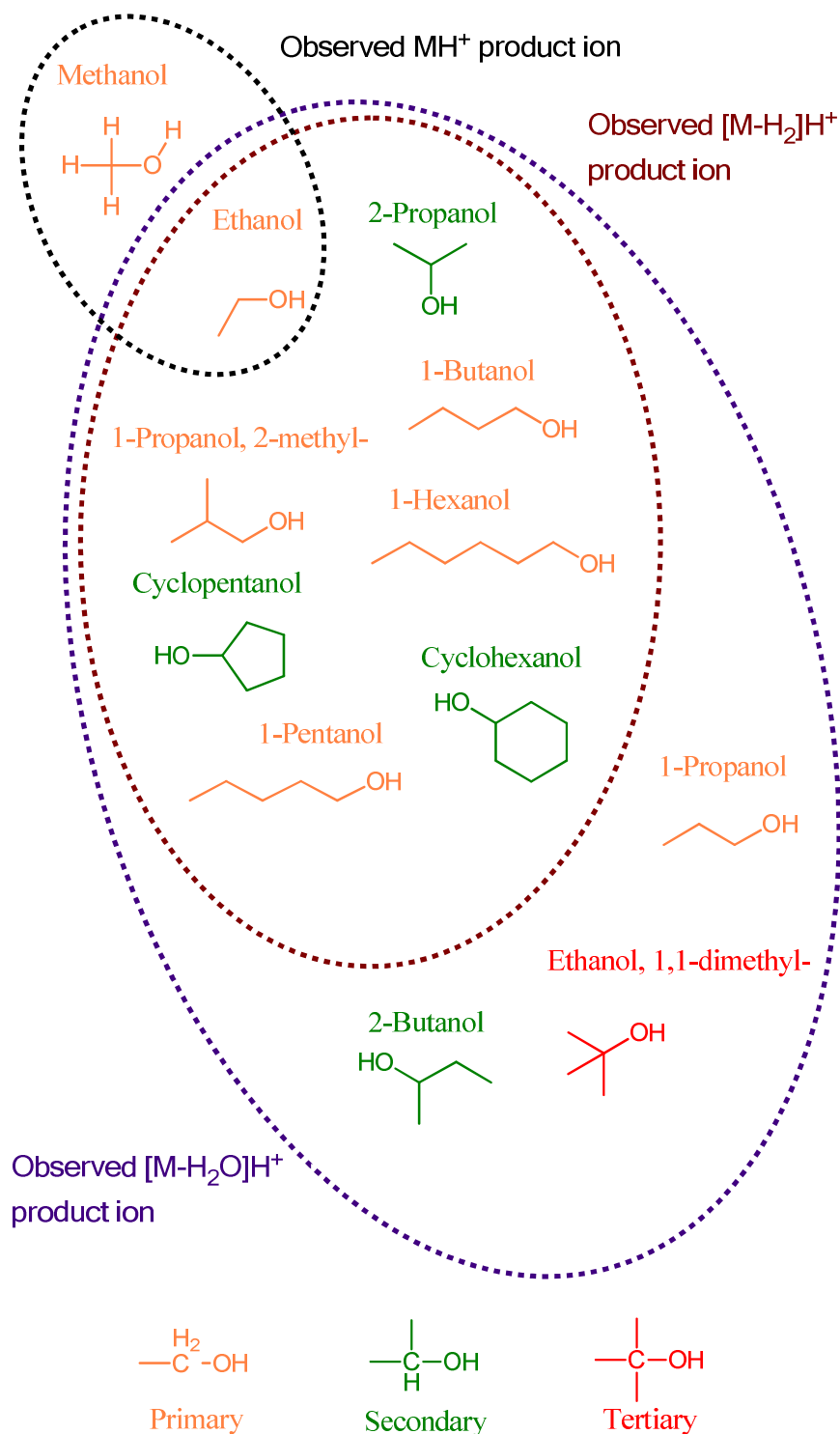
adjacent to the oxygen. This may explain why no loss of H₂ is exhibited from the tertiary butyl alcohol. An extension of the idea may also be possible to the 2-butanol isomer where the single hydrogen atom on the carbon adjacent to the oxygen may be unavailable to form molecular hydrogen.

This basis of thought does not provide a full understanding of the isomeric dependence of the H₂ loss; it particularly does not explain the isomeric dependence of the propyl alcohols. However, it may provide a basis for an investigation of the isomeric dependence and may be tested against further work to examine the hollow cathode dependence of each butyl alcohol.

Methanol showed no fragmentation with any applied reduced electric field, whereas ethanol was the only other alcohol to show an identifiable intensity of protonated monomer. The collation of previous research, [55, 73] particularly that of Inomata and Tanimoto, [59] helped understand the behaviour of ethanol in a PTR-MS, previously described as anomalous [2]. The observed loss of signal intensity was explained by fragmentation, leading to formation of a H₃O⁺ product ion.

The propyl alcohols, 1-pentanol and 1-hexanol were found to show the production of a common C₃H₇⁺ carbocation fragment ion at *m/z* 43. Whereas the butyl alcohols and 1-hexanol fragmented to produce a common C₄H₉⁺ product ion at *m/z* 57. Many other common fragment ions were observed, particularly at higher reduced electric fields and found notably at *m/z* 39 and 41 where the carbocations: C₃H₃⁺ and C₃H₅⁺ were identified. The fact that these common fragment ions were found to exist provides further evidence of the need for careful chemical study, as has been carried out in this chapter.

Figure 44: Summary diagram of the initial fragmentations of each of the protonated monomers, MH^+ .



The diagram groups the fragmentation of each alcohol depending on how its protonated monomer was seen to fragment; either observed MH^+ , observed $[M-H_2]H^+$ or observed $[M-H_2O]H^+$. The structural nature of each alcohol is colour coded for.

The demonstration of the hollow cathode dependence on branching ratios has enlightened a hitherto unmentioned effect on product ion formation in a PTR-MS. The origin of this effect has been examined to reveal and explain possible theories, namely the extension of the plasma from the ion source, or the production of H_3O^+ reagent ions in an internally excited state. A more detailed knowledge of theoretical plasma conditions and accurate modelling of the conditions in the ion source may allow a more definitive understanding to be found.

This chapter has shown that as an analytical instrument, the PTR-MS can be used to detect and differentiate between many of these aliphatic alcohol compounds by their product ions' behaviour at different reduced electric field settings.

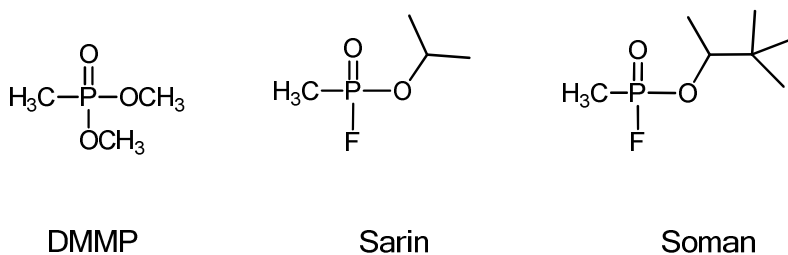
3 Proton Transfer Reaction Mass Spectrometry of Organophosphates Related to Chemical Warfare Agents and Pesticides

3.1 Introduction

The use of mass spectrometry techniques for chemical warfare detection has been a long standing area of scientific exploration. Many mass spectrometric techniques have been employed to analyse organophosphates as surrogates for chemical weapons [20, 21, 74-79]. Organophosphates act to inhibit acetyl cholinesterase in mammals and insects. The toxicity of organophosphates varies; the less toxic compounds can be used as pesticides, while the more toxic organophosphates are used as nerve agents, e.g. sarin. Due to the acute toxicity of nerve agents, structurally similar compounds are used for analytical purposes by researchers. Dimethyl methylphosphonate (DMMP) has been used particularly extensively in mass spectrometric studies of chemical warfare agents (CWAs) and pesticides [20, 21, 74-78].

The structure of DMMP ($\text{CH}_3\text{PO}(\text{OCH}_3)_2$) is shown in Figure 45, along with the structures of sarin and soman. The similarity of the compounds' structures allows DMMP to be used, for certain detectors, as a detection surrogate for CWAs.

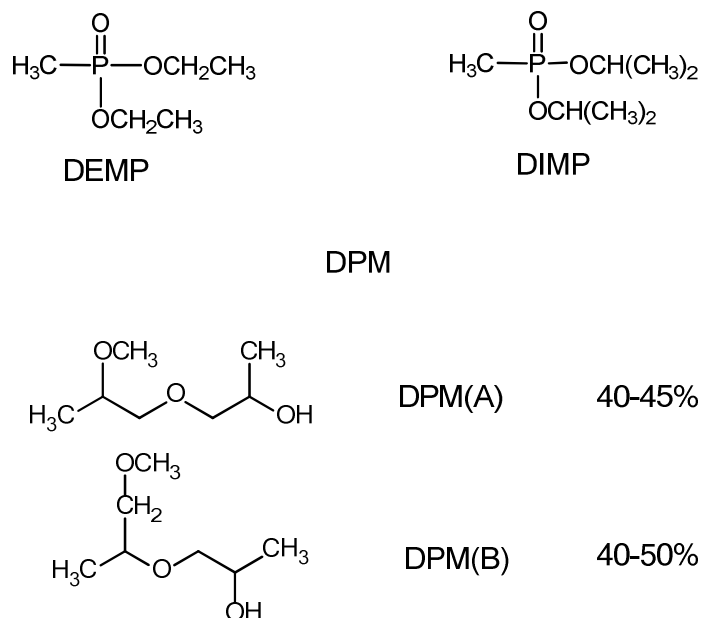
Figure 45: Chemical structures of DMMP, sarin (GB) and soman (GD).



Proton transfer reaction mass spectrometry has been used less extensively than other mass spectrometric techniques in the study of threat agents, but current research is correcting this [18-20, 37]. A recent paper in this vane, by F. Petersson et al., examined the detection of DMMP, along with other organophosphates [21]. Their published results showed two product ions for DMMP; at m/z 125, the protonated monomer (MH^+) and m/z 111. This section of the report will be mostly concerned with investigating the mechanism of formation leading to the product ion at m/z 111 in a PTR-MS. Although the magnitude of the product ion signal is small, the mechanism was found to create significant interest due to the effort required to explain it.

The investigation will centre on the analysis of DMMP, a deuterated isotopomer of DMMP, DMMPd6 ($CH_3PO(OCD_3)_2$) and an isomer of DMMP, trimethyl phosphite, TMP ($P(OCH_3)_3$). The results will also include the analysis of three further CWA simulants to allow comparison with the work of Petersson et al. [21]; diethyl methylphosphonate, DEMP ($CH_3PO(OC_2H_5)_2$), diisopropyl methylphosphonate, DIMP ($CH_3PO(OC_3H_7)_2$) and dipropylene glycol monomethyl ether, DPM ($CH_3(OC_3H_6)_2OH$). See Figure 46 for these molecules' structural information. The structure of DPM shown is for its two most common isomers; labelled for convenience DPM(A) and DPM(B). The sample used was a mixed isomer sample.

Figure 46: Chemical structures of DEMP, DIMP and DPM.

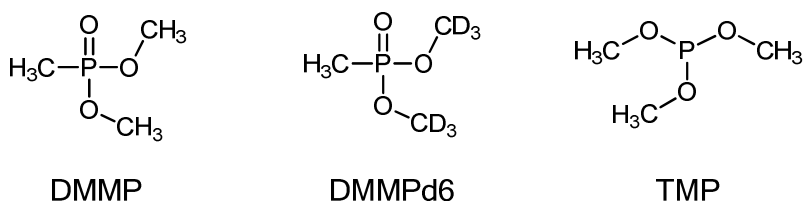


3.2 Background

The work by Petersson et al. hypothesised that the product ion at m/z 111 is formed by fragmentation of DMMPH^+ via the loss of methanol, to form a product ion at m/z 93, with subsequent reaction with water to form m/z 111, as has been observed with an ITMS [75, 76]; or a similar reaction where methanol is lost from a DMMPH^+ and water complex. An earlier study by Cordell et al. used a chemical ionisation reaction mass spectrometer (CIR-MS) to observe the reaction of H_3O^+ with DMMP [20]. They did not report a definite product ion at m/z 111, however a low intensity ion at m/z 111 could be seen in their published mass spectrum. Published results [77, 78] of the reaction between DMMP and H_3O^+ in a selected ion flow tube mass spectrometer (SIFT) show no product ion at m/z 111. However, the product ion may have been present in small quantities, similar to the data of Petersson et al. [21] and Cordell et al. [20]. Measurements of the reaction between DMMP and H_3O^+ taken using the SIFT at Birmingham have shown a very low intensity ion signal at m/z 111.

Measurements of DMMP made with an Electrospray ionisation ion trap mass spectrometer (ESI-ITMS) have recorded the presence of a fragment ion at m/z 111 [75, 76]. These investigations attributed the production of this ion to the association of water to a fragment ion at m/z 93. Unpublished measurements of DMMP, taken by a colleague at Birmingham on a Finnigan LCQ ESI-ITMS showed a product ion at m/z 111 resulting from the trapping and fragmentation of the protonated monomer, DMMPH⁺ (m/z 125).

Figure 47: Chemical structure of DMMP and DMMP d6 showing comparison of the deuterated sites. The structure of TMP is also shown.



The DMMP d6 compound was produced by Dstl Porton Down, Salisbury. The DMMP d6 compound has been deuterated at each methoxy methyl group, allowing analysis of fragmentation involving either of the methoxy groups. The obvious loss sites of methanol from DMMPH⁺ would be at one of the methoxy groups. However, it is possible that the phosphonyl methyl may migrate to the phosphoryl oxygen to form a phosphite; because of this TMP was also studied. Each analyte was obtained from Sigma-Aldrich, except DMMP d6.

3.3 Experimental and Results

The presentation of this study's results will start with those of DMMP, DMMPd6 and TMP. The results of DEMP, DIMP and DPM will then be shown and discussed.

3.3.1 The study of DMMP, DMMP d6 and TMP to identify the product ion at m/z 111 observed from the reaction of DMMP with H_3O^+

The experiment and its results will be discussed in this section. First the results obtained for the reaction of H_3O^+ with DMMP will be discussed with particular relation to the observed ion at m/z 111. The potential reaction mechanism involving association with water will be analysed with reagent ions of D_3O^+ and in sample mixtures of changing humidity.

Analysis of DMMP d6 will follow to understand a potential reaction mechanism involving the phosphonyl methyl of DMMP. The reaction of TMP will also be analysed, as fragmentation via the phosphonyl methyl may involve an intermediate phosphite compound. Finally the possible reaction mechanisms leading to the formation of the product ion at m/z 111 will be discussed.

3.3.1.1 DMMP with H_3O^+

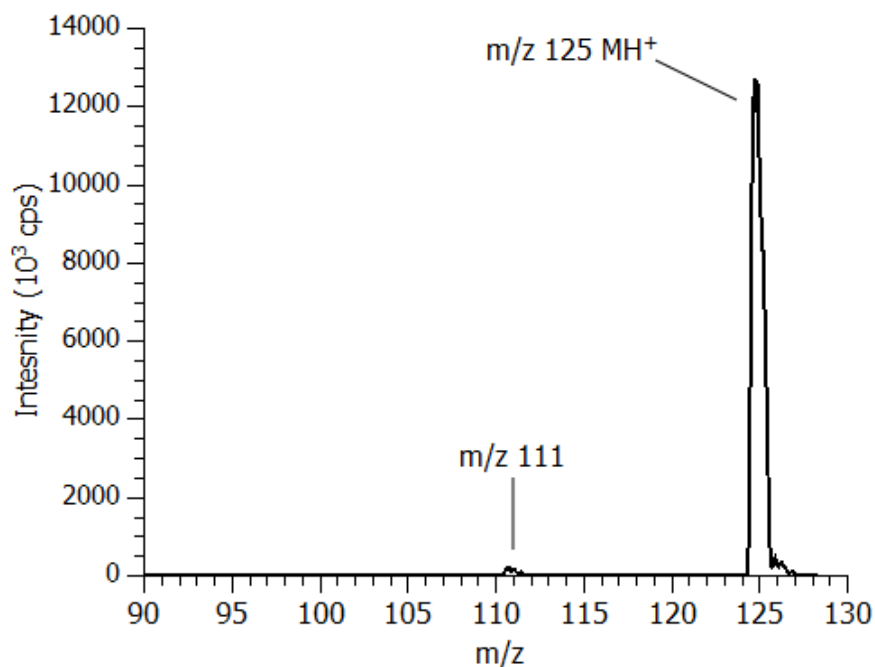
DMMP vapour diluted in nitrogen was measured using a PTR-MS. Nitrogen was used rather than air to reduce the amount of oxygen in the drift tube, effectively limiting the amount of oxygen back-streaming effect into the hollow cathode, thereby reducing the O_2^+ signal to <0.1 % of the total reagent ion signal. This improves confidence when assigning the observed product ions as the result of only proton transfer reactions.

The sample was introduced to the instrument similarly to the alcohol vapour in nitrogen, explained in Section 2.3.2. The experimental set-up is illustrated in Figure 19. The sample of DMMP vapour in nitrogen was produced by transferring a couple of drops of DMMP onto a piece of cotton wool, placed in a 10 ml plastic syringe. The liquid transfer was performed using a 250 μ l glass syringe. The needle of the 10 ml syringe was inserted into a nitrogen gas stream. The syringe was empty except for the cotton wool,

such that when the plunger of the syringe was retracted the syringe filled with a nitrogen and DMMP vapour mixture. Using a syringe drive, this vapour could then be injected back into the flow of nitrogen, creating a stable concentration of DMMP vapour in nitrogen to be analysed by the PTR-MS. Varying the flow rate from the syringe drive would vary the concentration of DMMP by a corresponding amount. This was used to investigate the possibility of a concentration dependence, no such dependence was observed.

A mass spectrum for this set-up is shown in Figure 48. The protonated monomer, MH^+ at m/z 125, was observed to be the most dominant ion, with a further signal observed at m/z 111 (branching ratio < 0.5 %). No product ion was initially observed at m/z 93, although during a later experiment a product ion at m/z 93 was observed with a signal an order of magnitude lower than the product ions at m/z 111. All product ions were observed across a 91-138 Td range of reduced electric fields, and for a range of hollow cathode emission current between 2-10 mA. The observed product ion branching ratios were independent for changes in both conditions.

Figure 48: Mass spectrum for DMMP with H_3O^+ recorded at a reduced electric field of 115 Td.



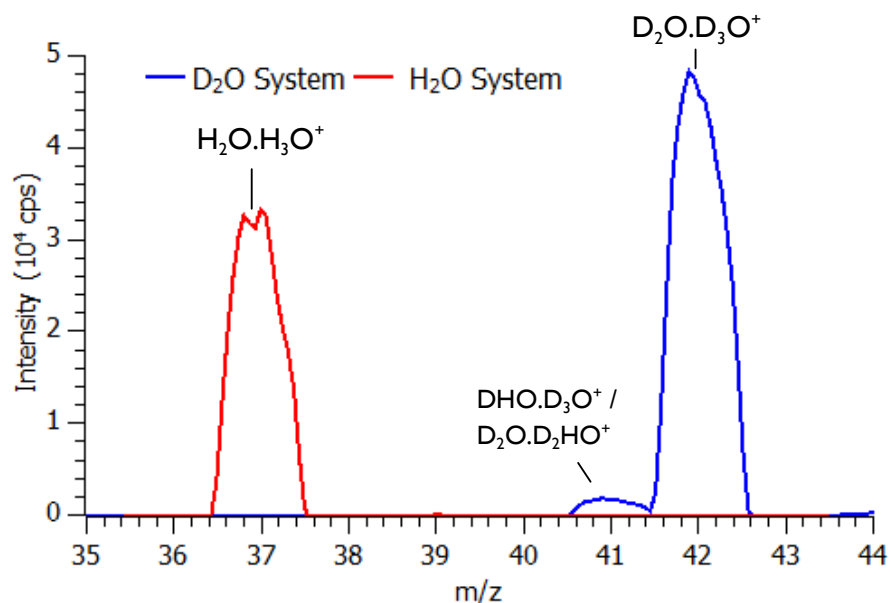
3.3.1.2 DMMP with D_3O^+

To test if the product ion at m/z 111 is formed by association with water, DMMP was analysed in a D_2O system. A D_2O system is described here as identical to a normal PTR-MS system, as described thus far, but with the H_2O water source replaced with D_2O . To achieve this state the water reservoir of the PTR-MS was modified. A septum connection was added to the reservoir for the addition of D_2O through a hypodermic needle and the reservoir was emptied of H_2O . To ensure as much H_2O was removed from the system as possible, the water flow controller was opened fully ($10 \text{ cm}^3 \text{ min}^{-1}$), pumping out any remaining water vapour from the reservoir. With the reservoir evacuated, a 10 ml plastic syringe was used to transfer 20 cm^3 of D_2O , injected through the septum. In this way, D_2O was added to the system with the minimum contamination of H_2O .

With the water reservoir containing D_2O , the PTR-MS will operate as normal, except with D_3O^+ ions as the predominant reagent ion. By using a carrier gas of white spot

nitrogen, filtered through a hydrocarbon trap, the high isotopic purity of the D_2O system will be best maintained. Lab air, which would contain naturally isotopic water vapour, would compromise the purity of the D_3O^+ signal. A mass scan from a D_2O and a H_2O system taken with a nitrogen carrier gas is shown in Figure 49.

Figure 49: Mass spectra of clean nitrogen for H_2O and D_2O systems.

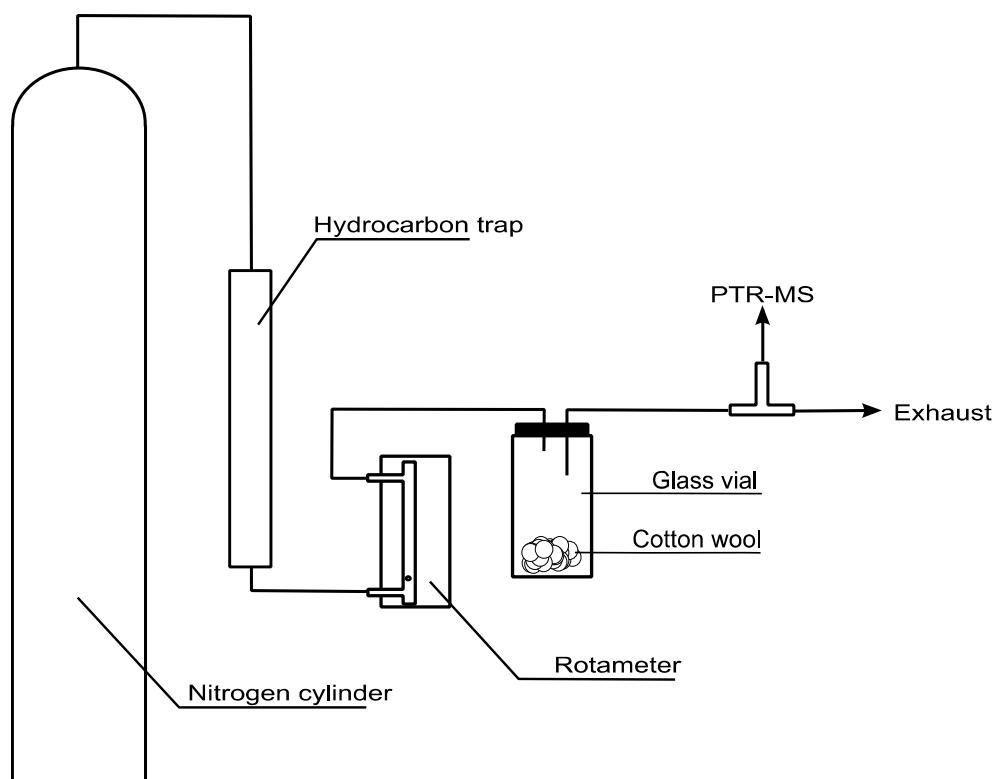


A 'shoulder' is seen next to the $D_2O.D_3O^+$ peak in the mass spectrum, corresponding to either $D_2O.D_2HO^+$ or $DHO.D_3O^+$ ions. That these ions are present indicates that some H_2O is still present in the system, but that D_2O is by far the dominant isotopic water species present in the ion source.

With the PTR-MS operating as a D_2O system the analysis of DMMP with D_3O^+ was performed. If the product ion of DMMP and H_3O^+ observed at m/z 111 is due to association with water, the product ion should appear at m/z 113 in a D_2O system, provided necessary D_2O is present in the drift tube. To test this, a sample was prepared using a piece of cotton wool inside a glass vial. A couple of drops of DMMP were added to the cotton wool. The vial was topped by a septum, such that an inlet and an outlet of

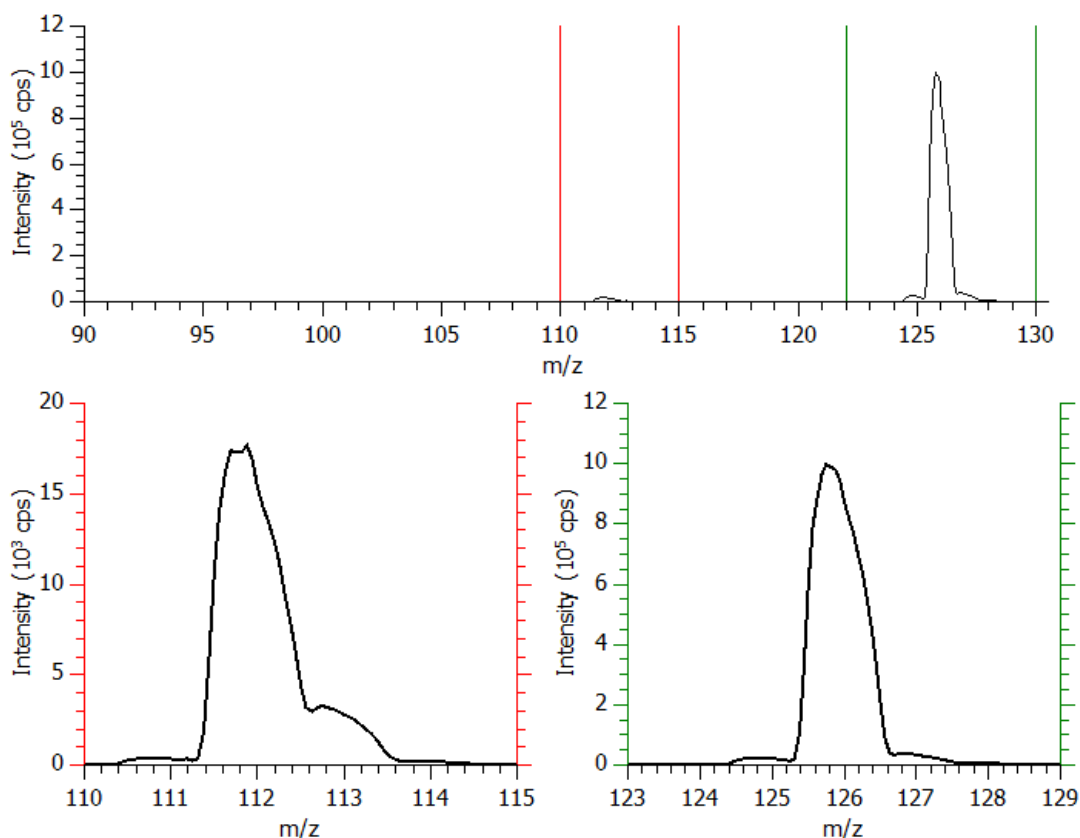
¼ inch Teflon tube could be added. A flow of white spot nitrogen, cleaned via a hydrocarbon trap and controlled by a rotameter, was passed through the vial, creating a flow of nitrogen with DMMP vapour. This flow was connected via a stainless steel T-piece to the PTR-MS, and an exhaust vent. The set-up is shown in Figure 50 and the mass spectrum obtained for this experiment is shown in Figure 51.

Figure 50: Experimental set-up used in the analysis of DMMP and DMMP d6.



Three major product ions were observed in the mass spectrum of DMMP with D_3O^+ ; at m/z 112, 113 and 126. The observed product ion branching ratios were independent of reduced electric field, suggesting no dependence on the reaction time. In a D_2O system deuterium transfer replaces proton transfer as the ionisation mechanism. The product ion at m/z 126 is assigned as the deuterated monomer of DMMP, $[DMMP]D^+$.

Figure 51: Mass spectrum of DMMP in a D₂O system.



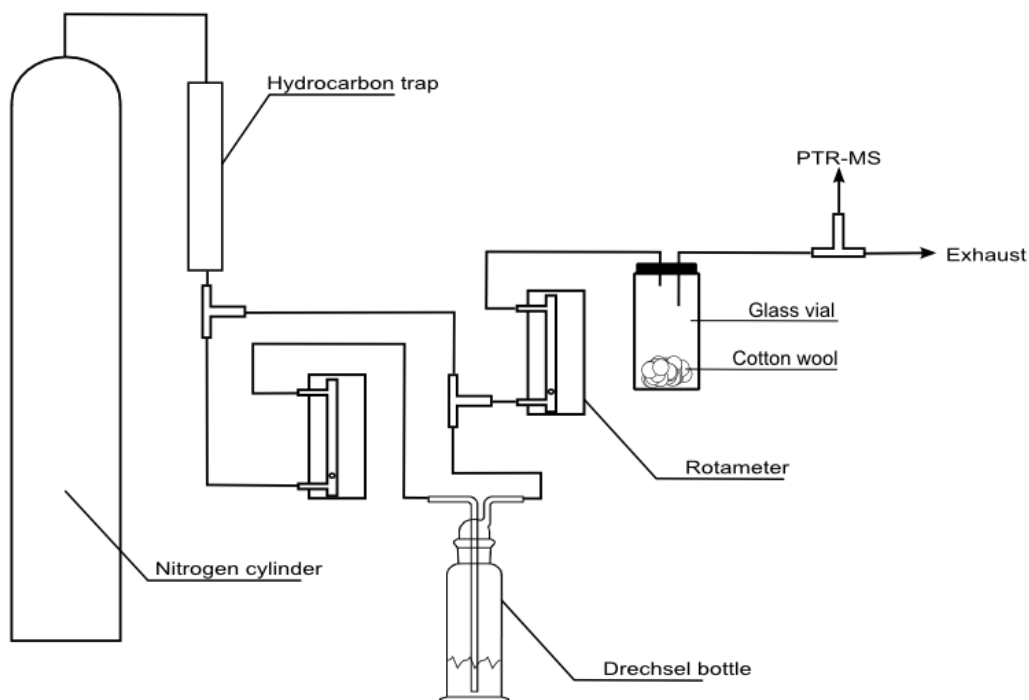
The peaks between m/z 110-115 and 123-129 are highlighted and magnified for clearer observation.

The product ions at m/z 112 and m/z 113, shown in Figure 51, reveal an apparent greater complexity to the reaction of DMMP. The product ion at m/z 113 may be produced by association of D₂O to a product ion at m/z 93; whereas, the product ion at m/z 112 requires further explanation.

3.3.1.3 DMMP with H₃O⁺/D₂O and D₃O⁺/H₂O

To further understand the possibility of a reaction involving water, it was decided to examine the behaviour of the product ions of DMMP in systems of altered humidity. The humidity was altered in two main ways; a reagent ion of H₃O⁺ with altered D₂O sample humidity and a reagent ion of D₃O⁺ with an altered sample humidity of H₂O. The experimental set-up used to achieve this is shown in Figure 52.

Figure 52: Experimental set-up to enable monitoring of DMMP with varied levels of humidity.



The experiment was designed, such that the humidity of the sample of DMMP could be altered in a controlled way. In Figure 52 the direction of nitrogen flow is left to right. The flow of nitrogen is provided by a white spot grade gas cylinder; cleaned further by a hydrocarbon trap. After the trap the gas flow is diverged by a T-piece, one divergence flows through a rotameter to a Drechsel bottle containing water. The outflow from the Drechsel bottle is connected to the second divergence from the hydrocarbon trap. This combined flow is controlled via a second rotameter which flows across a glass vial containing a few drops of DMMP on cotton wool. The flow is then side sampled by the PTR-MS, with the excess flow removed via an exhaust.

By keeping the flow rate of the second rotameter constant, at $1100 \text{ cm}^3 \text{ min}^{-1}$ and varying the flow of the first rotameter it was possible to alter the sample humidity. Two experiments were carried out with this set-up; firstly with a reagent ion of H_3O^+ and a

Drechsel bottle containing D_2O and secondly a D_3O^+ reagent ion and a Drechsel sample of H_2O .

The intensity of the water cluster signals are shown in Figure 53 for both the H_3O^+ and D_3O^+ reagent ions with increasing humidity.

Figure 53: Graph showing the water clusters for a) a H_3O^+ system with D_2O and b) a D_3O^+ system with H_2O .

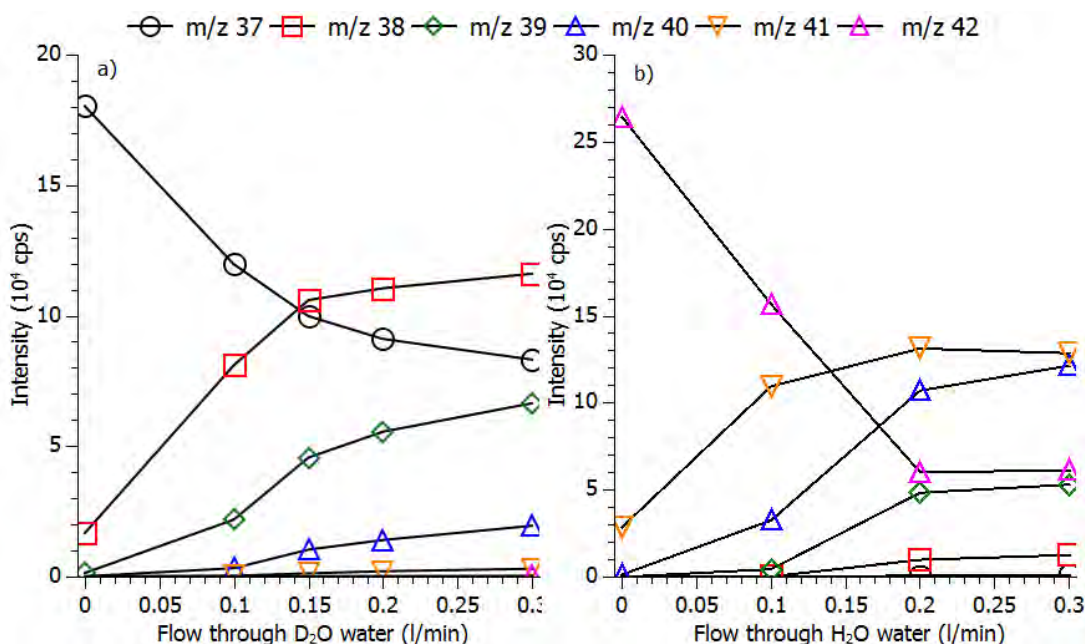


Figure 53 shows that at zero flow rate through the Drechsel bottle the produced water clusters are of relatively pure isotopic composition. As the flow through the Drechsel bottle is increased the isotopic purity of the clusters is diminished. For the H_3O^+ system the increased D_2O humidity in the sample causes an increase in higher mass water clusters, at the expense of the hydrate cluster at m/z 37. For the D_3O^+ system, the dominant hydrate cluster for zero flow through the Drechsel bottle is the cluster at m/z 42. A rise in the signal intensity of lower mass hydrate cluster ions is observed when the flow through the Drechsel bottle is increased. The composition of the hydrate clusters are shown in Table 8.

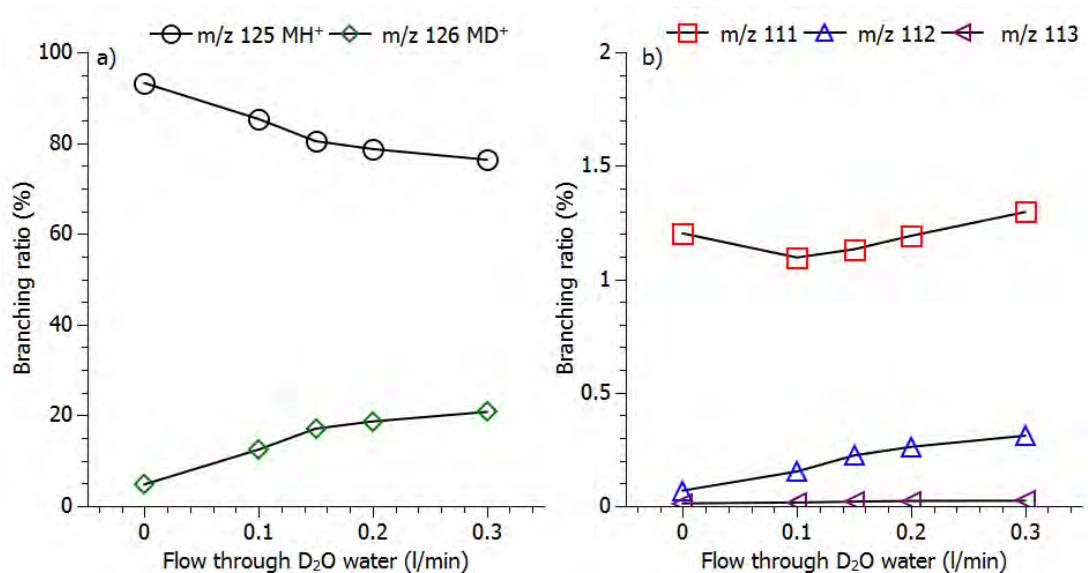
Table 8: Composition of each water cluster in a isotopic mix. Not including O¹⁸ considerations.

<i>m/z</i>	Chemical formula
37	H ₃ O ⁺ .H ₂ O
38	H ₃ O ⁺ .HDO / H ₂ DO ⁺ .H ₂ O
39	H ₃ O ⁺ .D ₂ O / H ₂ DO ⁺ .HDO / HD ₂ O ⁺ .H ₂ O
40	H ₂ DO ⁺ .D ₂ O / HD ₂ O ⁺ .HDO / D ₃ O ⁺ .H ₂ O
41	HD ₂ O ⁺ .D ₂ O / D ₃ O ⁺ .DHO
42	D ₃ O ⁺ .D ₂ O

The isotopic mixing observed in the hydrate clusters indicates isotopic scrambling by either association and dissociation reactions of water clusters in the drift tube, or by direct ionisation in the ion source. Humidity may be increased in the ion source by the flow of humid gas from the drift tube.

Figure 54 shows the product ion branching ratios of DMMP in a system of H₃O⁺ with increasing D₂O, sample humidity. No signal is observed at *m/z* 113 for any flow rate through the Drechsel bottle, whereas a signal was observed in the D₃O⁺ system, shown in Figure 51. Good correlation is observed between the increase in deuterated monomer and the increase in the sample's D₂O humidity.

Figure 54: Graph of the product ion branching ratios of DMMP as a function of flow through D₂O in a H₃O⁺ system, product ions *m/z* 125 and *m/z* 126 are shown in a) and product ions *m/z* 111, 112 and 113 in b).



That no product ion is observed at *m/z* 113, indicates that the origin of this product ion is not from association of water to the *m/z* 93 product ion. This further implies that for the reaction of DMMP with H₃O⁺ the product ion at *m/z* 111 is not formed by association with water.

Figure 55: Graph showing the product ions a) at m/z 125 and 126 and b) at m/z 111, 112 and 113 observed from the reaction of DMMP in a D_3O^+ system as a function of H_2O humidity.

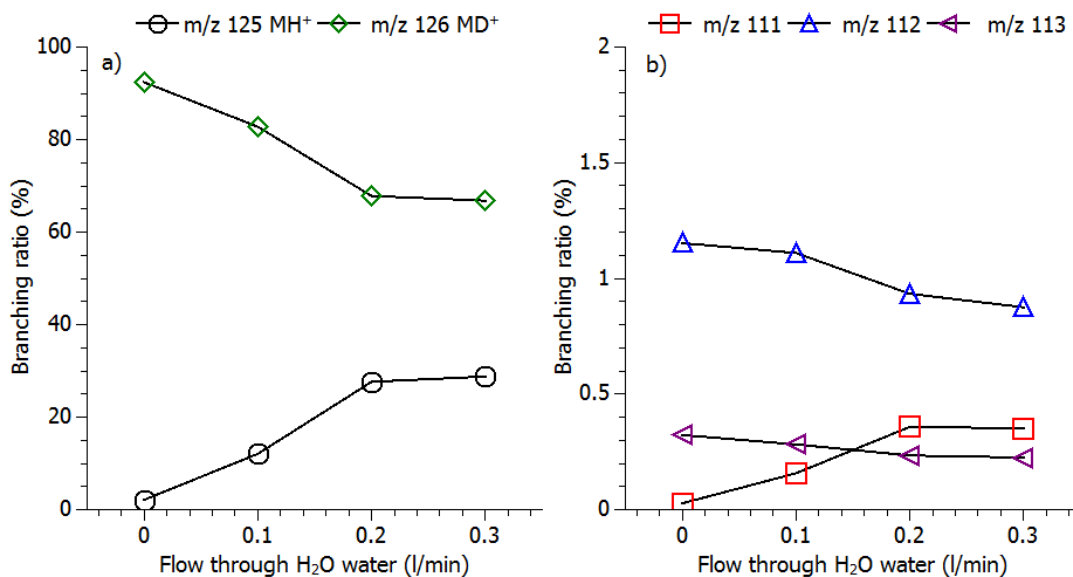


Figure 55 shows how the increase in H_2O humidity in a D_3O^+ system affects the branching ratios. A strong correlation is observed between the production of protonated DMMP and the increase in flow through the Drechsel bottle. The product ion at m/z 111 correlates well with the $DMMPH^+$ ion at m/z 125, suggesting that the product ion at m/z 111 results from the protonated monomer and not the deuterated monomer. This may indicate that the donated proton or deuteron is sequestered to the product ion.

3.3.1.3 DMMP d_6 and TMP with H_3O^+

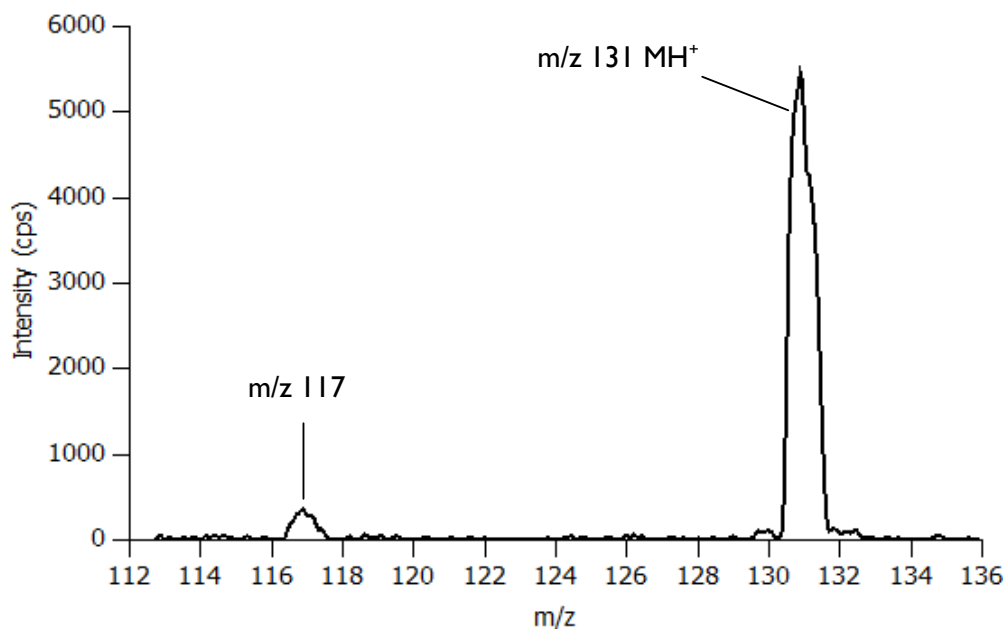
With an association reaction with water being disproven as the source of the product ion at m/z 111, further measurements were carried out to help explain the ion's formation. The product ions produced from the reaction between DMMP d_6 and TMP were both analysed using the PTR-MS. DMMP d_6 was analysed to understand the involvement of the methyl and methoxy groups of DMMP in the ion-molecule reaction. The structure of DMMP d_6 is shown in Figure 47, with the deuteration occurring at each of its methoxy groups. TMP was analysed to help understand possible rearrangement of

the DMMPH⁺ protonated monomer to a phosphite type molecular ion. To this end a study was initiated into DMMP d6 and TMP, the results are explained in this section.

The results of DMMP d6 and TMP will be presented with an explanation of the reaction based on DFT calculations provided by a colleague, Dr. Peter Watts. A review of advances in computational chemistry, applied to gas-phase ion chemistry is provided by Alcami et al. [80]. The results will be compared with later, repeat results taken with the isotopologue of DMMP, where the previous recorded product ions are shown to have been affected by an impurity or artefact ion.

A sample of DMMP d6 in nitrogen was analysed using the same method illustrated in Figure 19; a syringe drive was used to inject a vapour and nitrogen mixture into a flow of nitrogen. A mass spectrum for the compound is shown in Figure 56. The mass spectrum shows two product ions: the protonated monomer, MH⁺ at *m/z* 131 and an ion at *m/z* 117. A further product ion was observed at *m/z* 114 at low intensity. The product ion branching ratios were observed to be independent of reduced electric field.

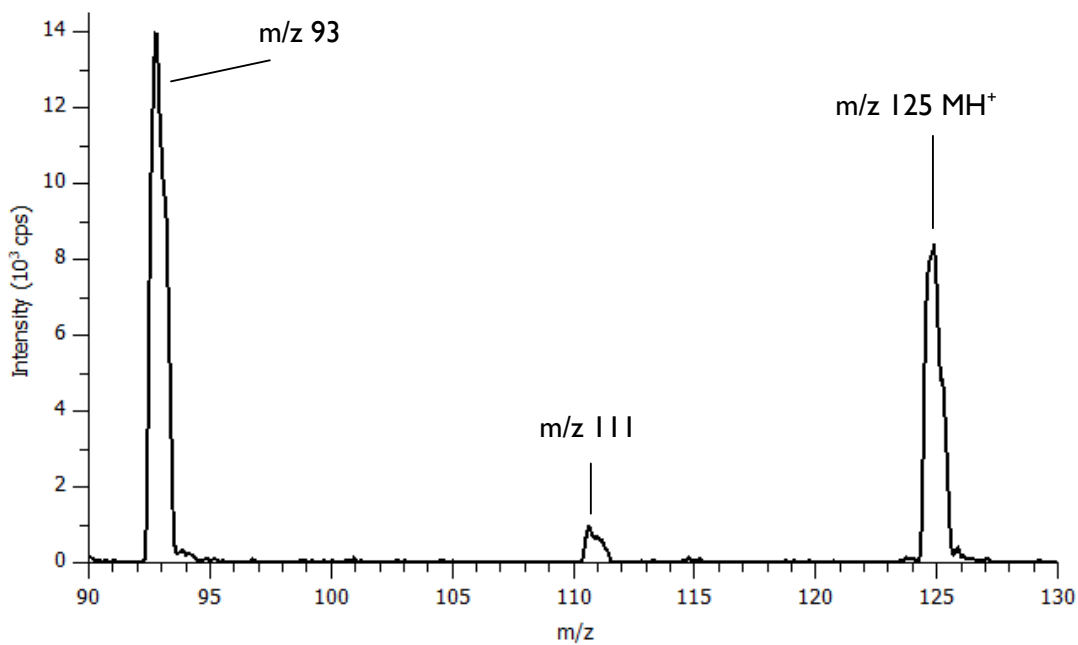
Figure 56: Mass spectrum of DMMP d6 reacting with H₃O⁺ at 115 Td.



A sample of TMP and nitrogen was analysed by employing an identical method of sample preparation, illustrated in Figure 19. The results are shown in Figure 57.

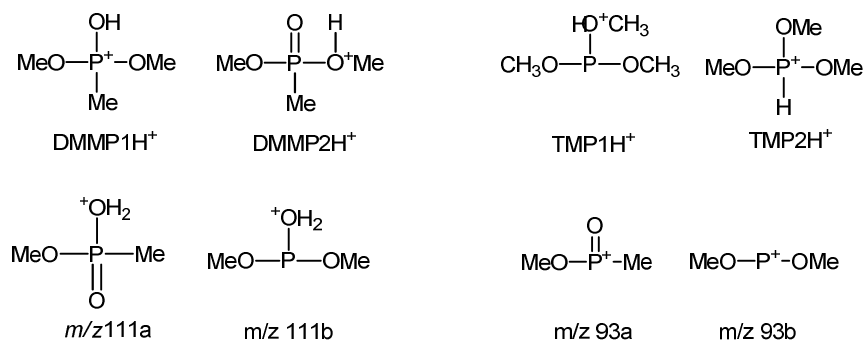
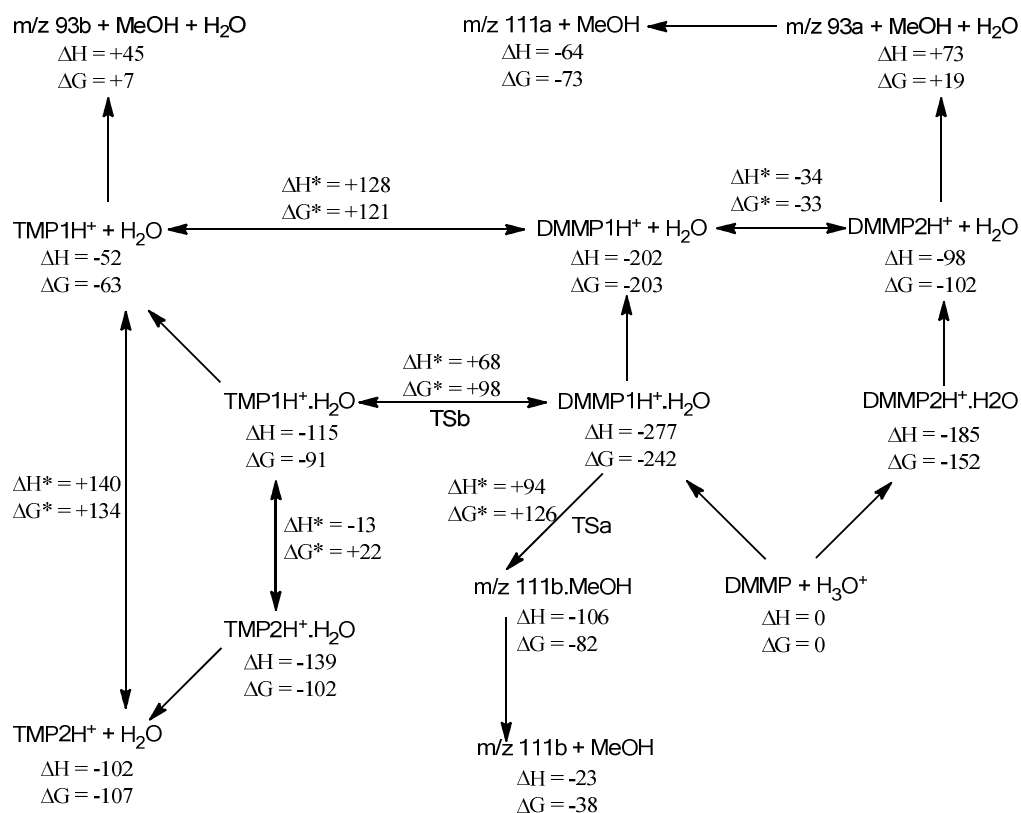
The protonated monomer is observed at m/z 125, as well as fragment ions at m/z 93 and m/z 111. The observed product ions were analysed over a range of reduced electric fields between 91-138 Td. The product ion branching ratios were found to be independent of reduced electric field (m/z 125: 30 %, m/z 111: 2 %, m/z 93: 68 %).

Figure 57: Mass spectrum of the reaction of TMP with H_3O^+ measured at a reduced electric field of 115 Td.



The results obtained in these experiments were supported by DFT calculations, the reaction scheme and associated molecular ion structures are shown in Figure 58.

Figure 58: Free energy, ΔG and enthalpy, ΔH changes for complexes and reactions relative to a starting point of DMMP + H_3O^+ .



All enthalpies and free energies in kJmol^{-1}

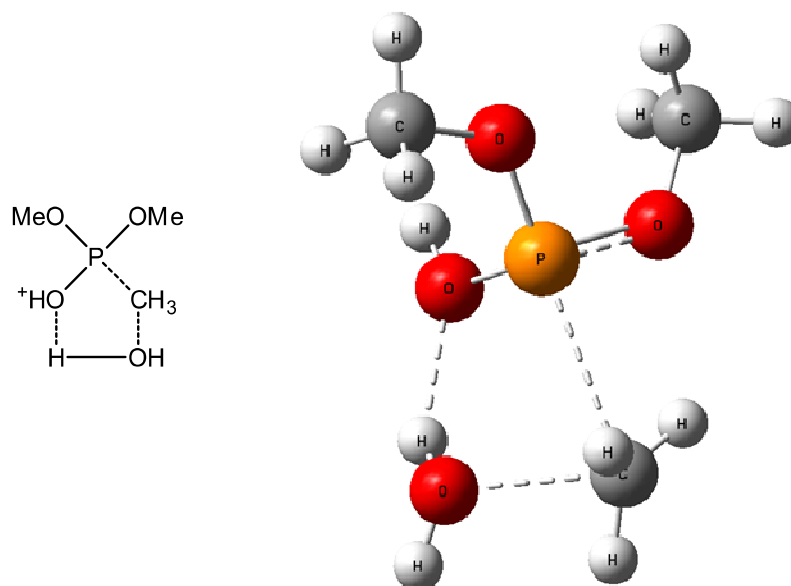
The calculated enthalpies and free energy in Figure 58 are provided using the Gaussian 03 programme with GaussView interface. The B3LYP functional with a 6-31+G(d,p) basis set has been used.

Figure 58 shows two possible arrangements of DMMP upon proton transfer, DMMP1H $^+$ and DMMP2H $^+$. An energetically available and reversible rearrangement of the

protonated DMMP molecule exists between its two isomers. The rearrangement depends on the position of the donated proton, either at the methoxy group, or the phosphoryl oxygen.

A product ion for DMMP d6 is recorded at m/z 117, corresponding to a loss of 14 amu from the protonated monomer; this implies that the fragmentation is involving the non-deuterated phosphoryl methyl. A transition state, TSa was found for the loss of the phosphoryl methyl via an association with the reagent ion. The transition state is shown in Figure 59. This transition state would require energy above that of the system of DMMP and H_3O^+ . The product ion at m/z 111, m/z 111b is formed from the DMMPH^+ isomer. The shape of the ion m/z 111b is that of a phosphite molecule.

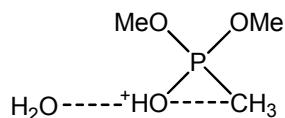
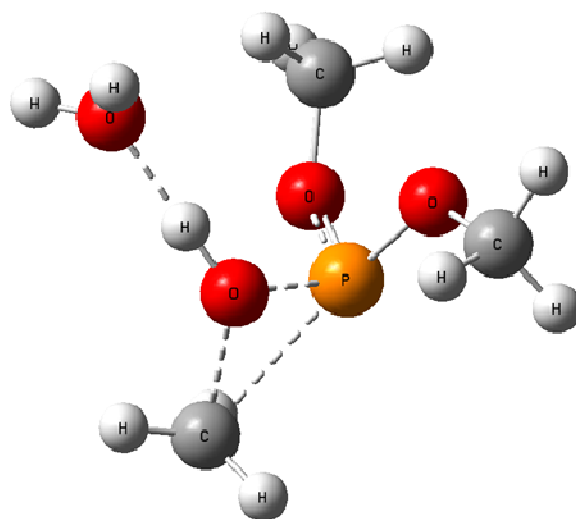
Figure 59: Structure of the transition state TSa.



In searching for the transition state, TSa, a further transition state, TSb was also found, allowing conversion from $\text{DMMPH}^+\cdot\text{H}_2\text{O}$ to a complex of a phosphite molecular ion and water. Should this transition state be formed, the product ion at m/z 125 may be composed of a mixture of ions: DMMPH^+ , DMMP2H^+ , TMPIH^+ and TMP2H^+ , as shown

in Figure 58. The fragmentation of TMPIH^+ to the product ion m/z 93b is not energetically favourable, indicating that the TMPIH^+ formed from TSb lacks sufficient energy to fragment.

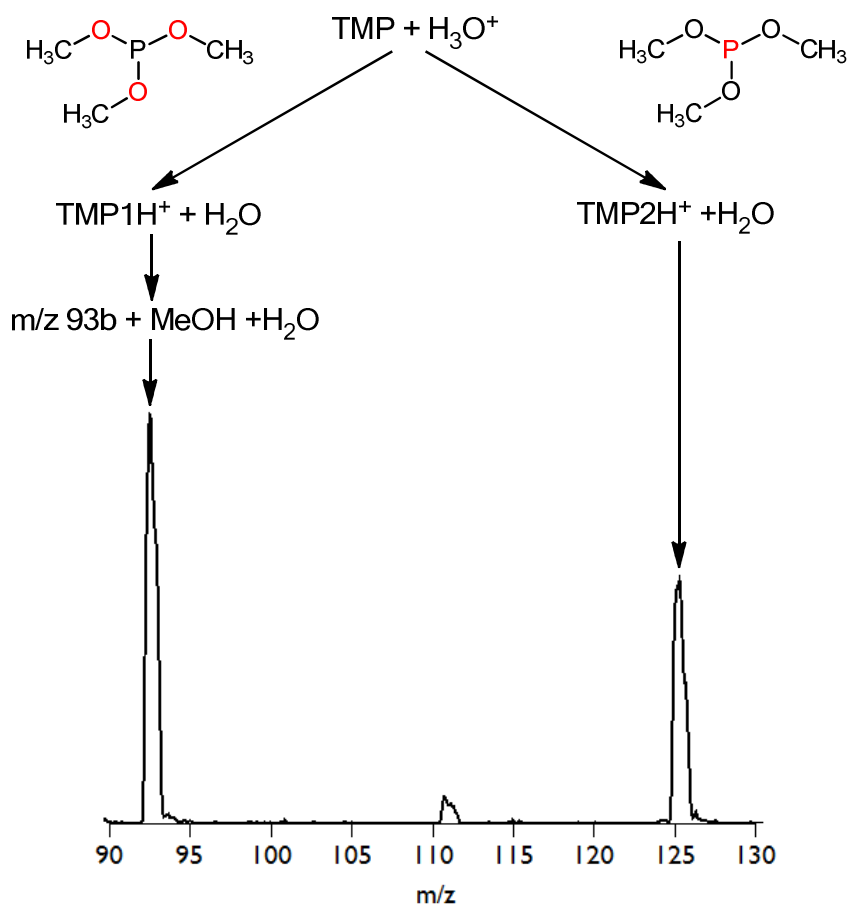
Figure 60: Structure of the transition state TSb.



Analysing the reaction of the neutral molecule of TMP with H_3O^+ , TMP has two possible sites of proton transfer, either to one of the oxygen atoms or to the phosphorus atom. The two major product ions at m/z 93 and 125 can be explained by protonation to either the phosphorus site or one of the oxygen sites, see Figure 47 for the chemical structure of TMP. The greater availability of the oxygen site, outnumbering the phosphorus site 3:1, would indicate the more abundant product ion, at m/z 93, is formed by oxygen site protonation. Whereas, the less abundant ion, at m/z 125, is formed by phosphorus site protonation.

This theory is supported by DFT calculations of the TMP molecule, performed in conjunction with this study, where the proton affinity of either of the oxygen sites of TMP is 853 kJ mol^{-1} and 903 kJ mol^{-1} for the phosphorus site; allowing proton transfer to either site. Danikiewicz [81] has compared the accuracy of computed proton affinities against measured values, finding good accuracy for the computed values.

Figure 61: The reaction of TMP with H_3O^+ showing the origin of the product ions at m/z 93 and 125 from the different protonation sites and subsequent isomers of TMPH^+ .



Protonation to an oxygen site creates an isomeric ion of TMPH^+ , TMP1H^+ , this ion will result in fragmentation to a product ion at m/z 93. The isomer formed by protonation to the phosphorus site, TMP2H^+ will result in the stable protonated monomer, at m/z 125. This is illustrated in Figure 61. The fragmentation of TMP1H^+ must be necessarily

rapid and/or an energy barrier to rearrangement exists, such that isomerisation between TMPIH^+ and TMP2H^+ may not occur.

Corroborating studies of DMMP d6 cast doubt on the validity of the product ion found at m/z 117. The syringe sample of DMMP d6 was taken for investigation at the Ionicon Analytik laboratory in Innsbruck, Austria. The obtained results were dissimilar to those this study had obtained. It was found that whilst product ions at m/z 131 and m/z 117 were observed, the branching ratio of the m/z 117 product ion was much reduced in comparison to the results obtained in Birmingham. The Innsbruck group also reported an ion at m/z 114.

To reconcile these results, a sample of DMMP d6 with DMMP was analysed as a function of time using the PTR-MS at Birmingham. The sample was produced by passing a flow of nitrogen through a glass vial containing cotton wool doped with a couple of drops of DMMP and DMMP d6. The lid of the glass vial had been adapted to allow for two PTFE tubes to be inserted; one as inlet, one as outlet. The flow of nitrogen was sampled by the PTR-MS, with the excess removed by an exhaust. The set-up is shown in Figure 50.

Multiple ions were analysed as a function of time, the results are shown in Figure 62. Ions at m/z 125 and 111, corresponding to DMMPH^+ and its fragment ion were analysed, along with m/z 131, 114 and 117, the protonated monomer of DMMP d6 and its two candidate product ions.

Figure 62: Selected ions of the reaction of DMMP and DMMP d6 with H₃O⁺ as a function of time

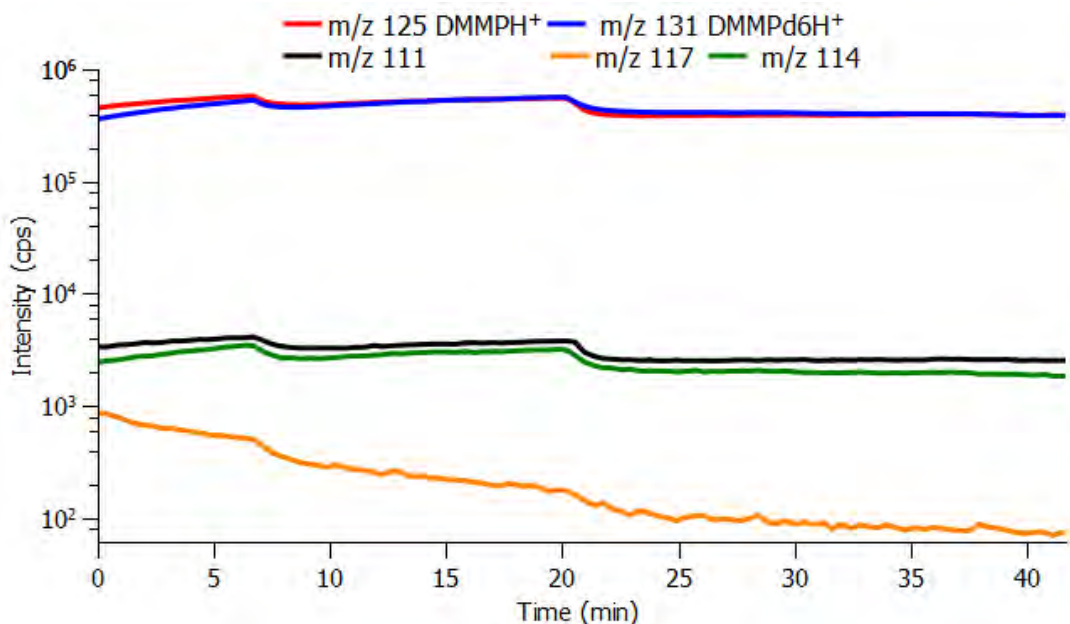


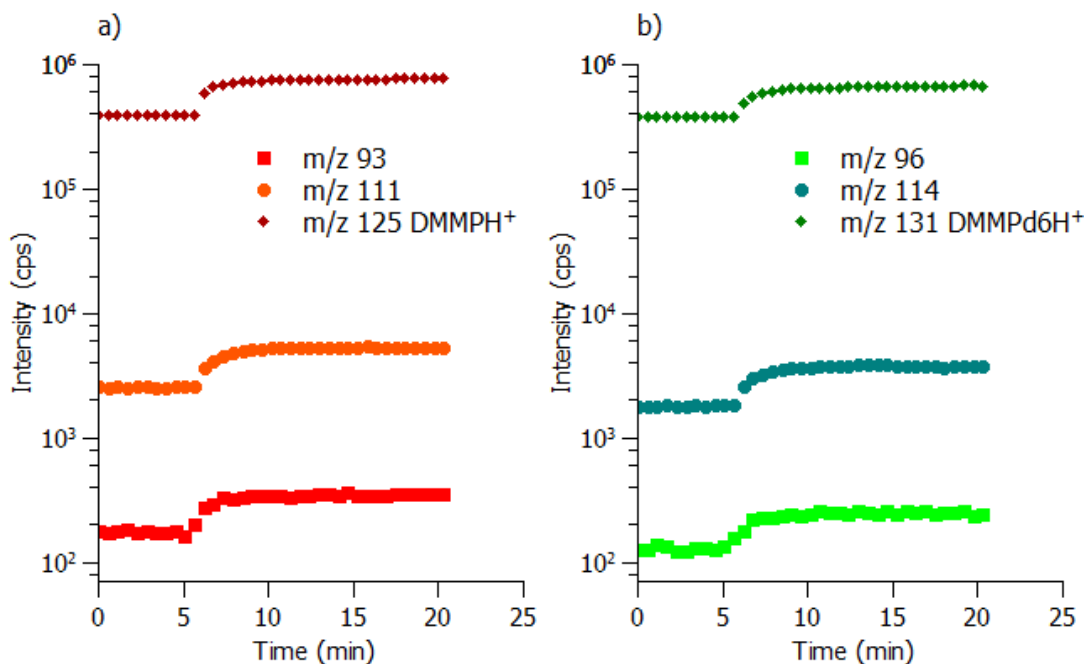
Figure 62 shows clear correlation between both the *m/z* 131 and 125 protonated monomers and the *m/z* 114 and 111 product ions. The product ion at *m/z* 117 decreases with time, demonstrating that it is the result of an impurity present in the sample and not as the result of the reaction scheme postulated earlier. The recognition of a product ion at *m/z* 114 suggests the fragmentation reaction involves a methoxy group.

The two variations in product ion intensity, shown in Figure 62 occurring just after 5 minutes and just after 20 minutes into the experiment were caused by altering the flow rate of nitrogen across the sample to vary the analyte concentration. Both the protonated monomer signals of DMMP and DMMP d6 are varying in harmony with their associated product ions at *m/z* 111 and 114.

Figure 63 shows separately the product ions recorded for a) DMMP and b) DMMP d6; the figure includes the *m/z* 93 and *m/z* 96 product ions for DMMP and DMMP d6,

respectively. The increase in signal at approximately 5 minutes is caused by reducing the flow speed of nitrogen over the sample.

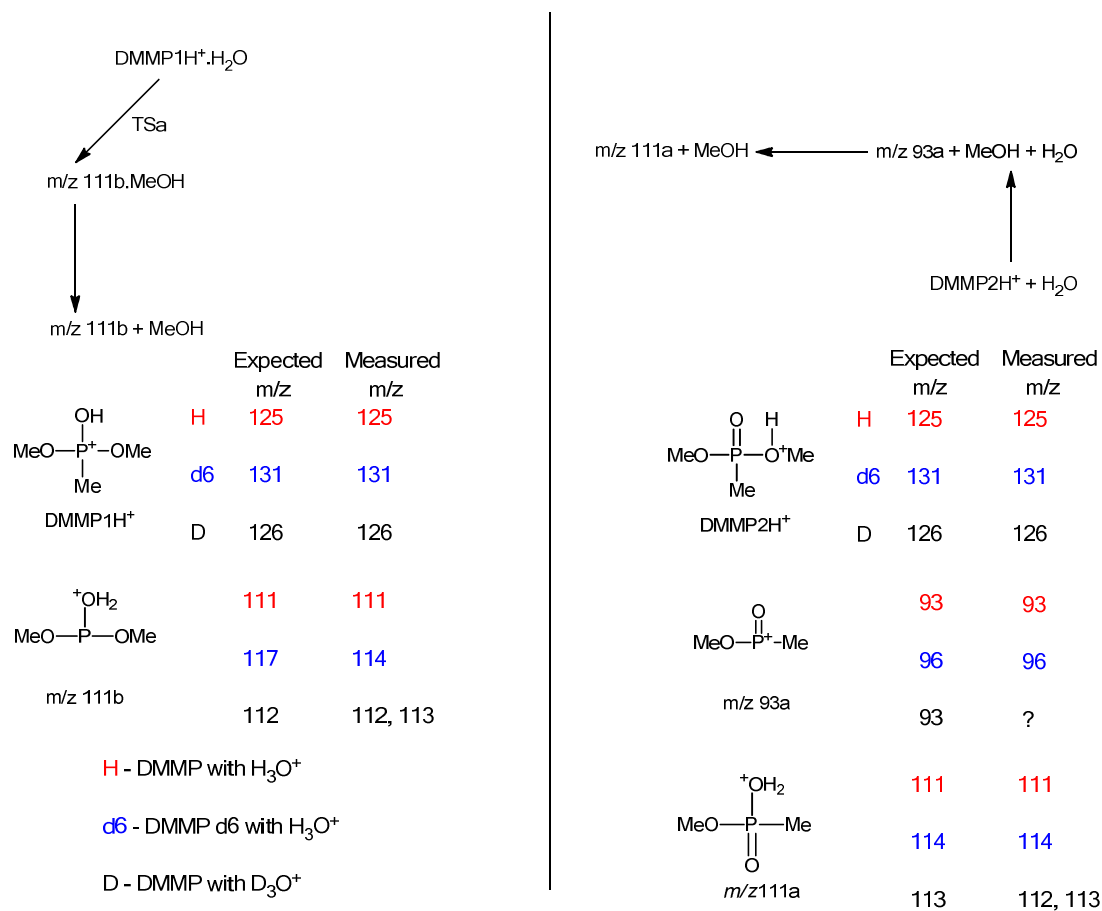
Figure 63: Time evolution spectra of a) product ions due to DMMP and b) product ions due to DMMP d6.



The product ions observed in Figure 63 show very close alignment between the fragment ions for each reaction; m/z 96 and 114 for DMMP d6 and m/z 93 and 111 for DMMP are similar fractions of their respective protonated monomers. This correlation is a strong indication that in both cases the correct product ions have been identified.

The evidence for the fragmentation mechanisms to m/z 111 identified in Figure 58 is summarised in Figure 64. Both proposed fragmentations leading to m/z 111 are shown and for each ion that we would expect to detect the predicted m/z values are also given. These values are compared to the values detected by experiment. No one suggested fragmentation provides a complete prediction of the observed product ions, thus neither theoretical pathway is deemed sufficient to explain the experimental data.

Figure 64: Comparison of the fragmentation proposed in Figure 58 with data collected using DMMP and DMMP d6.



3.3.1.4 DMMP d6 with D₃O⁺

For completeness, the reaction of DMMP d6 in a D₂O system was also studied. The sample was measured by passing a flow of white spot nitrogen through a glass vial containing a few drops of DMMP d6. The experimental set-up is shown in Figure 50, with the observed mass spectrum shown in Figure 65.

Figure 65: Recorded product ions for DMMPd6 in a D₂O system.

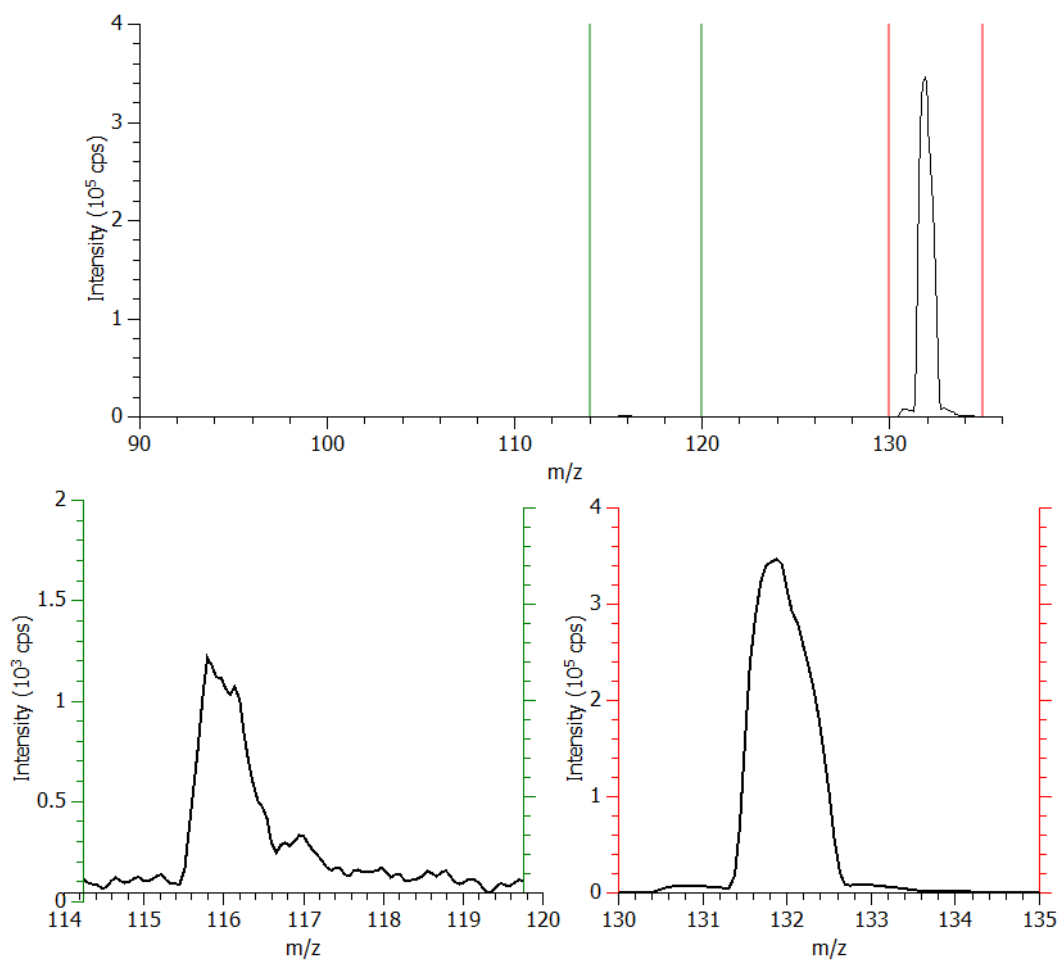


Figure 65 shows a product ion at m/z 132 corresponding with the deuterated monomer, $[\text{DMMPd6}]\text{D}^+$. A second peak is observed at m/z 116; this product ion would be consistent with association of D_2O with a product ion at m/z 96. An alternative route should be preferred however, given comparison with the DMMP and D_2O data, where association of water with the ion at m/z 93 was not occurring. A further possible peak is also observed at m/z 117.

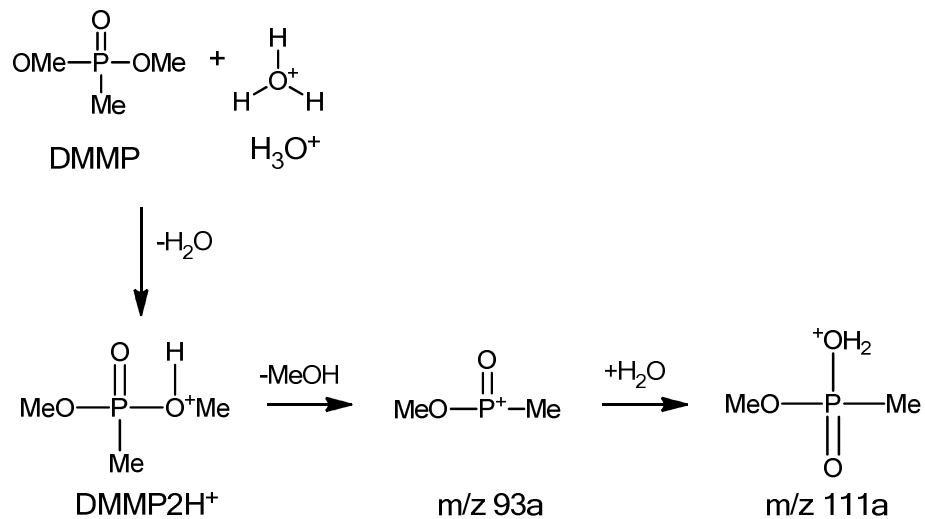
3.3.1.5 Discussion of the reactions of DMMP and DMMP d6

To study the formation of a product ion at m/z 111 from the reaction of DMMP with H_3O^+ the reactions of DMMP, one of its isomers (TMP) and an isotopologue (DMMPd6)

have been investigated using a PTR-MS. Progress has been made toward this aim, and a discussion of that progress follows.

ESI-ITMS studies [75, 76] of DMMP observed a product ion at m/z 111 attributed to the association of water to a product ion at m/z 93, the reaction is shown in Figure 66. Experiments performed as part of this investigation have shown that the product ion at m/z 111 is not formed by this mechanism. By studying the behaviour of product ions in a humidity of D_2O no signal was observed at m/z 113, indicating no association between an ion at m/z 93 and D_2O . In a PTR-MS system with D_3O^+ as the reagent ion, a product ion at m/z 113 was observed, but its signal was less prominent than the signal detected at m/z 112.

Figure 66: Reaction mechanism producing a product ion at m/z 111, m/z 111a via loss of methanol and association of water. Reaction pathway taken from Figure 58.



A further possible fragmentation mechanism was found by DFT calculation involving a transition state, TSa; see Figure 58 for the reaction pathway and Figure 59 for the diagram of TSa. This reaction mechanism involved loss of the phosphonyl methyl. Experiments with DMMP d6 confirmed a product ion at m/z 114. The detection of this

product ion indicates its formation occurs via the loss of a neutral fragment from either of the methoxy groups and not the phosphoryl methyl.

The preferred reaction is one where loss of methanol from one of the methoxy groups occurs from an association of water and DMMPH⁺. In the experiments of Section 3.3.1.2 and Section 3.3.1.3 reactions involving the protonated monomer and deuterated monomer of DMMP were studied. From the complex DMMPH⁺.H₂O, loss of CH₃OH would result in a product ion at *m/z* 111, and loss of CH₃OD from the complex DMMPD⁺.D₂O would result in a product ion at *m/z* 113.

This reaction scheme does not seem to allow for the recorded product ion at *m/z* 112. However, even with the PTR-MS being operated with a reagent gas of D₂O some background H₂O will be present in the drift tube. The complexes of DMMPH⁺.H₂O and DMMPD⁺.D₂O will quickly dissociate to form DMMPH⁺ and DMMPD⁺, or eliminate CH₃OH and CH₃OD, respectively. The DMMPH⁺ and DMMPD⁺ may react with H₂O or D₂O in the drift tube to form new complexes, which may in turn eliminate methanol.

In experiments using D₃O⁺ as the reagent ion association of H₂O and the DMMPD⁺ ion may occur to form a DMMPD⁺.H₂O complex; loss of CH₃OH from this complex would result in an ion at *m/z* 112. That no product ion is observed at *m/z* 111 indicates that the deuteron donated to the DMMP molecule is sequestered to the phosphoryl oxygen, as in the structure of DMMPID⁺, see Figure 58 for the structure of DMMPID⁺. Where a humidity of H₂O is added to the sample, a product ion is observed at *m/z* 111. This ion is the result of protonation of DMMP by H₃O⁺ to form DMMPH⁺, the H₃O⁺ being formed by back-streaming of H₂O into the ion source. A greater incidence of back-streaming will be caused by the greater number density of H₂O in the drift region. When using H₃O⁺ as the reagent ion and adding D₂O no ion at *m/z* 113 was observed,

suggesting that no CH_3OH is lost from the complex of $\text{DMMPH}^+\cdot\text{D}_2\text{O}$. This further indicates that the donated proton is sequestered to the phosphoryl oxygen.

The ratio of the product ions produced at m/z 111, 112 and 113 in a system of DMMP with differing components of deuterated and undeuterated water will depend on the relative number density of neutral water molecules in the drift tube. This is not a value that we can know easily, the relative abundance of water clusters gives the best indication, but may not be an accurate reflection of the relative number density of D_2O and H_2O in the drift tube. The water clusters, if formed in the source drift region would represent a good measure of the composition of water in the ion source only. A fraction of water molecules from the drift tube may be capable of back flow into the source drift region, explaining the hydrate clusters observed in Figure 53, where a higher humidity sample was analysed. The formation of hydrated reagent ion clusters is a complex reaction; dependent on the humidity in the drift tube and ion source, as well as the drift velocity and drift time. Some of these factors are intrinsically linked, making experimental study difficult.

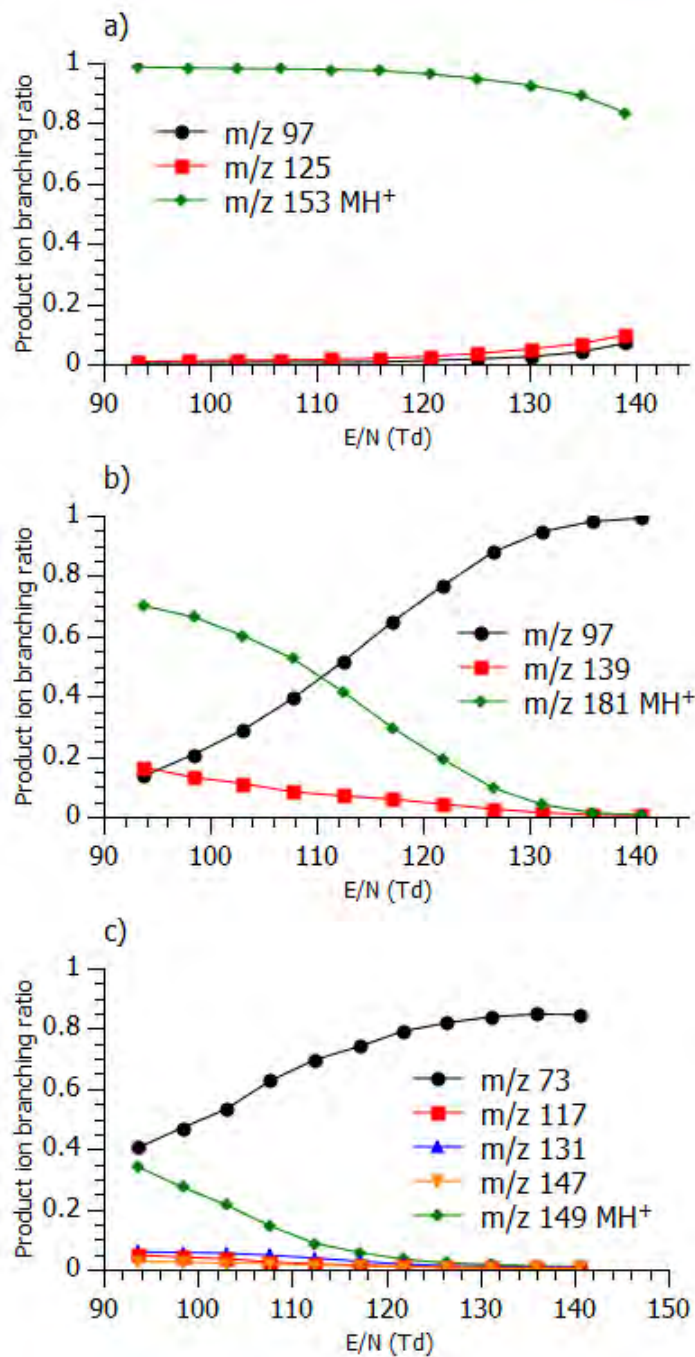
For results taken with DMMP d6 this reaction mechanism remains applicable. In its reaction with H_3O^+ , loss of CD_3OH from $\text{DMMPd6H}^+\cdot\text{H}_2\text{O}$, formed from either the initial transient complex, or a later association between H_2O and DMMPd6H^+ would produce an ion at m/z 114. When studied with a reagent ion of D_3O^+ , loss of CD_3OD from a complex of $\text{DMMPd6D}^+\cdot\text{D}_2\text{O}$ would produce a product ion at m/z 116; whereas, loss of CD_3OH from a complex of $\text{DMMPd6D}^+\cdot\text{H}_2\text{O}$ would produce an ion at m/z 117. Both these product ions are observed in the mass spectrum for the reaction of DMMP d6 with D_3O^+ .

3.3.2 DEMP, DIMP and DPM analysed with H_3O^+ in a PTR-MS

For complete comparison with the work by Petersson [21] and to complete the study of DMMP by analysing further CWA simulants, the compounds DPM (dipropylene glycol monomethyl ether), DEMP (diethyl methylphosphonate), and DIMP (diisopropyl methylphosphonate) were analysed in the PTR-MS (structures of each chemical are shown in Figure 46). DPM is used as a simulant for CWAs because of its similar physical properties; boiling point, vapour pressure etc. [82]. Similar to DMMP, DIMP and DEMP are also both used as CWA simulants because of their organophosphate nature, to simulate nerve agents in particular.

Samples of chemical vapour and nitrogen were produced using the same method of preparation used to analyse the reactions of TMP and DMMP with H_3O^+ in Section 3.3.1.1 and Section 3.3.1.2. A dependence on reduced electric field was observed for each compound and the observed product ions are shown in Figure 67.

Figure 67: Product ions of a) DEMP, b) DIMP and c) DPM as a function of reduced electric field.



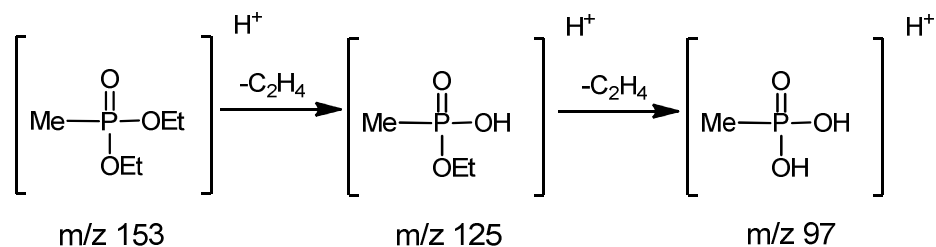
3.3.2.1 DEMP

Of the three compounds the protonated monomer of DEMP showed the least dependence on reduced electric field, producing mostly protonated monomer (MH⁺) across the range of reduced electric fields studied. Two fragment ions were observed at

m/z 125 and m/z 97, corresponding to loss of one and two molecules of ethene, respectively ($[M-C_2H_4]H^+$, $[M-2C_2H_4]H^+$). Both these product ions were also observed in ESI-ITMS studies of DEMP [75]. The product ion branching ratios agree very strongly with those reported by Petersson [21].

The ESI-ITMS study observed a product ion at m/z 97 resultant from trapping the m/z 125 product ion, indicating that the elimination of ethene molecules observed is sequential as shown in Figure 68. Both the protonated monomers of DPM and DIMP showed more considerable dependences on the reduced electric field

Figure 68: Proposed sequential fragmentation of protonated DEMP.



3.3.2.2 DIMP

The observed product ions of DIMP agree very well with those observed by Petersson [21]. A protonated monomer, $\text{DIMP}H^+$ is observed along with two fragment ions at m/z 139 and 97 corresponding to losses of one and of two propene molecules, respectively ($[M-C_3H_6]H^+$, $[M-2C_3H_6]H^+$). These two fragment ions were also observed in a study by Bell et al. by MS/MS of $\text{DIMP}H^+$ using an ESI-ITMS [75]. In that study trapping the ion at m/z 139 resulted in a fragment ion at m/z 97, again suggesting a sequential loss of alkenes, similar to the fragmentation of DEMP.

Figure 69: Proposed sequential fragmentation of protonated DIMP.

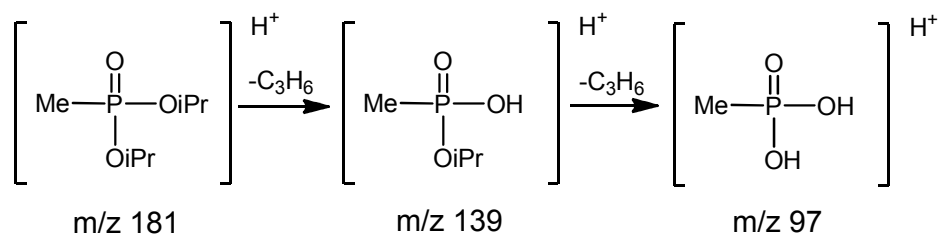


Figure 69 shows the proposed fragmentation of DIMP. The pathway is strikingly similar to that of DEMP, the pathway in both cases involving sequential elimination of the alkene corresponding to each compound; propene for DIMP, and ethene for DEMP. The two reaction schemes are also fragmenting to a common ion at m/z 97.

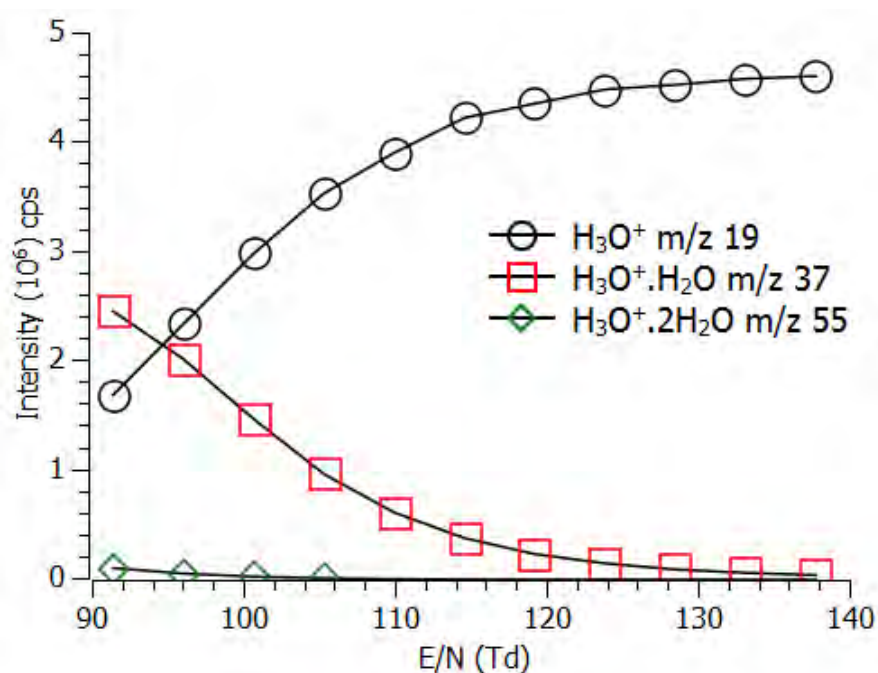
3.3.2.3 DPM

Two major product ions were observed for DPM; the protonated monomer, DPMH^+ and a fragment ion at m/z 73. Two further, minor ions are seen at m/z 117 and m/z 131, both peaking at a 5 % branching ratio for a reduced electric field of 90 Td. DPM was the only compound studied that showed considerable difference from the reported results of Petersson et al. [21]. Petersson observed a fragment ion at m/z 147 with an approximate branching ratio of 30 % for 90 Td, the signal was attributed to loss of H_2 from the protonated monomer, $[\text{M}-\text{H}_2]\text{H}^+$. This ion very closely followed the signal due to the protonated monomer, MH^+ over the 90-140 Td range of reduced electric fields recorded by Petersson. In our study such a product ion was observed, but not at a branching ratio greater than 3 % at any reduced electric field. The ion is shown in Figure 67. The reason for this discrepancy in the observed product ions for the reaction of DPM is unclear. One postulated reason may be a difference in sample; DPM being manufactured for industrial solvent applications.

The minor product ions at m/z 131 and 117 are attributed to loss of water and methanol from the protonated monomer, respectively. The product ion at m/z 73 is attributed to a sequential loss; loss of water from the protonated monomer, followed by loss of propanal. The loss site for water is attributed to the OH group, forming the product ion at m/z 131; further loss of propanal results in the fragment ion at m/z 73.

The fragmentation may be the result of dissociative proton transfer from the H_3O^+ reagent ion. At lower reduced electric field the number density of protonated water clusters in the drift tube will be increased. The proton affinity of water clusters is greater than that of water; resulting in less energetic proton transfer, so less proton transfer induced dissociation should occur. The profile of the protonated water clusters produced from a nitrogen sample gas is shown in Figure 70.

Figure 70: Water clusters observed in a drift gas of dry nitrogen.



The shape of this profile is similar to the shape observed for the monomer and product ion at m/z 73 of DPM, seen in Figure 67. This indicates that the fragment ion may be

formed by the more energetic proton transfer from the H_3O^+ ion and the monomer resulting from the softer ionisation involving the $\text{H}_3\text{O}^+\cdot\text{H}_2\text{O}$ water cluster.

3.4 Conclusions and Further Work

The bulk of this study has been concerned with a succession of measurements to understand the formation of the product ion at m/z 111 from the reaction of DMMP with H_3O^+ . Possible reaction schemes leading to the ion's formation were proposed and tested with experiment. The investigation proposed a final possible reaction mechanism involving the loss of methanol from a methoxy methyl via an association complex of DMMPH^+ and H_2O , producing the ion at m/z 111 directly.

During the course of the investigation DFT calculations, provided by Dr. Peter Watts have been interpreted to help decide on reliable reaction processes. A suitable transition state has not yet been found by DFT calculations of the DMMP and H_3O^+ system to match the proposed scheme. The proposed reaction scheme has been realised by eliminating other possible schemes; namely association between DMMP and H_3O^+ to lose methanol from the phosphonyl methyl and loss of methanol from the protonated monomer followed by association with water. It is planned that Dr. Peter Watts will continue DFT calculations on this system in order to find a transition state, so that the results of this section may be published.

The DMMP data, along with data taken from DIMP, DEMP and DPM has shown the PTR-MS to be very capable at the detection of chemical warfare simulants agreeing with the data of Cordell et al. [20] and Petersson et al. [21]. Comparison of this data, with results collected by Petersson et al. has been made. The data collected with the organophosphates has been compared particularly to results taken on ESI-ITMS [75, 76]

and SIFT-MS [77, 78] instruments, deepening the understanding of PTR-MS comparative to other mass spectrometry techniques.

4 Using a PTR-MS for Breath Analysis of Patients with Liver Disease

4.1 Introduction

The potential for breath analysis as a diagnostic medical tool has been known about since doctors first noticed patients developed an odour on their breath indicative of their disease. Patients suffering from diabetes develop an acetone-like smell to their breath, while the breath of patients with lung infection has a putrid odour [83].

Currently, breath analysis is used for a limited number of clinical practice applications [84]. Breath analysis has been used clinically to monitor bacterial growth in the gut and to diagnose bacterial infection. The urea breath test is used to identify infections of *helicobacter pylori* in the stomach [85], while the hydrogen breath test is used to monitor the growth of bacteria in the bowel [86], helping to diagnose irritable bowel syndrome [87]. Breath analysis is also beginning to be used clinically in identification of airway inflammation, with the fractional exhaled nitric oxide breath test being implemented in a clinical setting to diagnose and monitor asthma [88].

Advances in the sensitivity of mass spectrometric measurements are allowing breath analysis to study the effects of metabolism by analysing the VOCs detected in breath [84, 89]. Metabolites in the blood may pass into the breath at exchange sites in the lungs or airways.

Within the lungs, air and blood exchange oxygen and carbon dioxide at the alveoli. At this exchange site, VOCs dissolved in the blood may be evaporated and become constituents of the air within the lungs. This mechanism may allow breath analysis to provide a surrogate for measurements of blood composition. What is more, breath

analysis may provide information not currently available in conventional blood tests by using the advances in gas analysis available to mass spectrometry. Medical research may be able to use information gained from breath analysis to learn more about metabolism and better understand a patient's illnesses or reactions to medication. This knowledge could then feed through to frontline medics to improve diagnoses and treatments of disease.

The study of VOCs of metabolic origin has a wide field of applications, with potential diagnostic and monitoring possibilities. Any disease state will impact on the body, producing an alteration in the body's metabolism, which may be detected by breath analysis. However, definitive identification of metabolic VOCs caused by disease is difficult. Careful understanding of the metabolic pathways and repeatable detection of compounds are two important limiting factors in the progression of breath markers for metabolic monitoring [84].

Breath analysis for metabolic markers has focussed strongly on isoprene [90-94] and acetone [90, 95, 96]. Isoprene has been identified as an endogenously produced compound in humans [92] and the compound has been linked to lipid peroxidation, cell damage [97]. However, this link has been shown to be less than straight forward [93]. Acetone, again has a complicated metabolic path [98], the compound has been observed variously as a marker for diabetes [96] and liver disease [99, 100].

Many mass spectrometric techniques are being exploited for the analysis of breath composition. These techniques include; selected ion flow tube mass spectrometry (SIFT) [96, 101-103], gas chromatography mass spectrometry (GC-MS) [93, 94, 97, 100, 104, 105] and ion mobility spectrometry (IMS) [106, 107]. Proton transfer reaction mass spectrometry is another such technique at the forefront of breath analysis [9, 13,

14, 90, 95, 108-112]. The technique combines real-time, high sensitivity analysis of breath with the ability to make suggested identifications, assets that may be very applicable to medical diagnoses and investigation.

4.2 Background

A good deal of investigation has been made into using breath analysis to aid in the diagnosis of lung disorders [88, 94, 103, 104, 107, 109, 111]. Although this association may seem an obviously fruitful theme for investigation, the differences in the lung function of patients with lung diseases and their controls may produce false positives, indicating difficulty breathing without furthering an ability to use breath analysis as an early stage diagnosis tool.

A more promising organ for study may be the liver. Diseases of the liver may have dramatic consequences for metabolic pathways, affecting concentrations of blood constituents. These constituents may not have been monitored before in blood samples of patients with liver disease and so mass spectrometric breath analysis may be a very innovative and interesting tool.

A good deal of research has been forthcoming in this field, but none utilising the properties and advantages of a PTR-MS [99, 100, 113-116]. This study aims to correct this by using a PTR-MS to study breath of patients with liver disease.

Patients suffering liver disease have been identified to produce a characteristic and foul odour on their breath, known as *foetor hepaticus*. Much of the effort to apply breath analysis to liver disease has focussed on identifying compounds that contribute to this foul odour. GC-MS studies by Tangerman et al. in 1994 [114] and Van den Velde et al. in 2009 [100] have both attributed the odour to dimethyl sulphide ((CH₃)₂S).

Tangerman et al. go further than detection, proposing the compound is a derivative of methanethiol (CH_4S) [115].

The importance of methanethiol in the effect of hepatic diseases was reported by Almardini et al. in 1984 [117]. Almardini et al. observed increased methanethiol in the blood of encephalopathic patients with liver disease compared to non-encephalopathic patients and healthy controls. A 2001 study by Sehnert et al., using GC-MS to examine breath, further linked the involvement of volatile sulphurous compounds to liver disease. The study observed that patients could be differentiated between groups with liver disease and those with healthy livers by their detected levels of carbonyl sulphide (COS), carbon disulphide (C_2S) and isoprene (C_4H_8).

Other compounds have been identified as possible markers of liver disease on breath. In 2009 study by Van den Velde et al. [100] increased acetone, 2-butanone and 2-pentanone were observed. In 2006, Solga et al. [99] reported ethanol and acetone as increased breath constituents of patients with liver disease, the origin of the compounds was thought to be due to a change in gut flora brought on by liver disease.

Using a GC-MS in 1994, Friedman et al. [116] found limonene on the expired breath of patients with liver disease. Limonene is a citrus essential oil found in fruit juices, it is also a common contributory of many air freshening scents. Patients suffering with liver disease reported an increased preference for citrus flavour. The origin of the elevated levels was not conclusively proved to be caused by either metabolic differences, or an increased preference for citrus flavour.

The importance of volatile sulphur compounds to the application of breath analysis toward liver disease is evidenced by previous studies. A recent study by Tangerman et

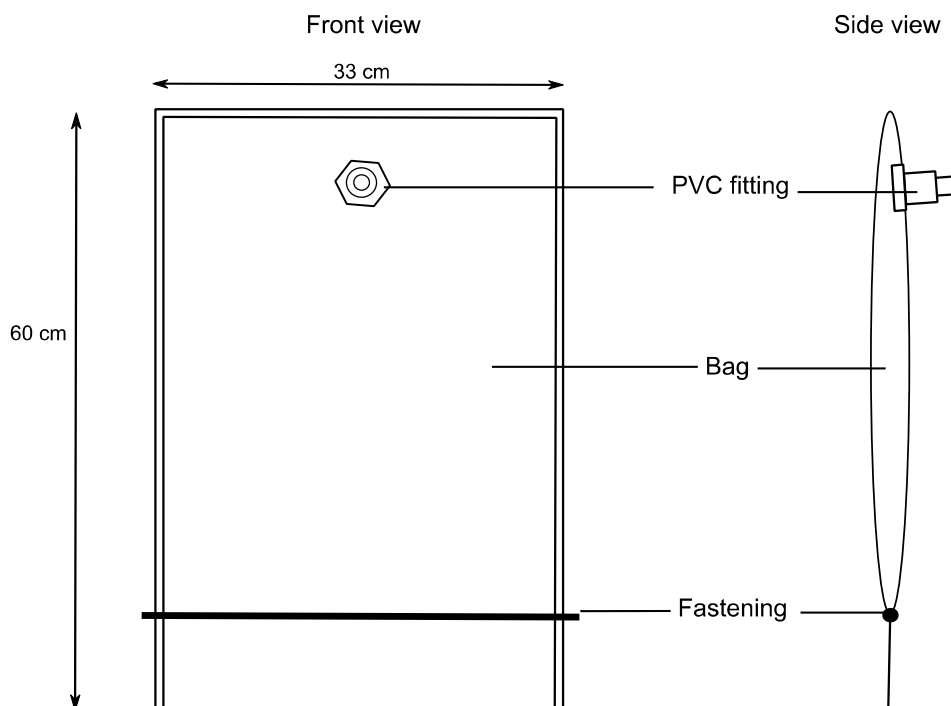
al. in 2009 [118] examined sulphurous compounds for detection; the compounds were recorded as highly volatile and often reactive.

4.3 Preliminary Study of Garlic Breath

With the reactivity of the sulphurous compounds in mind, a preliminary study was undertaken to test the quality of our breath testing procedures using garlic to elicit sulphurous compounds on the breath. The ingestion of garlic has been linked previously to the observation of sulphurous compounds on breath [119, 120]. Concentrations of allyl methyl sulphide and dimethyl sulphide were found to contribute to the characteristic odour of 'garlic breath'.

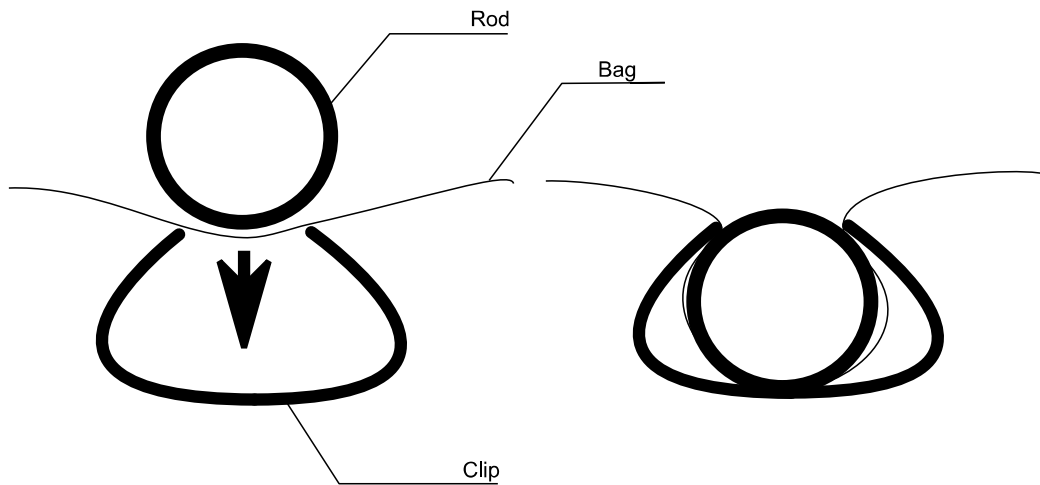
To test the suitability of our proposed breath sampling procedure, a volunteer was instructed to ingest half a clove of raw garlic two hours before giving a breath sample. The sample was collected by asking the volunteer to provide a single exhalation collected in a Teflon bag. The bag's construction is outlined in Figure 71.

Figure 71: Teflon bags used for breath sampling.



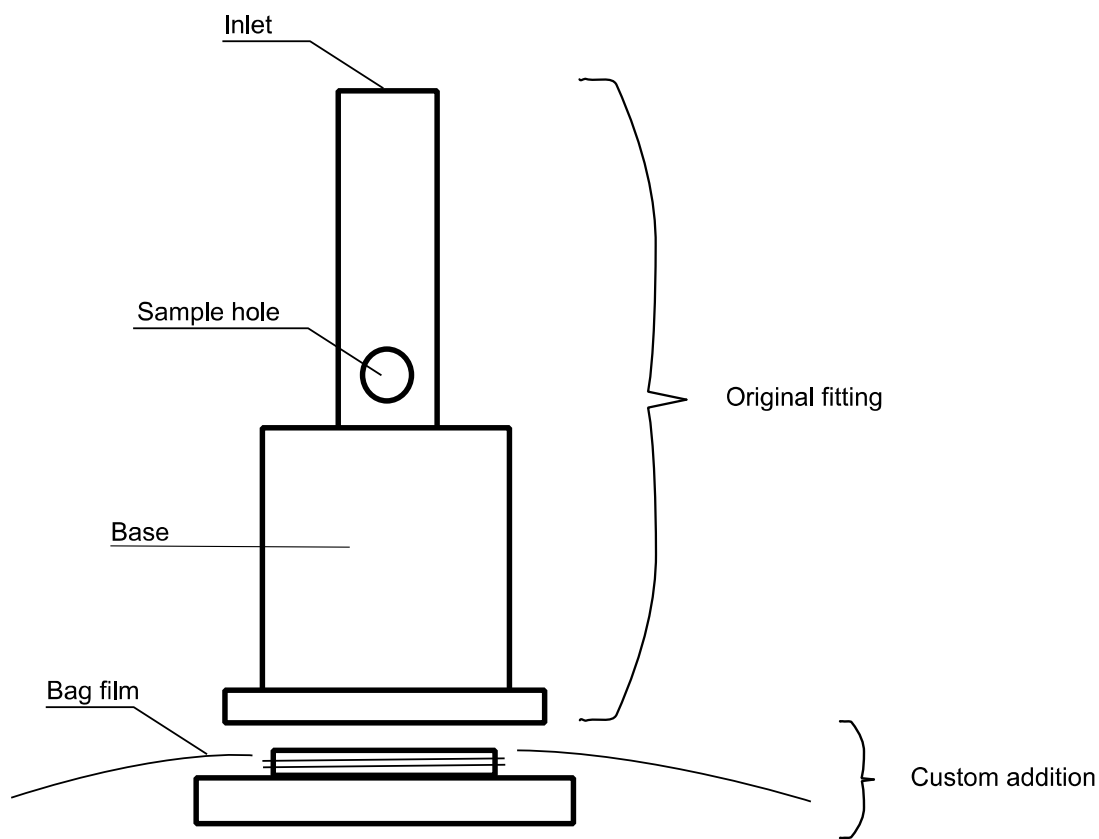
The breath sampling bag is permanently sealed at three edges, with a temporary fastening along the fourth edge. The temporary fastening uses a rod and clip mechanism outlined in Figure 72. The fastening is designed such that it can be placed at any position across the width of the bag to tune the bag's volume to the patient's lung capacity; i.e. a large person would have a greater expected lung volume than a small person.

Figure 72: Temporary fastening strip shown in the action of fastening.



The bags are filled and emptied through a PVC fitting adapted from exhaled breath fittings (EAF) produced by SKC Inc. The fittings are push to open, and have been adapted by the addition of screw-on bases to fix them to the PTFE film bags, allowing the fittings to be reused. A diagram of the fittings is shown in Figure 73.

Figure 73: PVC fitting used for breath analysis.

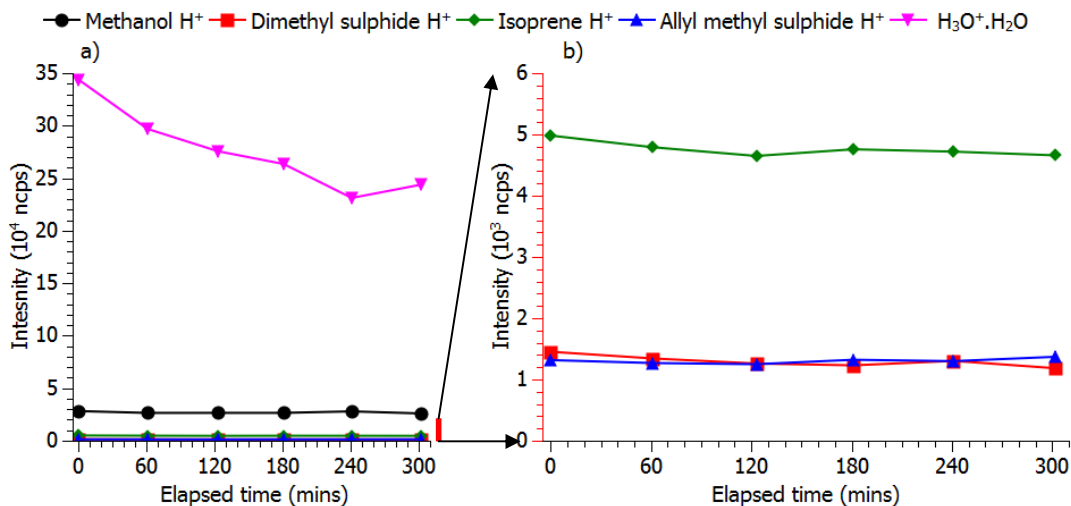


With the sample hole visible the fitting valve is closed, and when the hole is pushed into the base, the valve is open. The fittings are cleaned before each use, using isopropyl alcohol, then sterilised with 2.5 g of sodium dichloroisocyanurate (PRESEPT) sterilisation tablet in 1 litre of clean water.

The sample was collected with the collection bag sitting in a heating jacket, set to 40 °C. The volunteer formed a seal around the fitting with their mouth and opened the valve of the fitting, exhaling fully. The volunteer then closed the valve and unsealed their mouth from the fitting, retaining the sample of breath inside the bag.

The sample was analysed by PTR-MS as soon as possible after the sample was taken. Subsequent measurements were made every hour afterwards, for approximately five hours. These results are summarised in Figure 74.

Figure 74: Time evolution of a breath sample to test the suitability of PTFE bags to storing volatile sulphurous compounds; b) shows a zoomed in portion of a).



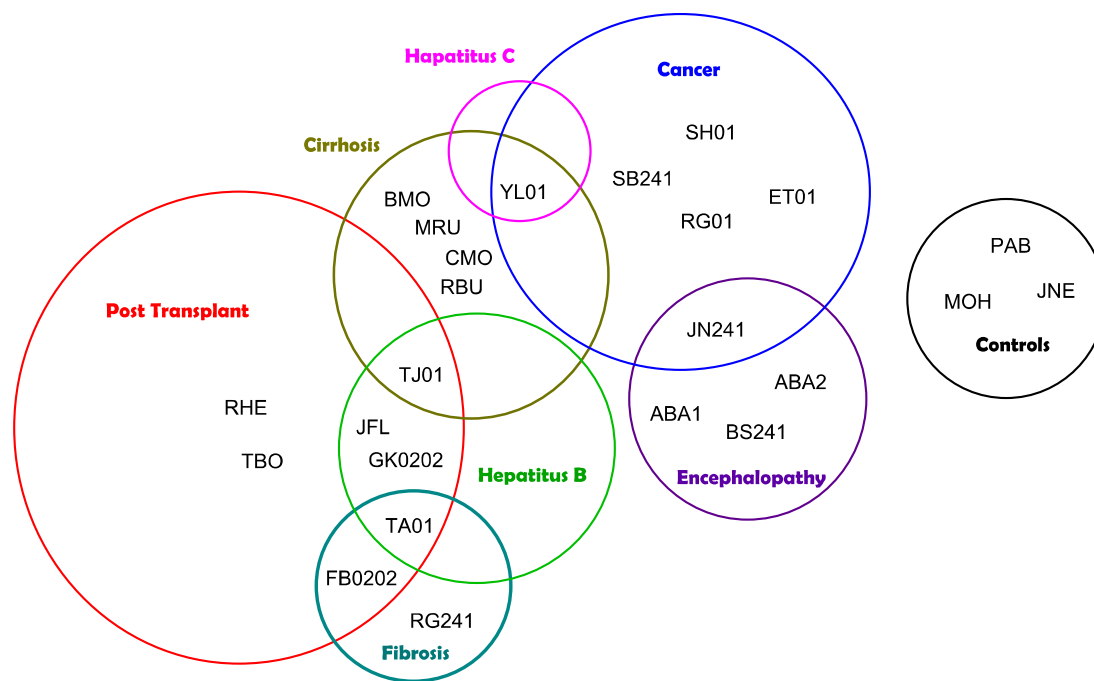
In between measurements the bag was left unheated, and then heated for five minutes before each measurement. The signal intensity of the H₃O⁺.H₂O water cluster has dropped over the five hours, indicating that the sample is becoming less humid. The other compounds (methanol, dimethyl sulphide, isoprene and allyl methyl sulphide) showed good stability over the five hour time period. This indicates that the PTFE sampling bags are suitable for use with volatile sulphurous compounds. The loss of water cluster signal, when compared to the other compounds is attributed to the greater concentration of water vapour in the sample and the comparatively smaller size of the water molecule.

4.4 Experimental Methodology

With confirmation that PTFE bags can maintain the verity of a breath sample containing sulphurous compounds for up to five hours, it was decided to collect breath samples from patients and transport them to the laboratory for analysis. This had the advantage that the PTR-MS did not need to be moved.

Volunteers were recruited by medical staff at the Liver Unit; particularly helpful in collaboration were Dr. Tahir Shah and Dr. Andrew Holt; consultant physicians in liver medicine and hepatology, respectively. The volunteers were selected from a range of liver disease states, ranging in condition and severity. A summary of the 21 patient volunteers, including 3 healthy controls is shown in Figure 75.

Figure 75: Summary of volunteers involved in Liver Study.



The volunteers were each given an alphanumeric code to ensure the anonymity of their data. Patients were asked to fill in a short questionnaire (attached in Appendix A) to detail some of their medical history and provide information about possible contaminants to their sample. Diet has a considerable impact on the chemicals detected in breath samples; volunteers were asked whether they had consumed garlic or coffee in the last 24 hours. Acetone is detected as a breath biomarker associated with fasting; as part of the questionnaire volunteers were asked the last time they ate a meal. Alcohol is another dietary factor that can affect breath samples; both in the detection directly of

ethanol, but also in the detection of acetaldehyde; a marker for hangovers. Volunteers were asked if they had drunk alcohol in the last 24 hours. Patients were also asked to provide information about non-prescribed medications or remedies they were taking.

The measurements were collected over nine separate days between May 2009 and February 2011. Each sample was collected from the hospital and transported to the laboratory for measurement. The time between sample and measurement was never more than four hours. Volunteers provided measurements in the Liver Unit of the Queen Elizabeth Hospital, Birmingham, except PAB, ABA1 and ABA2. PAB provided a sample of breath in the laboratory of the Molecular Physics Group after ingesting half a clove of garlic, and ABA1 and ABA2 gave samples in the Liver Ward of the Queen Elizabeth Hospital after both had been admitted. Volunteers all arrived to give samples from their home environments, except ABA 1 and ABA 2.

4.4.1 A note on breathing technique

O'Hara et al. investigated breath sampling techniques with particular respect to the effect the style of breathing had on the sample obtained [121, 122]. The study reported discrepancies in the composition of breath samples dependent on the way that a single breath was delivered. Work by Anderson et al. has summarised this effect and explained it with theoretical calculations [123]. The effect is dependent on the varied solubility of compounds observed. The compounds solubility affects the exchange site of the gas between the air and the blood. High solubility gases may exchange in the airways, for lower solubility compounds exchange will be limited to the thinner membrane alveoli. Classically, gas exchange in breath is assumed to occur only at the alveoli. The concentration of a low solubility gas in the final portion of a breath sample, known as end exhaled breath will represent an alveolar concentration.

For high solubility gases, exchange will occur on inspiration and expiration in the airways. On inspiration, soluble compounds in the blood diffuse through the airway's mucus lining to enter the air, depleting their concentration in the mucus. The lining of the airways has many layers of tissue and because of this it takes time for the soluble gases in the blood to replenish concentrations in the mucus. When the breath is expired, the mucus has not yet been replenished and some soluble gas in the breath will now be reabsorbed by the mucus. Thus, for highly soluble compounds, end exhaled breath is not a true reflection of alveolar air. For ethanol, the magnitude of this effect has been shown to be dependent on both lung volume and exhalation speed [124, 125].

Greater equilibration of air in the airways with the blood and mucus of the lining would help to minimise this effect. An isothermal rebreathing procedure was implemented to equilibrate the airway air, mucus and blood, by extending the time the breath sample will be in contact with the airway. This procedure was first implemented for measurements with a PTR-MS by O'Hara et al. [121]. This helped to ensure against variability caused by breathing pattern, and lung volume.

The procedure required each volunteer to take a full inhalation and deliver one full exhalation into a breath sample bag, heated to 40 °C. The valve is then closed, sealing the bag. This bag of air is then used as a reservoir for rebreathing. Volunteers fully exhale outside the bag and then inhale from the bag, and exhale that breath back into the bag. They complete this cycle five times, finishing on an exhalation into the bag, after which the valve is closed. While doing this the volunteer is required to use a nose clip and a diver's style mouthpiece to assure a good seal between the volunteer's airways and the bag.

The volunteer's blood oxygen content is monitored using a pulse oximeter, if the blood oxygen concentration is seen to fall below 90 % or to change by more than 5 %, the procedure is aborted. This action was not necessary. Volunteers repeat the cycle of 5 breaths 3 further times, making 4 cycles and 20 breaths in total. Between rebreathing cycles the volunteer is allowed to rest to maintain their blood oxygen levels and prevent undue discomfort.

This procedure was deemed very successful for eliminating the variability of single exhalations caused by breathing style in healthy volunteers, under clear instruction [121]. However, the technique has been found to be somewhat more difficult to use on patients who may have breathing disorders or a more general lack of fitness that could preclude them from the procedure. In these events, patients were asked to give single exhalation samples only. The breath sample procedure for each volunteer, along with their age and gender is shown in Table 9.

Table 9: Table showing the age, gender and sample method for each participant in the study

Volunteer	Age Range: 81-23 Mean: 56	Gender Male: 14 Female: 10	Sample method
ABA1	52	M	Single exhalation
ABA2	58	M	3 cycle rebreathe
BS241	62	M	Single exhalation
JN241	70	F	Single exhalation
SB241	45	F	4 cycle rebreathe
RG01	81	M	Single exhalation
ET01	61	M	Single exhalation
SH01	66	F	Single exhalation
YL01	47	F	Single exhalation
RBU	44	F	4 cycle rebreathe
CMO	67	F	3 cycle rebreathe
MRU	69	M	Single exhalation
BMO	63	F	Single exhalation
TJ01	52	M	Single exhalation
GK0202	56	M	Single exhalation
JFL	62	M	Single exhalation
RHE	46	F	Single exhalation
TBO	52	F	4 cycle rebreathe
TA01	46	M	Single exhalation
FB0202	62	M	Single exhalation
RG241	63	M	Single exhalation
PAB	23	M	Single exhalation
MOH	39	F	4 cycle rebreathe
JNE	59	M	4 cycle rebreathe

4.4.3 Measurement details

To maximise the useful measurements of each breath sample a standard measurement procedure was decided upon. Samples were brought to the laboratory and measured from the earliest time of collection to the latest. The sample bag was placed in a heating jacket for at least 5 minutes to reach 40 °C. The PTR-MS was set-up with consistent lens voltages and hollow cathode conditions for each measurement. Before a measurement was taken, the background conditions of the PTR-MS were analysed by

recording the mass spectrum of a cleaned flow of nitrogen. This measurement provided an instrumental background.

After this background was taken, the sample bag was connected to the PTR-MS via a stainless steel and PTFE adapter. A set of two adapters were kept heated at 55 - 60 °C between measurements. The adapter was kept insulated while connecting the bag to the inlet of the PTR-MS. The PVC valve of the bag is opened with the mass spectrometer set up to monitor ions at m/z 37 (hydrate cluster), m/z 33 (methanol) and m/z 59 (acetone); three major contributions of breath. When each of these ion signals is viewed to have stabilised, it is assumed the PTR-MS is sampling air collected in the breath sample bag and mass spectra of the breath sample can be collected.

Mass spectra were collected from m/z 20 to 200 with a 0.5 second dwell time. Mass spectra were recorded first at a reduced electric field of ~138 Td, then ~115 Td and ~91 Td. This ensured that a 138 Td mass spectrum was recorded for each breath sample, and if enough sample remained further spectra would be collected at 115 Td and 91 Td. Two mass spectra were taken at each reduced electric field, sample volume allowing.

Where more than one sample was to be analysed in a session, the recorded sample was discarded, and the next sample was placed in the heating bag to warm. The stainless steel and PTFE adapter was cleaned by wiping the inlet with a 50:50 iso-propanol and water mix, followed by a flow of cleaned nitrogen. The adapter was returned to the oven to be heated to 55 - 60 °C. The PTR-MS background was again analysed using a clean flow of nitrogen. The second bag would be analysed using the same procedure as the first, using the second adapter. This procedure was repeated, alternating adapter, until each sample had been analysed.

4.5 Results

For each volunteer's breath sample a mass spectrum was recorded at a reduced electric field of 138 Td. The mass spectra were normalised to 5 million cps of the signal intensity of the H_3O^+ ion calculated from the $\text{H}_3^{18}\text{O}^+$ ion at m/z 21 and the hydrate cluster ($\text{H}_2\text{O}.\text{H}_3\text{O}^+$) at m/z 37. This allowed spectra to be compared without bias from the reagent ion signal.

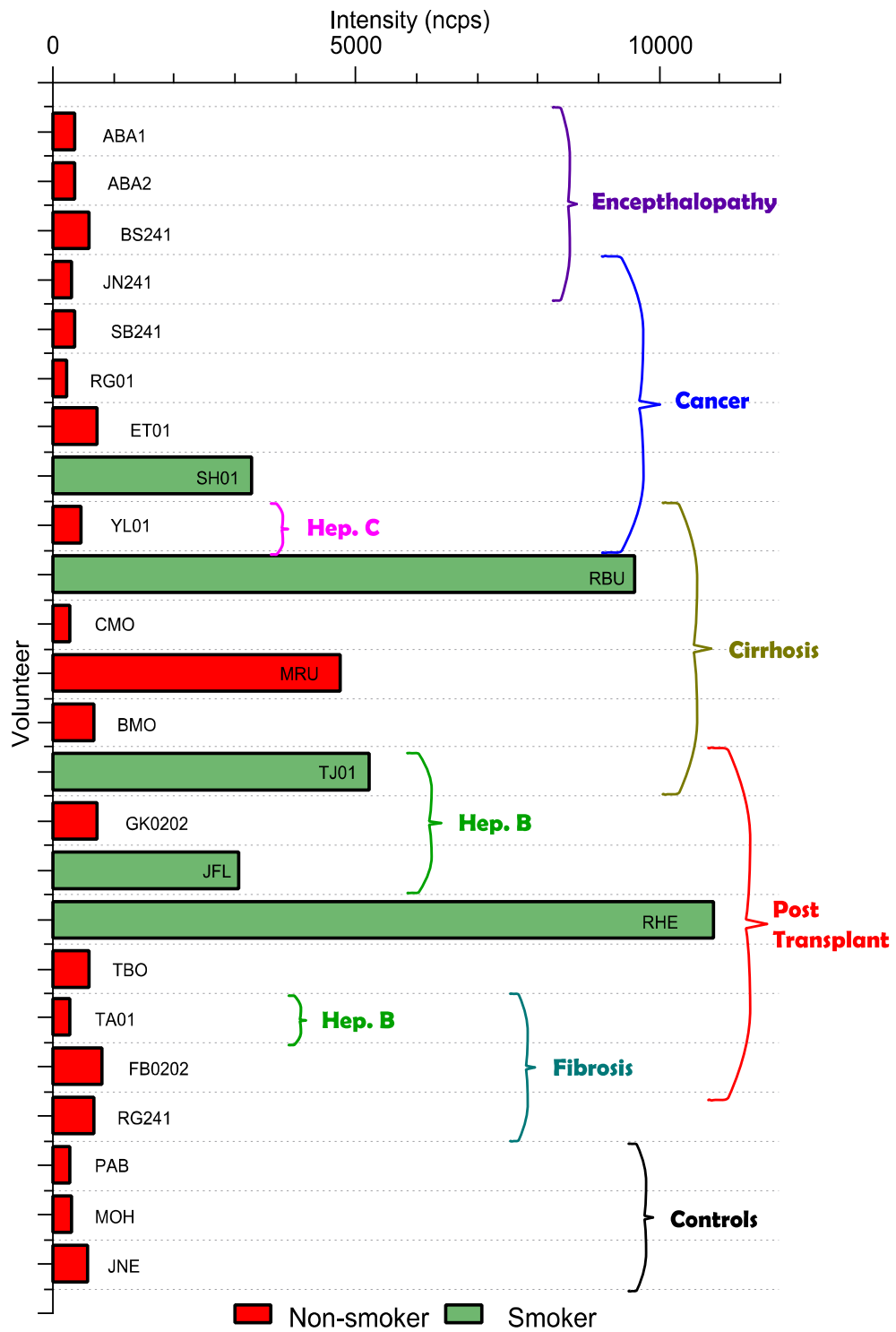
Peaks in the spectra that display interest, either as potential markers for liver disease, or comparison with markers found in other studies have been selected. To allow for distortions in the peak shape, the recorded intensity for each m/z value is taken as the maximum intensity found within 0.5 amu either side of the m/z .

4.5.1 Smokers

A previously identified and understood set of markers exist for smokers [111]. These markers are acetonitrile (MH^+ - m/z 42), benzene, (MH^+ - m/z 79) and toluene (MH^+ - m/z 93). The compounds are indicators of biomass burning; chemical constituents of smoke.

The signal detected at m/z 42 corresponding to protonated acetonitrile is shown in Figure 76 for each volunteer. The volunteers are divided in to two groups; those who identified themselves as smokers and those who identified as non-smokers. A clear correlation is observed between those patients who smoke and the prevalence of acetonitrile on their breath. The volunteer, MRU claims to have given up smoking, but the high signal of acetonitrile indicates that this patient is still a smoker. The volunteer has been left in the non-smoker bracket however, based on their response to the questionnaire.

Figure 76: Chart showing the intensity of the signal recorded at m/z 42 for each volunteer in the study.

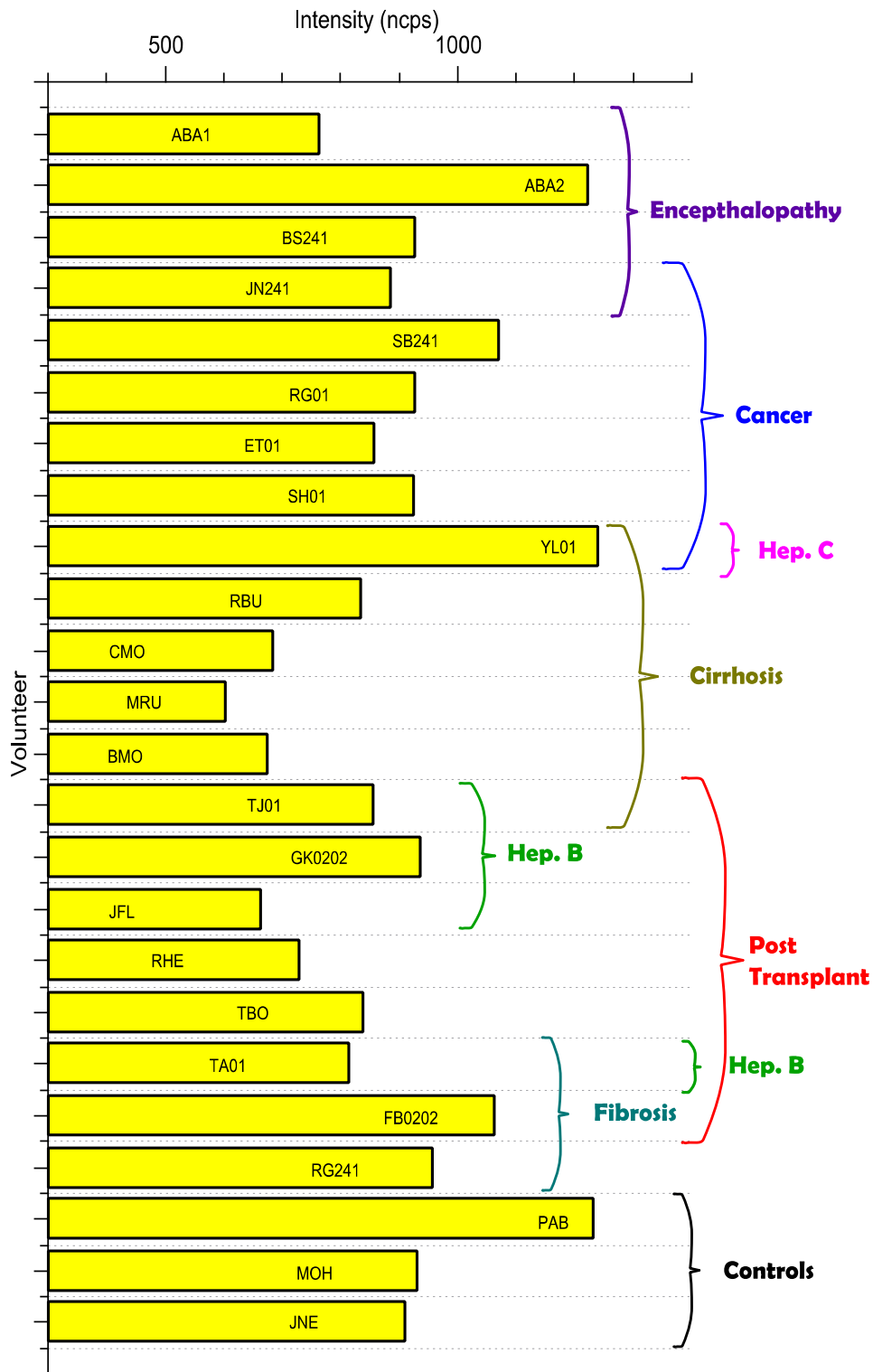


The good correlation observed for smokers and acetonitrile, provides a good confidence that the breath sampling has functioned well, allowing a clear distinction and grouping of patients to be made. With this confidence further correlations may be examined.

4.5.2 Volatile sulphurous compounds

Volatile sulphurous compounds have been the most abundantly reported compounds on the breath of those with liver disease. Dimethyl sulphide is one of these sulphurous compounds and has been associated with *foetor hepaticus* [100, 114, 115]. The protonated monomer, MH^+ of the compound would be present at m/z 63. The signal detected at m/z 63 was picked out from each mass spectrum and is shown in Figure 77.

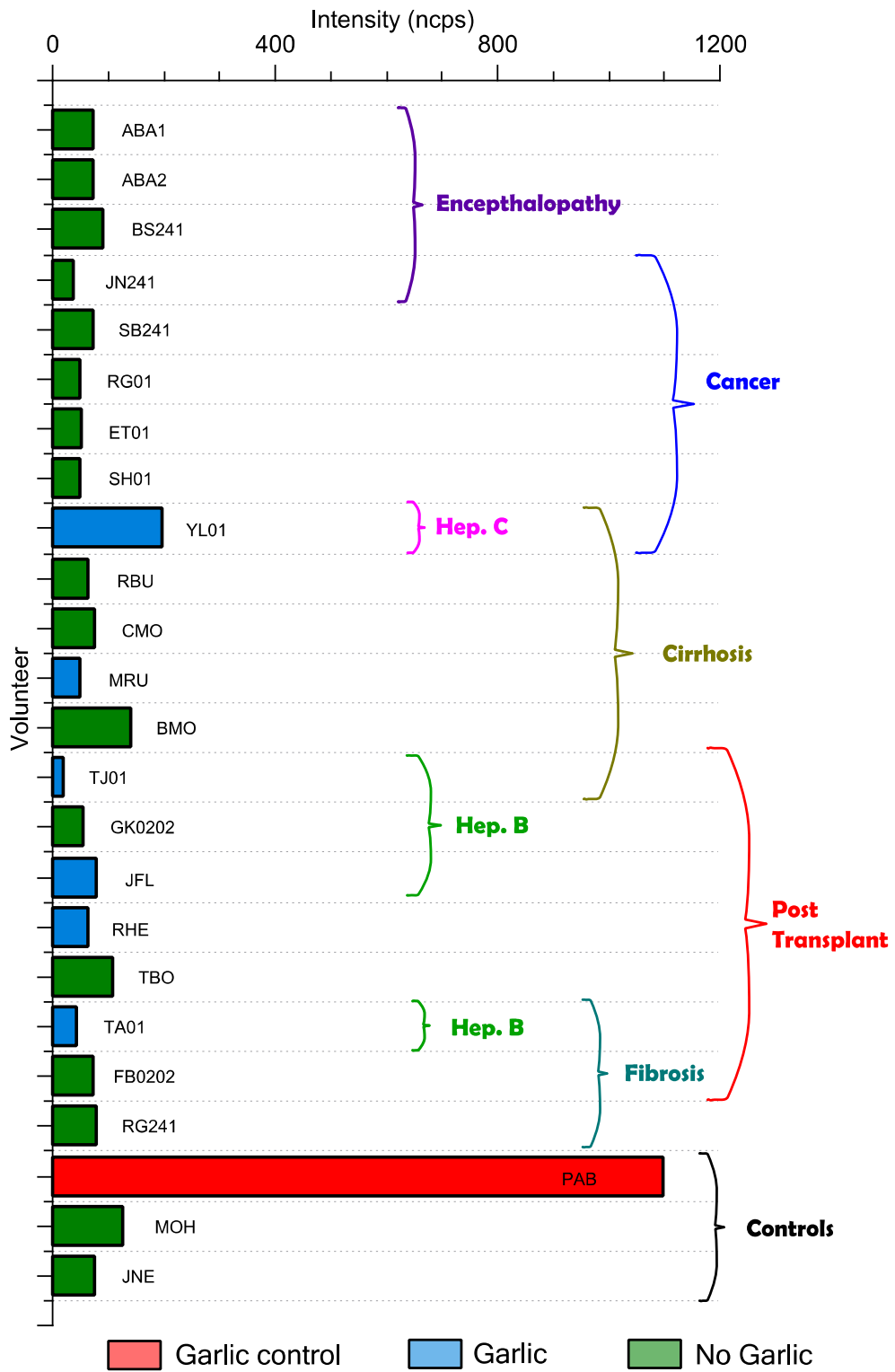
Figure 77: Data for each volunteer at m/z 63, which would correspond to the protonated monomer of dimethyl sulphide recorded at 138 Td.



No clear pattern for the appearance of m/z 63 is seen with either group, or between patients and controls. The highest intensity signals were observed for the volunteers, PAB, YL01 and ABA2. As described in Section 4.3, PAB had ingested a half clove of raw garlic; dimethyl sulphide has been reported as a constituent of 'garlic breath' [119, 120].

Figure 78 shows the collected data for each mass spectrum at m/z 49. A clear increase is shown for PAB. Methanethiol, CH_4S is a sulphurous compound, which is observed in elevated levels on the breath of PAB. The recorded levels of methanethiol indicate its possible use as a marker for the consumption of garlic. Figure 78 also shows how volunteers responded when asked if they had ingested garlic in the last 24 hours. Correlation of garlic consumption may depend on the raw or cooked nature of the garlic, or on time after ingestion. Methanethiol is broken down by bacteria in the gut to form dimethyl sulphide [114].

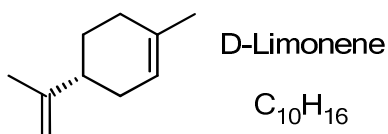
Figure 78: Data for each volunteer at m/z 49, which would correspond to the protonated monomer of methanethiol recorded at 138 Td.



4.5.3 Limonene

Limonene is a monocyclic monoterpene responsible for a large component of the flavour of citrus fruit. Monoterpenes are a class of hydrocarbon made of two isoprene molecules to form the chemical formula $C_{10}H_{16}$. A chemical structure diagram of limonene is shown in Figure 79.

Figure 79: Chemical structure of D-limonene



The report by Friedman identified limonene as a compound on the breath of patients with liver disease [116]. The patients suffered from a range of liver illnesses, not including encephalopathy. Elevated levels of limonene were recorded as seeming dependent on the type of liver disease; non-cholestatic liver disease patients showed increased levels of limonene when compared to cholestatic patients.

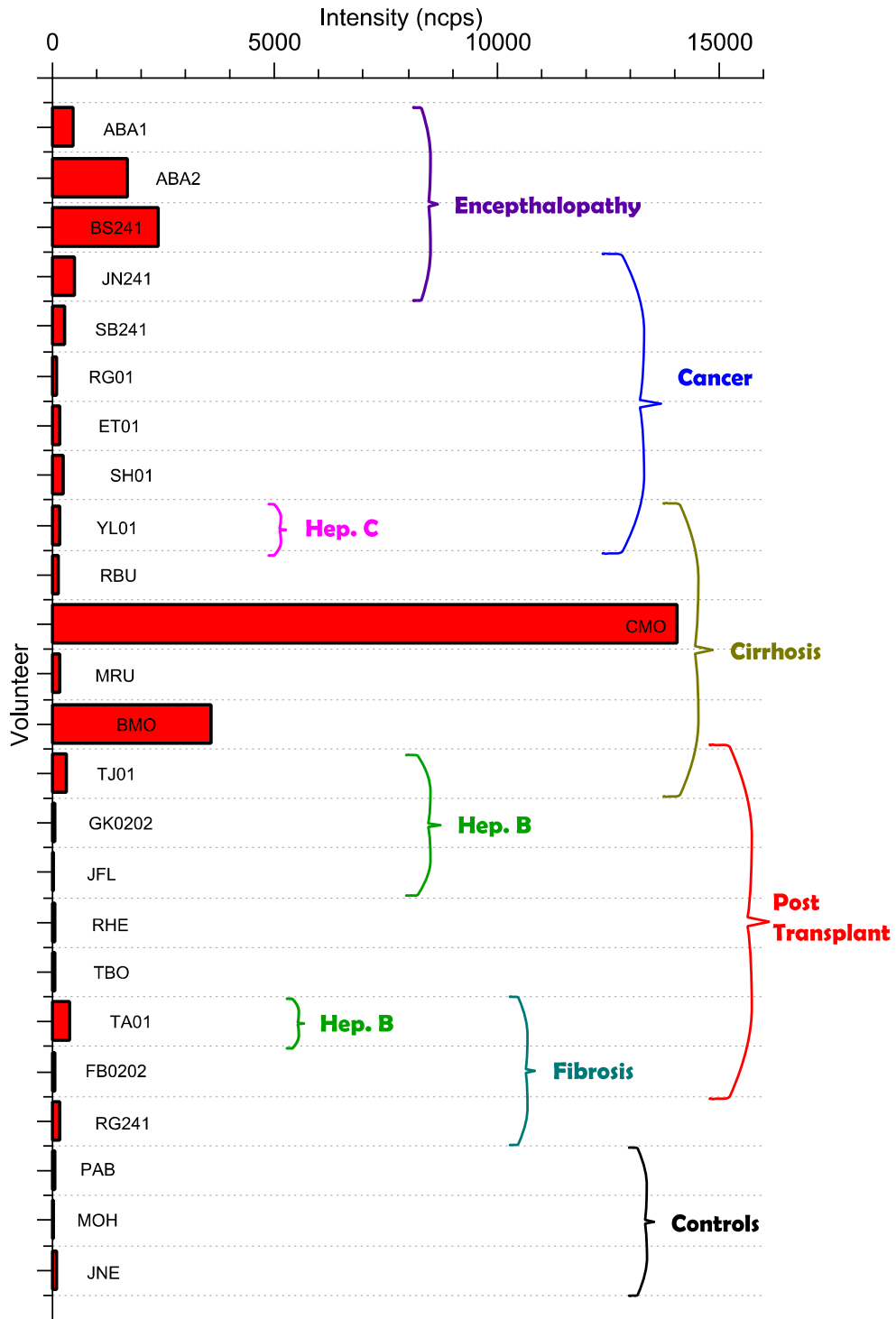
Cholestasis is a disease where bile is prevented from flowing from the liver to the duodenum. Hepatic and cirrhotic patients are not normally cholestatic, but the patients in our study were not formally defined with regards to cholestasis.

A recent report by Beauchamp and Buettner [126] indicated that limonene could be absorbed by the body from the environment and then released in a breath sample.

For this study, the collated data recorded for each volunteer at m/z 137 is shown in Figure 80. High signal peaks are observed for CMO and BMO, cirrhotic patients from the liver unit's clinic session. Elevated levels are also observed for each member of the encephalopathic group; ABA1, ABA2, BS241 and JN241. ABA1 and ABA2 were both

patients admitted to the liver ward for observation; BS241 and JN241 were patients at the liver unit's clinic.

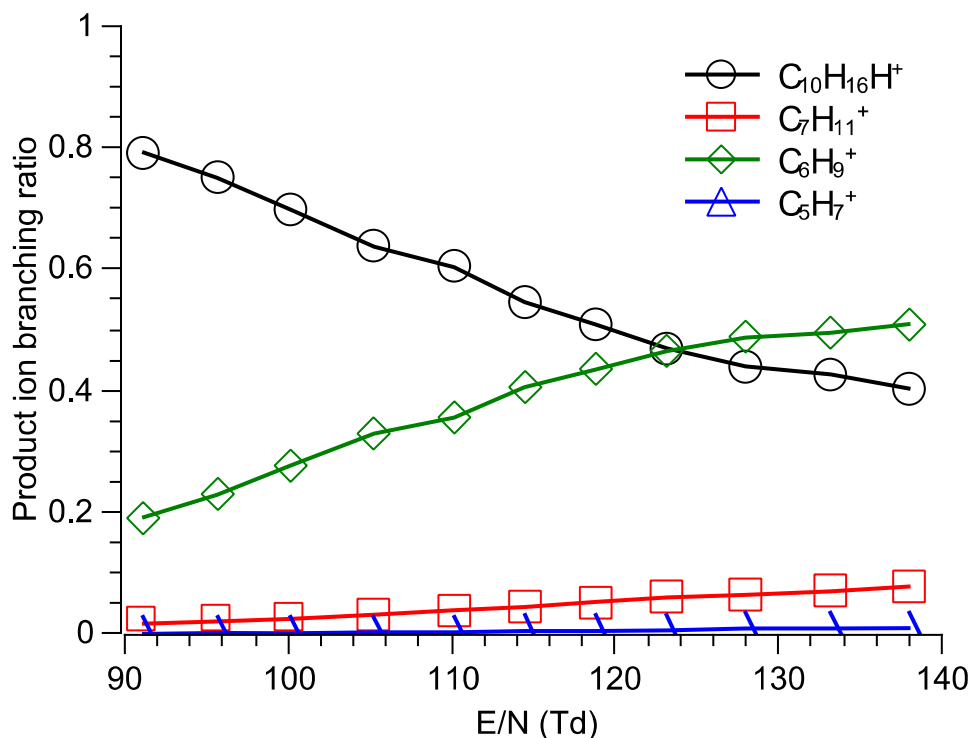
Figure 80: Data for each volunteer at m/z 137, which would correspond to the protonated monomer of limonene recorded at 138 Td.



To further understand the origin of the m/z 137 signal the product ions of D-limonene were recorded as a function of reduced electric field. A sample of limonene was measured with the PTR-MS via a similar method used to analyse the saturated alcohols, explained in Section 2.3.2. A couple of drops of limonene were transferred to a piece of cotton wool placed inside the barrel of a 10 ml plastic syringe. The plunger of the syringe was inserted to evacuate the barrel. With the syringe needle inserted into a flow of nitrogen the plunger was retracted, filling the syringe with limonene vapour and nitrogen, which could be injected into the flow of nitrogen to be measured by the PTR-MS. This set-up is outlined in Figure 19.

The results of this experiment are shown in Figure 81. Two major product ions were observed from the reaction between limonene and H_3O^+ ; MH^+ , m/z 137 ($\text{C}_{10}\text{H}_{16}\text{H}^+$) and $[\text{M}-\text{C}_4\text{H}_8]\text{H}^+$, m/z 81 (C_6H_9^+). Two lesser intensity product ions were observed at m/z 95 ($\text{C}_7\text{H}_{11}^+$) and m/z 67 (C_5H_7^+), corresponding to losses of C_3H_6 and C_5H_{10} respectively.

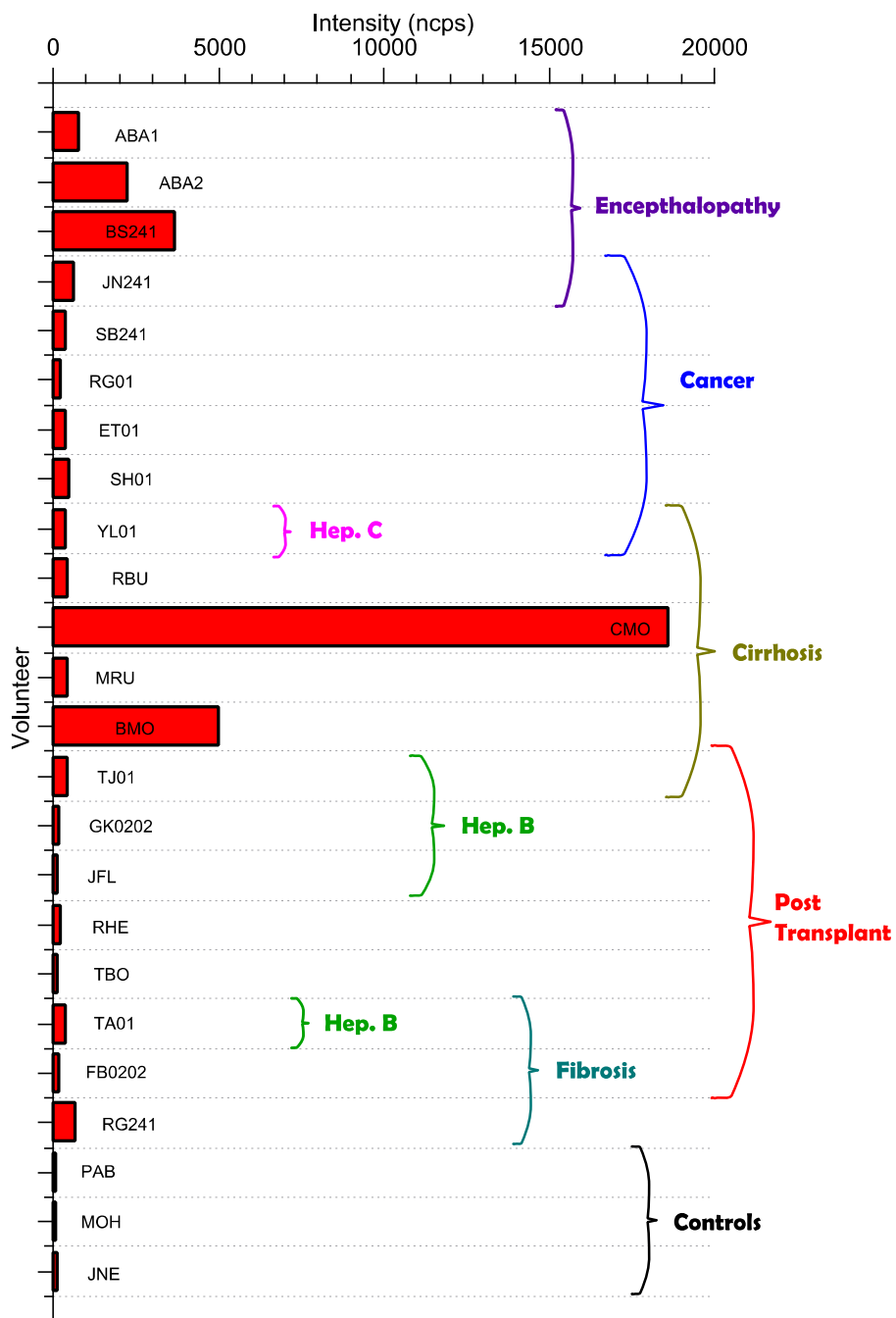
Figure 81: Product ion branching ratios for the reaction of limonene with H_3O^+ between a reduced electric field of 91-138 Td.



The data recorded in this study agrees well with the results reported by Tani et al. [39] and Steeghs et al. [44], who observed identical product ions. Tani et al. also report a very similar set of product ions produced for each monoterpene they analysed.

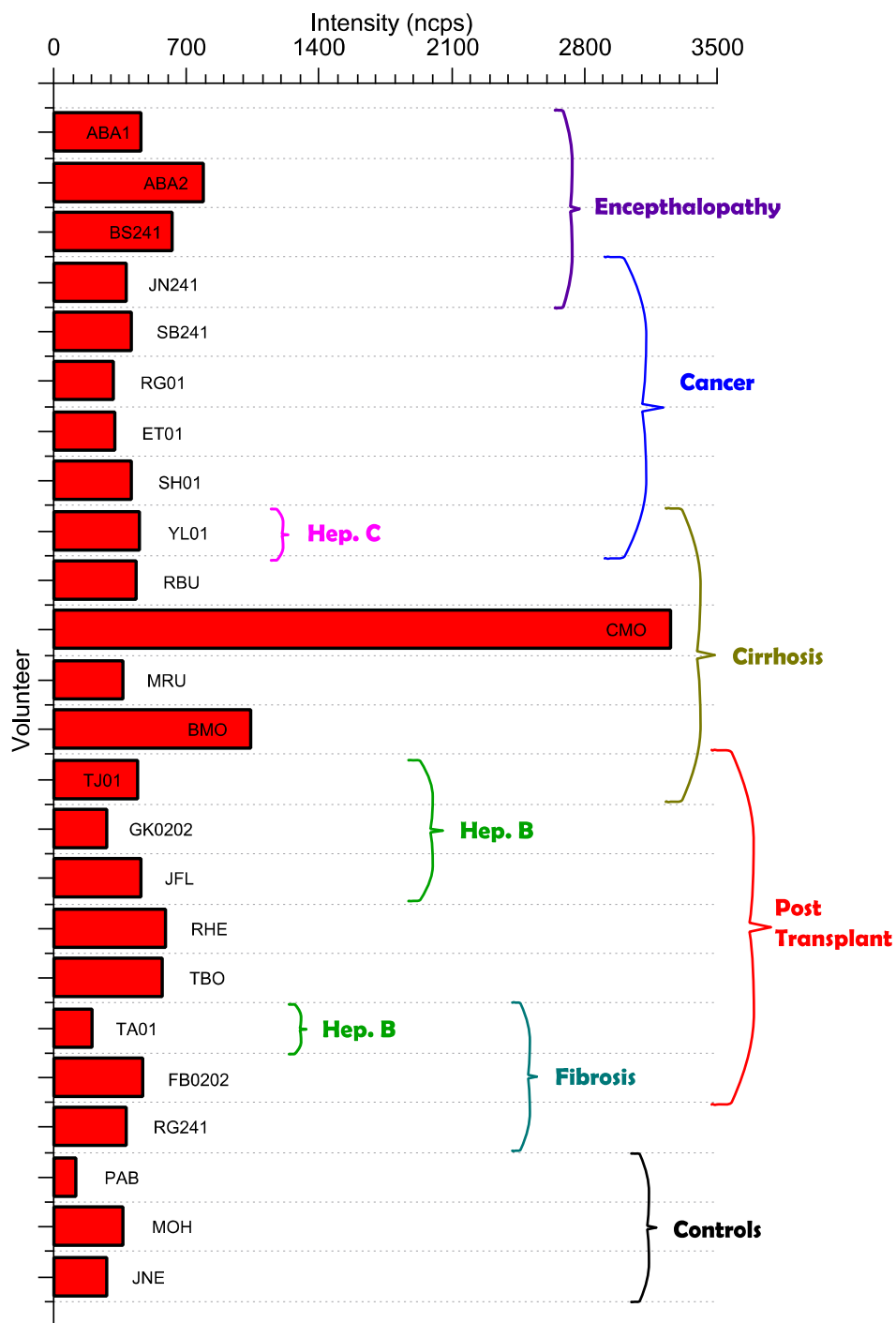
A strong correlation is observed for the peaks at m/z 81 and m/z 137 for each volunteer. The peak values recorded for m/z 81 are shown in Figure 82. Again very strong signals are recorded for both CMO and BMO, with visible signals seen for the encephalopathic group also. This gives a strong indication that the m/z 137 and m/z 81 peaks in the mass spectra of the volunteers are due to limonene, or another monoterpene.

Figure 82: Data for each volunteer at m/z 81, which would correspond to the $C_6H_9^+$ fragment ion of limonene recorded at 138 Td.



The fragment ion at m/z 95 records a similar effect, as shown in Figure 83. The correlation remains strong for CMO and BMO, but becomes less so for the encephalopathic patients, possibly due to a competing compound at m/z 95.

Figure 83: Data for each volunteer at m/z 95, which would correspond to the $C_5H_7^+$ fragment ion of limonene recorded at 138 Td.



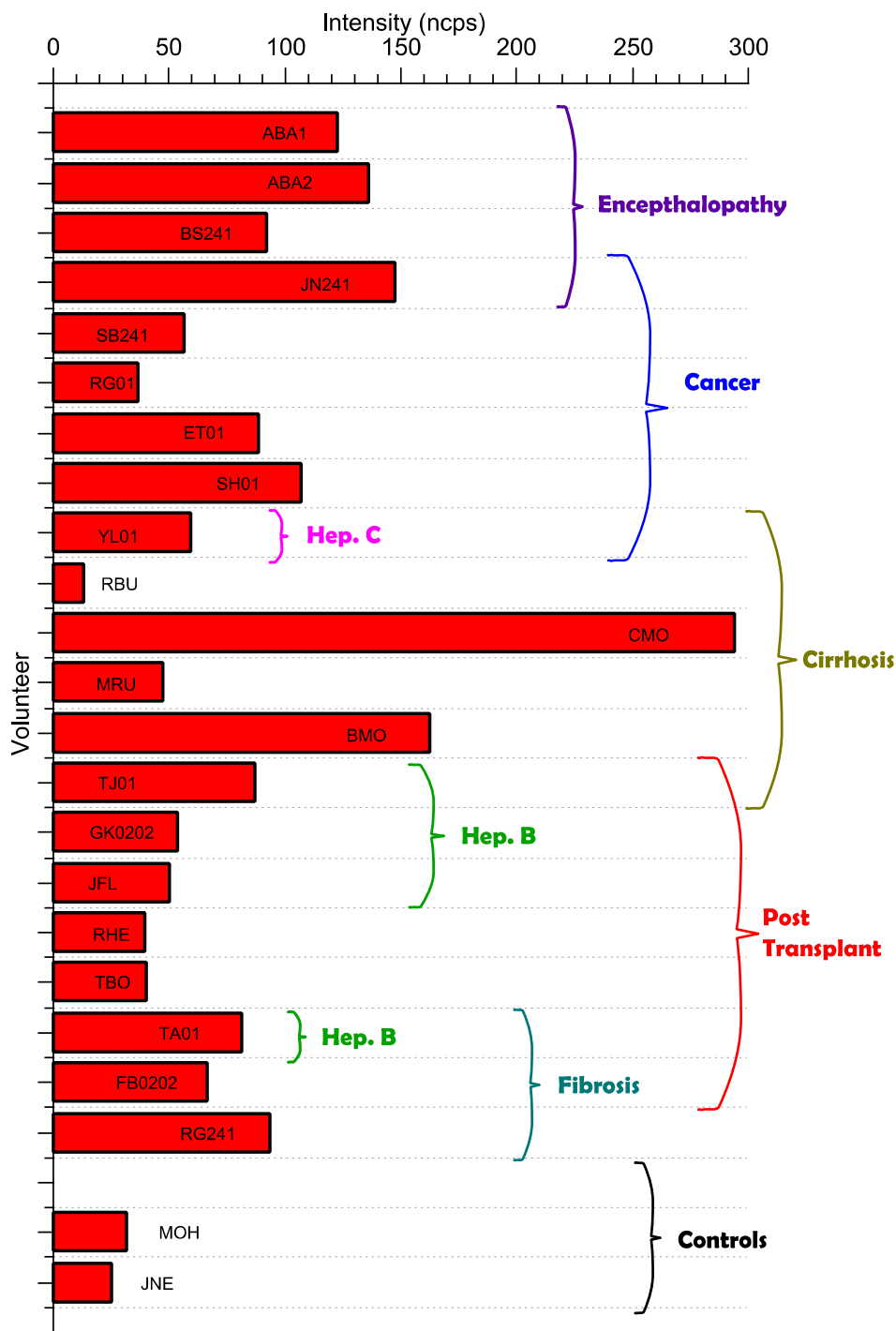
The interpretation of these results must be a cautious one. The low number of volunteers in each group negates the usefulness of treating the groups statistically as one.

The possibility exists, particularly given the use of monoterpenes as flavour and

fragrance additives, that the detected signals may be contaminants. An easily imaginable route to a monoterpene contamination may be from topical decongestants which contain the monoterpene pinene. Another ingredient in topical decongestants is camphor, $C_{10}H_{16}O$. The protonated monomer of camphor would appear at m/z 153. Figure 84 shows the data collected for each volunteer at m/z 153.

A correlation is observed between the appearance of the m/z 137 ion, for CMO and BMO. It may suggest that the CMO and BMO signals may be the result of contamination with a topical ointment, but no conclusions can be drawn. The source of the signals may be common to both CMO and BMO, given their consistent branching ratios for the product ions observed.

Figure 84: Data for each volunteer at m/z 153 recorded at 138 Td.



What can be proposed more definitely is that the signals in question at m/z 137, 81 and 95 do appear to be from a monoterpene. Whether this is due to contamination, or a possible marker for liver disease is a point that will be discussed later. To aid such a

discussion the reproducibility of breath sampling has also been analysed and commented upon.

4.6 Consistency of Breath Samples

No repeat samples were taken during the liver study, preventing any measurement of the sampling consistency. However, a second, uncompleted study did take repeat measurements and samples of breath. The study was initiated to monitor the effects of chemotherapy using breath analysis. The study failed to engage a large enough patient sample to analyse the effects of chemotherapy, but the data has been used to analyse the consistency of breath sampling using a PTR-MS. The results of this analysis are displayed in this section, along with descriptions of the trial's initial purpose and methodology.

4.6.1 Purpose of the chemotherapy study

As part of the PhD studies of a research colleague, Dr. Shane O'Hehir [127] ethical approval was achieved for a study using the PTR-MS to analyse the breath of patients undergoing chemotherapy; for which O'Hehir was the chief investigator. Comparison was to be made with blood tests to gain an insight into the possible effectiveness of breath sampling as a technique in optimising chemotherapy dosing.

The trial was organised in conjunction with a larger trial, for which Dr. Dan Rea of the oncology department at the Queen Elizabeth Hospital, Birmingham was principal investigator. The trial was begun by me with guidance from O'Hehir; all sample collection, measurements and analyses presented as part of this trial were performed by me.

The trial's aim was to recruit 10 patients undergoing their initial chemotherapy treatment and take three samples from each patient, on three occasions. Samples were

to be taken before their first treatment, at their nadir; midway between their first and second treatments, and before their second treatment.

The full criteria of patients were not measured by the study. Four patients gave at least one sample, two reaching completeness, giving 9 sampling opportunities and 27 samples in total. With only two patients recruited who completed the trial procedure, any conclusions about the effectiveness of breath sampling to monitor chemotherapy dosing have been inhibited. However, the results have been analysed toward a discussion of the consistency of sampling and measurement techniques.

4.6.2 Methodology of the chemotherapy study

For each sampling opportunity, three samples were taken and transported to the Molecular Physics lab to be analysed by the PTR-MS. Patients received a patient code to make their data anonymous. A summary of the patient samples collected is shown in Table 10. Patient code; PAB001 withdrew from the study without submitting a sample.

Table 10: Table of patient samples collected for the chemotherapy study.

Patient	1 st sample	Nadir sample	Final sample
PAB002	07.05.2010	19.05.2010	x
	The patient was unable to provide a final sample due to an MRSA infection which precluded her access to the CRF.		
PAB003	05.08.2010	x	x
	The patient gave only a first sample, this was because of hardware failure.		
PAB004	15.10.2010	25.10.2010	05.11.2010
	Patient completed trial.		
PAB005	24.05.2011	04.06.2011	13.06.2011
	Patient completed trial.		

Samples were obtained using a rebreathing protocol developed and explained by O’Hara et al. [121, 122] and commented on in Section 4.4.1. The protocol required patients to provide a sample by filling a sampling bag with a full exhalation from a full inhalation. The bag’s valve was then closed. The patient was then fitted with a nose clip and asked to wear a pulse oximeter to monitor their percentage of oxygenated haemoglobin.

Patients were then asked to complete 4 cycles of 5 breaths using the bag as a reservoir for inhalation. The patient began each cycle by breathing out fully, then inhaling from the bag and exhaling this breath back into the bag, all with their mouth connected to the bag by a diver’s style mouth piece. Four further breaths would be taken in this style to complete a cycle, each without removing the mouth piece. After each cycle the valve was closed and the patient rested. During these cycles the bag was heated to 40 °C, maintaining isothermal conditions. If the patient’s level of oxygenated haemoglobin dropped below 90 % or changed by greater than 5 %, they would be instructed to stop the protocol; no such action was necessary.

For each sampling occasion three samples of breath were taken from each patient, the samples were stored in Teflon sample bags with 0.5 mm wall thickness, similar in construction to the bags illustrated in Figure 71 with fastenings and valves shown in Figure 72 and Figure 73 and explained in Section 4.3.

It was aimed that each sample would be analysed at three different values of reduced electric field; 138, 115 and 91 Td. Each sample was analysed with the PTR-MS using an analogue mass scan between m/z 20 and 200, with a 0.5 second dwell time.

The bags were heated to 40 °C for each measurement. Two machined stainless steel adapters were used to connect the customised EAF fittings to the PTR-MS inlet. One adapter would be used at a time; the adapter was flushed with nitrogen and heated to 55 - 60 °C before measurement, and an insulating synthetic fabric was placed around the adapter during measurement to prevent cold spots. Adapters were cleaned with a 50:50 iso-propanol and water mix and flushed with nitrogen after measurement and heated again to 55 - 60 °C; using alternate adapters the bags could be measured in efficient time.

Between each new sample a flow of white spot nitrogen was measured to set the instrumental background of the PTR-MS, and to check that the compounds in the previous sample had cleared sufficiently from the system to avoid contamination.

Each sample was analysed at three settings of reduced electric field; 91, 115 and 138 Td. At each reduced electric field three scans were taken, where sufficient sample was available. Often software glitches could occur in recorded spectra, so three scans were taken to allow for this. Scans were always recorded at 138 Td first to ensure that all samples would have a comparable reduced electric field. Later scans were taken at 115

Td and 91 Td provided sufficient sample remained. Analysis in this section will be concerned only with scans taken at 138 Td.

The resulting data set is large in terms of repeat measurements in comparison with the data set collected from liver patients where no repeats were available. Data collection for both studies was performed using the same 0.5 second dwell time. This will allow the chemotherapy data to provide some information about the reproducibility of breath samples taken as part of the liver study.

4.7.3 Results

Five m/z values have been selected for analysis. Ions at m/z 59 and 69 were selected, corresponding to acetone and isoprene; two compounds that have been studied on breath using PTR-MS [90, 95, 128, 129], particularly by O'Hara et al. in comparison with blood values [128]. Isoprene and acetone have been chosen for analysis to enable comparison with some of these previous studies.

Further ions at m/z 33 and 47 were analysed, corresponding to methanol and ethanol respectively, again commonly observed breath compounds. Methanol and ethanol are both alcohol compounds with similar properties, but are detected at very different signal intensities; for this reason they were chosen to reflect the repeatability of the technique over a range of intensity. Finally ions at m/z 137 were also picked out for analysis to try to observe evidence of monoterpene detection to compare with the signal observed with the liver patients.

Signal intensity was calculated for the five m/z values by finding the maximum signal intensity within a 0.5 amu range of the m/z value being investigated. This value was then normalised to 5 million cps of the sum of the m/z 19 (H_3O^+) and 37 ($\text{H}_3\text{O}^+\cdot\text{H}_2\text{O}$) signals.

4.6.3.1 Statistical analysis for repeatability

For a comparison of repeatability it is useful to have a standard method to calculate a value by which the repeatability may be judged. Work by O'Hara et al. [130] used a method suggested by Bland and Altman [131] to calculate a repeatability factor, R. factor. As a comparison between the study of O'Hara et al. and this study may be beneficial, the same technique will be used.

For a series of repeat measurements of the same subject, it is generally assumed the measurements will not be the same. The variation may be caused by natural changes in the subject, the sample's consistency as a reflection of the subject, or the accuracy of the measurement procedure itself.

For a set of repeat measurements an average value can be calculated. If the distribution of measurements is assumed to be normal, the mean should reflect a true value for the measurement. The standard deviation of these measurements will give an understanding of the repeatability of the technique; 68 % of measurements should lie within one standard deviation of the mean.

This trial can examine two sources of error affecting the repeatability; the measurement accuracy and the sample consistency. The repeatability of measurements taken from the same sample should be affected only by the measurement accuracy. Whereas, repeat samples will be affected by the accuracy of the measurements, the sample's consistency and the patient's natural variability.

4.6.3.1.1 Analysis of measurement accuracy

The analysis of repeat measurements from the same sample has been performed by finding the mean and variance for each set of repeats. Each measurement produces a spectrum. 27 samples were analysed in total; of these samples, 14 had three useable

spectra recorded, 9 had two usable spectra, and 4 had one useful spectrum recorded. Samples with only one spectrum recorded have been omitted from this section of the analysis.

For samples with more than one spectrum the mean and variance for each sample was calculated. The average variance across all samples was used to find the average standard deviation, σ . The average of the mean was also taken for each m/z value. These values are shown in Table I I.

In accordance with work by Bland and Altman [131], and to compare the data with the results of O'Hara et al. [122] the samples repeatability factor was also calculated. The value, 1.96σ is the range either side of the mean that a measurement will lay within 95 % of the time. For two measurements, they are expected to lie within the range, $\sqrt{2} \times 1.96 \sigma$ or 2.77σ for 95 % of measurements. This factor is known as the repeatability factor and is shown in Table I I for the five investigated m/z values.

Table I I: Scan accuracy for measurements of acetone, isoprene, methanol, ethanol and monoterpene, showing standard deviation and repeatability.

Compound	Mean ncps	St. Dev. ncps	St. Dev. % of mean	R. factor ncps	R. factor % of mean
Acetone	49830	2789	6	7724	16
Isoprene	6482	420	7	1165	18
Methanol	8412	545	7	1510	18
Ethanol	1000	185	19	513	51
Monoterpene	187	35	19	96	51

4.6.3.1.2 Analysis of sample consistency

A further examination of repeatability can be made by examining the sample consistency. Using the mean values for each sample with more than one spectrum, along with each single spectrum sample's value, the variance and mean of a patient's samples on a particular day can easily be calculated. Each of the nine sampling opportunities yielded three samples.

Each mean and variance from the nine sampling days can be used to calculate an average standard deviation for each of the five m/z values. The standard deviation is shown in Table 12, along with the repeatability factor, calculated again as 2.77σ .

Table 12: Sample consistency for measurements of acetone, isoprene, methanol, ethanol and monoterpene, showing standard deviation and repeatability.

Compound	Mean ncps	St. Dev. ncps	St. Dev. % of mean	R. factor ncps	R. factor % of mean
Acetone	49205	4157	8	11515	23
Isoprene	6674	1150	17	3185	48
Methanol	7801	684	9	1896	24
Ethanol	1047	275	26	762	73
Monoterpene	187	42	22	115	62

4.6.4 Discussion of repeatability

The measurement repeatability and sample repeatability will be discussed in turn, with appropriate comparison made between the two. A comparison with the data of this study and similar results for methanol, acetone and isoprene collected by Steeghs et al. [129] will be made, along with results recorded by O'Hara et al. [122] for acetone and isoprene.

4.6.4.1 Discussion of measurement repeatability

For every compound analysed the measurement repeatability was better than the sample repeatability. This is an obvious expectation as the sampling repeatability will be limited by the measurement repeatability.

The measurement repeatability is shown in Table I I. At higher mean signal intensity the repeatability improves as a fraction of that mean. At greater signal intensity the statistical error in measurement becomes less effective, thus the repeatability should improve for higher intensity ion signals.

Acetone shows the best measurement repeatability as a fraction of the mean and the highest signal intensity, (10^4) of all five compounds examined. Methanol and isoprene show similar intensity (10^3) and similar repeatability. Ethanol and monoterpene both show similar repeatability, in spite of their different signal intensities; ethanol – 10^3 , monoterpene - 10^2 .

4.6.4.2 Discussion of sample repeatability

The repeatability of the sample is less clearly dependent on the mean intensity, with the nature of the compound also affecting its repeatability. Isoprene shows a worse repeatability than methanol, whereas their measurement repeatability was similar. This implies that the isoprene concentration in repeat samples is more variable than the methanol concentration.

Changes in the concentration of isoprene have been observed to be rapid at the onset of exercise [90]. The rebreathing technique may be causing similar metabolic mechanisms to become active, thus varying the concentration of isoprene during the sampling procedure, contributing to the poorer repeatability.

Solubility may also affect a compound's repeatability. The solubility of isoprene is lower than that of methanol and acetone. Table 13 shows the blood : gas partition coefficients for the compounds analysed; the higher the coefficient the more soluble the gas is in blood. Higher solubility compounds can exchange between blood and breath higher in the respiratory system; in the airways rather than the alveoli [123]. This would increase the volume over which exchange can occur, which for a rebreathing technique, may cause a more representative and reproducible concentration of the compound in the breath sample. This may also contribute to the better repeatability when sampling methanol as opposed to isoprene.

Table 13: Values of blood : gas partition coefficients for acetone, isoprene, methanol, ethanol and limonene.

Compound	Blood : Gas partition coefficients
Acetone	341 [123]
Isoprene	0.75 [132]
Methanol	2709 [123]
Ethanol	1756 [123]
Limonene	36 [133]

To aid the comparison with other studies into the repeatability of breath sampling, Table 14 and Table 15 show the results obtained by Steeghs at al. [129] and O'Hara et al. [122], respectively. The data is in reasonable agreement with that of our study. Steeghs et al. observed similar standard deviations for methanol, acetone and isoprene. Methanol was observed to have the best repeatability, as reported by Steeghs et al., using a single exhalation sampling method of the American Thoracic Society to measure end exhaled breath.

Table 14: Table showing sample reproducibility for methanol, isoprene and acetone; as found by Steeghs et al. [129].

Compound	Volunteer 1		Volunteer 2	
	Mean / ppb	Relative standard deviation / %	Mean / ppb	Relative standard deviation / %
Methanol	32	5.6	67	4.9
Acetone	158	11	80	5.6
Isoprene	18	29	17.9	6.6

O'Hara et al. used the same rebreathing technique as was employed by our study. Their results show better repeatability, but they are in reasonable agreement; with acetone measurements observed to be more repeatable than isoprene.

Table 15 shows the results presented by O'Hara et al., also showing the repeatability of acetone and isoprene measured by GC-MS in arterial and venous blood. The repeatability values for this study, shown in Table 12 are better than those reported for both venous and arterial blood by O'Hara et al. [122].

Table 15: Table showing sample reproducibility for acetone and isoprene for breath, arterial blood and venous blood; as found by O'Hara et al. [122].

Compound	Breath		Arterial blood		Venous blood	
	Mean / ppb	R. factor / %	Mean / ppb	Repeatability / %	Mean / ppb	R. factor / %
Acetone	956	19	21	101	17	79
Isoprene	465	27	6.8	79	14	81

4.6.5 Conclusion of the study into the repeatability of breath analysis

The repeatability of breath analysis using the PTR-MS and rebreathing technique has been examined in this section. The repeatability of both the measurement and sampling

has been analysed. The measurement has been shown to be a major contribution to the overall sample accuracy. In part, measurement accuracy of breath samples is hampered by sample volume constraints; more time measuring the sample can improve statistical accuracy, but the time that the sample can be scanned for is limited by the sample volume available to measure.

Measurement methods like TOF or ITMS can overcome this scanning problem, by capturing a wide range mass spectrum in less time, using up less of the sample than quadrupole scanning [13, 134-137]. Quadrupole mass analysers are still very useful in proton transfer reaction mass spectrometry, owing to their very high sensitivity; where sampling time is of limited concern, or where the ions to be monitored are already known the technique remains useful.

4.7 Discussion of Limonene

In analysis of the monoterpene at m/z 137, the repeatability factor of 62 % suggests that the monoterpene signal observed for encephalopathic patients is a real signal. The signals measured for encephalopathic patients are in some cases more than three times the signal observed for non-encephalopathic patients. However, the importance of the signal cannot be understood without further examination of breath samples from encephalopathic patients.

The origin of the compound is most likely exogenous, either dietary or an inhaled citrus scent. It is interesting that in considering this, Friedman [116] was not able to explain the increased limonene observed as purely the result of increased limonene consumption. Encephalopathy is a condition caused by excessive amounts of nitrogen compounds in the blood, affecting brain function. The excessive nitrogen compounds originate in the gut, and are allowed to enter the systemic circulation because of

impaired liver function. The condition is managed in part by nutritional control; consumption of protein is reduced to allow recovery, and slowly increased to tolerable levels [138].

These factors indicate that the study of limonene concentration on the breath of liver disease patients, with particular focus on encephalopathic patients may yield some interesting discoveries.

4.8 Conclusions and Further Work

This study has highlighted a possibly exciting area of breath research; the analysis of liver function by means of proton transfer reaction mass spectrometry of breath. Although only tentative, initial conclusions about possible markers can be drawn and other comments may be made.

A monoterpene signal at m/z 137 was observed to be elevated in encephalopathic patients. Encephalopathy is a disorder characterised by a nutritional dependence. The disease is often difficult to diagnose, requiring a non-empirical and time consuming evaluation of a patient's mental capabilities. With further cooperation the condition may be well suited to monitoring with breath analysis, providing the validity of markers can be realised.

The rebreathing sampling procedure implemented by O'Hara et al. [121] was found inadequate for use with patients due to its complexity. Encephalopathic patients were particularly troubled at having to perform this procedure due to their reduced mental capacity. Single exhalations were taken from patients where either their health or mental capacity prevented rebreathing. A further improvement to the sampling procedure beyond this may be the implementation of an end tidal volume breath

sampler. This type of sampler allows the end exhaled breath to be sampled, providing a more accurate value for alveolar air than a single full exhalation.

The repeatability for rebreathed samples taken as a part of an aborted study into chemotherapy dosing has also been presented. Good comparison has been observed with the repeatability of other breath sampling investigations using a PTR-MS.

Further studies in this field are of clear importance to developing the use of breath analysis as a serious diagnostic tool in medical research. A larger scale study of liver disease patients, focusing on encephalopathic patients with the possibility of time evolved data and control of diet would provide a sounder basis on which to found further research. The possible benefits of this research implore its development, and the contribution of proton transfer reaction mass spectrometry to this development could be of great importance.

References

- [1] W. Lindinger, A. Hansel, A. Jordan, *International Journal of Mass Spectrometry and Ion Processes*, (1998) 191-241.
- [2] R.S. Blake, P.S. Monks, A.M. Ellis, *Chemical Reviews*, 109 (2009) 861-896.
- [3] J. de Gouw, C. Warneke, *Mass Spectrometry Reviews*, 26 (2007) 223-257.
- [4] A. Lee, A.H. Goldstein, J.H. Kroll, N.L. Ng, V. Varutbangkul, R.C. Flagan, J.H. Seinfeld, *Journal of Geophysical Research-Atmospheres*, 111 (2006).
- [5] C.N. Hewitt, S. Hayward, A. Tani, *Journal of Environmental Monitoring*, 5 (2003) 1-7.
- [6] Y. Wang, C. Shen, J. Li, H. Jiang, Y. Chu, Proton Transfer Reaction Mass Spectrometry (PTR-MS), in: M.S. Lee (Ed.) *Mass Spectrometry Handbook*, John Wiley & Sons, 2012, pp. 605-631.
- [7] M. Steeghs, H.P. Bais, J. de Gouw, P. Goldan, W. Kuster, M. Northway, R. Fall, J.M. Vivanco, *Plant Physiology*, 135 (2004) 47-58.
- [8] R. Fall, T. Karl, A. Jordan, W. Lindinger, *Atmospheric Environment*, 35 (2001) 3905-3916.
- [9] E. Crespo, M.M.L. Steeghs, S.M. Cristescu, F.J.M. Harren, Proton Transfer Reaction Mass Spectrometry: Applications in the Life Sciences, in: M.S. Lee (Ed.) *Mass Spectrometry Handbook*, John Wiley & Sons, 2012, pp. 1257-1281.
- [10] S.L. Shaw, F.M. Mitloehner, W. Jackson, E.J. Depeters, J.G. Fadel, P.H. Robinson, R. Holzinger, A.H. Goldstein, *Environmental Science & Technology*, 41 (2007) 1310-1316.
- [11] M. O'Hara, C.A. Mayhew, *Journal of Breath Research*, (2009) 027001.
- [12] M.M.L. Steeghs, B.W.M. Moeskops, K. van Swam, S.M. Cristescu, P.T.J. Scheepers, F.J.M. Harren, *International Journal of Mass Spectrometry*, 253 (2006) 58-64.
- [13] H. Jens, M. Markus, S. Simon, T. Thorsten, G. Martin, H. Armin, *Journal of Breath Research*, (2009) 027004.
- [14] G.R. Harrison, A.D.J. Critchley, C.A. Mayhew, J.M. Thompson, *British Journal of Anaesthesia*, 91 (2003) 797-799.
- [15] K. Schwarz, W. Filipiak, A. Amann, *Journal of Breath Research*, (2009) 027002.
- [16] F. Wieland, A.N. Gloess, M. Keller, A. Wetzel, S. Schenker, C. Yeretian, *Analytical and Bioanalytical Chemistry*, 402 (2012) 2531-2543.
- [17] C. Soukoulis, E. Aprea, F. Biasioli, L. Cappellin, E. Schuhfried, T.D. Märk, F. Gasperi, *Rapid Communications in Mass Spectrometry*, 24 (2010) 2127-3134.
- [18] S. Jurschik, P. Sulzer, F. Petersson, C.A. Mayhew, A. Jordan, B. Agarwal, S. Haidacher, H. Seehauser, K. Becker, T.D. Mark, *Analytical and Bioanalytical Chemistry*, 398 (2010) 2813-2820.
- [19] C.A. Mayhew, P. Sulzer, F. Petersson, S. Haidacher, A. Jordan, L. Märk, P. Watts, T.D. Märk, *International Journal of Mass Spectrometry*, 289 (2010) 58-63.
- [20] R.L. Cordell, K.A. Willis, K.P. Wyche, R.S. Blake, A.M. Ellis, P.S. Monks, *Analytical Chemistry*, 79 (2007) 8359-8366.
- [21] F. Petersson, P. Sulzer, C.A. Mayhew, P. Watts, A. Jordan, L. Märk, T.D. Märk, *Rapid Communications in Mass Spectrometry*, 23 (2009) 3875-3880.
- [22] D.A. Steele, R.D. Short, P. Brown, C.A. Mayhew, *Plasma Processes and Polymers*, 8 (2011) 287-294.
- [23] P. Brown, P. Watts, T.D. Mark, C.A. Mayhew, *International Journal of Mass Spectrometry*, 294 (2010) 103-111.
- [24] J. Gross, Efficiency of Electron Ionization, in: *Mass Spectrometry: A Textbook*, Springer, 2004, pp. 196-197.

- [25] S.G. Lias, J.E. Bartmess, J.F. Liebman, J.L. Holmes, R.D. Levin, W.G. Mallard, Gas-Phase Ion and Neutral Thermochemistry, American Chemical Society and the American Institute of Physics, 1988.
- [26] E. Hunter, S. Lias, NIST Chemistry WebBook, Proton Affinities, in, 2009.
- [27] D. Smith, P. Španěl, Mass Spectrometry Reviews, 24 (2005) 661-700.
- [28] A. Hansel, A. Jordan, R. Holzinger, P. Prazeller, W. Vogel, W. Lindinger, International Journal of Mass Spectrometry, 150 (1995) 609-619.
- [29] F. Clementschitsch, K. Bayer, Microbial Cell Factories, 5 (2006) 19.
- [30] K.H. Schoenbach, A. El-Habachi, W. Shi, M. Ciocca, Plasma Sources Science and Technology, (1997) 468.
- [31] S. Lias, NIST Chemistry WebBook, Ionization Energy Data, in, 2009.
- [32] Y. Kawai, O. Yamaguchi, K. Takeuchi, Y. Yamauchi, S. Ozawa, H. Nakai, Chemical Physics Letters, (2003) 69-73.
- [33] Balzers, Partial Pressure Measurement in Vacuum Technology, Principality of Lichtenstein, 1989.
- [34] P.E. Miller, M.B. Denton, Journal of Chemical Education, 63 (1986) 617-622.
- [35] C. Dass, Fundamentals of contemporary mass spectrometry, John Wiley and Sons, 2007.
- [36] C. Warneke, C. van der Veen, S. Luxembourg, J.A. de Gouw, A. Kok, International Journal of Mass Spectrometry, 207 (2001) 167-182.
- [37] P. Sulzer, F. Petersson, B. Agarwal, K.H. Becker, S. Jurschik, T.D. Mark, D. Perry, P. Watts, C.A. Mayhew, Analytical Chemistry, 84 (2012) 4161-4166.
- [38] Sigma-Aldrich Safety Data Sheet, in: S.-A. Co. (Ed.), 2011.
- [39] A. Tani, S. Hayward, C.N. Hewitt, International Journal of Mass spectrometry, 223-224 (2003) 561-578.
- [40] A. Tani, S. Hayward, A. Hansel, C.N. Hewitt, International Journal of Mass spectrometry, 239 (2004) 161-169.
- [41] S. Kim, T. Karl, D. Helmig, R. Daly, R. Rasmussen, A. Guenther, Atmospheric Measurement Techniques, (2009) 99-112.
- [42] M. Demarcke, C. Amelynck, N. Schoon, F. Dhooghe, J. Rimetz-Planchon, H. Van Langenhove, J. Dewulf, International Journal of Mass spectrometry, 290 (2010) 14-21.
- [43] M. Demarcke, C. Amelynck, N. Schoon, F. Dhooghe, H. Van Langenhove, J. Dewulf, International Journal of Mass spectrometry, 279 (2009) 156-162.
- [44] M.M.L. Steeghs, E. Crespo, F.J.M. Harren, International Journal of Mass Spectrometry, 263 (2007) 204-212.
- [45] I. Dotan, D.L. Albritton, W. Lindinger, M. Pahl, Journal of Chemical Physics, 65 (1976) 5028-5030.
- [46] M. McFarland, D.I. Albritton, F.C. Fehsenfeld, E.E. Ferguson, A.L. Schmeltekopf, Journal of Chemical Physics, 59 (1973) 6620-6628.
- [47] G.H. Wannier, Physical Review, 83 (1951) 281-289.
- [48] G.H. Wannier, Physical Review, 87 (1952) 795-798.
- [49] D.R. Lide, CRC Handbook of Chemistry and Physics, 82nd ed., 2001 - 2002.
- [50] B.T. Jobson, M.L. Alexander, G.D. Maupin, G.G. Muntean, International Journal of Mass Spectrometry, 245 (2005) 78-89.
- [51] A.D.J. Critchley, C.R. Howle, C.A. Mayhew, R.P. Tuckett, Chemical Physics, 303 (2004) 235-241.
- [52] K. Buhr, S. van Ruth, C. Delahunty, International Journal of Mass Spectrometry, 221 (2002) 1-7.
- [53] R.S. Blake, K.P. Wyche, A.M. Ellis, P.S. Monks, International Journal of Mass Spectrometry, 254 (2006) 85-93.

- [54] C. Warneke, J.A. De Gouw, W.C. Kuster, P.D. Goldan, R. Fall, *Environmental Science & Technology*, 37 (2003) 2494-2501.
- [55] R.S. Mason, J.C. Naylor, *J. Phys. Chem. A*, 102 (1998) 10090-10098.
- [56] D.J. Swanton, D.C.J. Marsden, L. Radom, *Organic Mass Spectrometry*, 26 (1991) 227-234.
- [57] S.C. Smith, M.J. McEwan, K. Giles, D. Smith, N.G. Adams, *International Journal of Mass Spectrometry and Ion Processes*, 96 (1990) 77-96.
- [58] R.S. Mason, A. Parry, *International Journal of Mass Spectrometry and Ion Processes*, 108 (1991) 241-253.
- [59] S. Inomata, H. Tanimoto, *International Journal of Mass Spectrometry*, 285 (2009) 95-99.
- [60] C. Warneke, J. Kuczynski, A. Hansel, A. Jordan, W. Vogel, W. Lindinger, *International Journal of Mass Spectrometry and Ion Processes*, 154 (1996) 61-70.
- [61] J. Taucher, A. Lagg, A. Hansel, W. Vogel, W. Lindinger, *Alcoholism-Clinical and Experimental Research*, 19 (1995) 1147-1150.
- [62] S.D. Maleknia, T.L. Bell, M.A. Adams, *International Journal of Mass spectrometry*, 262 (2007) 203-210.
- [63] J. Williams, U. Poschl, P.J. Crutzen, A. Hansel, R. Holzinger, C. Warneke, W. Lindinger, J. Lelieveld, *Journal of Atmospheric Chemistry*, 38 (2001) 133-166.
- [64] J. de Gouw, C. Warneke, T. Karl, G. Eerdekens, C. van der Veen, R. Fall, *International Journal of Mass spectrometry*, 223 (2003) 365-382.
- [65] T. Wang, P. Spanel, D. Smith, *International Journal of Mass spectrometry*, 239 (2004) 139-146.
- [66] P. Spanel, D. Smith, *International Journal of Mass Spectrometry and Ion Processes*, 167-168 (1997) 375-388.
- [67] A.J. Bell, K. Giles, S. Moody, P. Watts, *International Journal of Mass spectrometry*, 173 (1998) 65-70.
- [68] A.J. Bell, K. Giles, S. Moody, N.J. Underwood, P. Watts, *International Journal of Mass spectrometry*, 165 (1997) 169-178.
- [69] R.M. Smith, *Understanding mass spectra: a basic approach*, John Wiley & Sons, 2004.
- [70] R.T. Morrison, R.N. Boyd, *Relative stabilities of carbocations*, in: *Organic Chemistry 4th Edition*, Allyn and Bacon, 1983, pp. 231-235.
- [71] D.H. Aue, *Wiley Interdisciplinary Reviews-Computational Molecular Science*, 1 (2011) 487-508.
- [72] E. Uggerud, *Mass Spectrometry Reviews*, 18 (1999) 285-308.
- [73] J.A. Stone, W.J. Wytenberg, *International Journal of Mass Spectrometry and Ion Processes*, 104 (1991) 95-107.
- [74] S. Price, *Ion mobility and mass spectrometric investigations of organophosphates related to chemical warfare agents and pesticides*, in: *School of Physics and Astronomy, University of Birmingham, Birmingham, 2010*.
- [75] A.J. Bell, D. Despeyroux, J. Murrell, P. Watts, *International Journal of Mass Spectrometry and Ion Processes*, 165-166 (1997) 533-550.
- [76] J.D. Barr, A.J. Bell, D.O. Konn, J. Murrell, C.M. Timperley, M.J. Waters, P. Watts, *Physical Chemistry Chemical Physics*, 4 (2002) 2200-2205.
- [77] A.J. Midey, T.M. Miller, A.A. Viggiano, *Journal of Physical Chemistry A*, 113 (2009) 4982-4989.
- [78] B.K. Chatterjee, R. Tosh, R. Johnsen, *International Journal of Mass Spectrometry and Ion Processes*, 103 (1991) 81-92.
- [79] A.J. Bell, F. Ferrante, S.E. Hall, V. Mikhailov, D. Mitchell, C.M. Timperley, P. Watts, N. Williams, *Int. J. Mass Spectrom.*, 269 (2008) 46-54.

- [80] M. Alcamì, O. Mo, M. Yanez, *Mass Spectrometry Reviews*, 20 (2001) 195-245.
- [81] W. Danikiewicz, *Int. J. Mass Spectrom.*, 285 (2009) 86-94.
- [82] B. Muir, H.B. Duffy, M.C. Moran, *Journal of Chromatography A*, 1038 (2004) 183-187.
- [83] A.K. Pavlou, A.P.F. Turner, *Clinical Chemistry and Laboratory Medicine*, 38 (2005) 99-112.
- [84] J. Dummer, M. Storer, M. Swanney, M. McEwan, A. Scott-Thomas, S. Bhandari, S. Chambers, R. Dweik, M. Epton, *Trac-Trends in Analytical Chemistry*, 30 (2011) 960-967.
- [85] D.Y. Graham, D.J. Evans, L.C. Alpert, P.D. Klein, D.G. Evans, A.R. Opekun, T.W. Boutton, *Lancet*, 1 (1987) 1174-1177.
- [86] G. Metz, M.A. Gassull, B.S. Drasar, D.J.A. Jenkins, L.M. Blendis, *Lancet*, 1 (1976) 668-669.
- [87] M. Pimentel, E.J. Chow, H.C. Lin, *American Journal of Gastroenterology*, 95 (2000) 3503-3506.
- [88] A. Sandrini, D.R. Taylor, P.S. Thomas, D.H. Yates, *Respirology*, 15 (2010) 57-70.
- [89] A. Amann, *International Journal of Mass Spectrometry*, (2004).
- [90] J. King, A. Kupferthaler, K. Unterkofler, H. Koc, S. Teschl, G. Teschl, W. Miekisch, J. Schubert, H. Hinterhuber, A. Amann, *Journal of Breath Research*, 3 (2009) 027006.
- [91] W. Miekisch, J.K. Schubert, G.F.E. Noeldge-Schomburg, *Clinica Chimica Acta*, 347 (2004) 25-39.
- [92] R. Salerno-Kennedy, K.D. Cashman, *Wiener Klinische Wochenschrift*, 117 (2005) 180-186.
- [93] L.T. McGrath, R. Patrick, B. Silke, *European Journal of Heart Failure*, 3 (2001) 423-427.
- [94] L.T. McGrath, R. Patrick, P. Mallon, L. Dowey, B. Silke, W. Norwood, S. Elborn, *European Respiratory Journal*, 16 (2000) 1065-1069.
- [95] K. Schwarz, A. Pizzini, B. Arendacka, K. Zerlauth, W. Filipiak, A. Schmid, A. Dzien, S. Neuner, M. Lechleitner, S. Scholl-Burgi, W. Miekisch, J. Schubert, K. Unterkofler, V. Witkovsky, G. Gastl, A. Amann, *Journal of Breath Research*, (2009) 027003.
- [96] M. Storer, J. Dummer, H. Lunt, J. Scotter, F. McCartin, J. Cook, M. Swanney, D. Kendall, F. Logan, M. Epton, *Journal of Breath Research*, 5 (2011) 046011.
- [97] D. Kohlmuller, W. Kochen, *Analytical Biochemistry*, 210 (1993) 268-276.
- [98] M.P. Kalapos, *Medical Hypotheses*, 53 (1999) 236-242.
- [99] S.F. Solga, A. Alkhouraishe, K. Cope, A. Tabesh, J.M. Clark, M. Torbenson, P. Schwartz, T. Magnuson, A.M. Diehl, T.H. Risby, *Biomarkers*, 11 (2006) 174-183.
- [100] S. Van den Velde, F. Nevens, P. Van Hee, D. van Steenberghe, M. Quirynen, *Journal of Chromatography B-Analytical Technologies in the Biomedical and Life Sciences*, 875 (2008) 344-348.
- [101] S.M. Abbott, J.B. Elder, P. Spanel, D. Smith, Quantification of acetonitrile in exhaled breath and urinary headspace using selected ion flow tube mass spectrometry, in: *Symposium in Honor of Helmut Schwaz*, Elsevier Science Bv, Berlin, Germany, 2003, pp. 655-665.
- [102] D. Smith, P. Spanel, *Mass Spectrometry Reviews*, 24 (2005) 661-700.
- [103] B. Enderby, D. Smith, W. Carroll, W. Lenney, Hydrogen Cyanide as a Biomarker for *Pseudomonas Aeruginosa* in the Breath of Children With Cystic Fibrosis, in: *104th International Conference of the American-Thoracic-Society*, Wiley-Liss, Toronto, CANADA, 2008, pp. 142-147.
- [104] Y. Jin, W. Di, W. Le, W. Ping, H. Yanjie, Y. Kejing, Detection of Lung Cancer with Volatile Organic Biomarkers in Exhaled Breath and Lung Cancer Cells, in: P. Matteo, S. Giorgio (Eds.), *AIP*, 2009, pp. 198-201.

- [105] M. Syhre, L. Manning, S. Phuanukoonnon, P. Harino, S.T. Chambers, *Tuberculosis*, 89 (2009) 263-266.
- [106] M. Westhoff, P. Litterst, L. Freitag, W. Urfer, S. Bader, J.I. Baumbach, *Thorax*, 64 (2009) 744-748.
- [107] A. Bunkowski, B. Bodeker, S. Bader, M. Westhoff, P. Litterst, J.I. Baumbach, *Journal of Breath Research*, 3 (2009).
- [108] J. Beauchamp, et al., *Journal of Breath Research*, 4 (2010) 026006.
- [109] S.M. Cristescu, H.A. Gietema, L. Blanchet, C. Kruitwagen, P. Munnik, R.J. van Klaveren, J.W.J. Lammers, L. Buydens, F.J.M. Harren, P. Zanen, *Journal of Breath Research*, 5 (2011).
- [110] S. Kamysek, P. Fuchs, H. Schwoebel, J.P. Roesner, S. Kischkel, K. Wolter, C. Loeseken, J.K. Schubert, W. Miekisch, *Analytical and Bioanalytical Chemistry*, 401 (2011) 2093-2102.
- [111] I. Kushch, K. Schwarz, L. Schwentner, B. Baumann, A. Dzien, A. Schmid, K. Unterkofler, G. Gastl, P. Spanel, D. Smith, A. Amann, *Journal of Breath Research*, 2 (2008).
- [112] B. Thekedar, W. Szymczak, V. Hollriegl, C. Hoeschen, U. Oeh, *Journal of Breath Research*, (2009) 027007.
- [113] T.H. Risby, S.S. Sehnert, *Free Radical Biology and Medicine*, 27 (1999) 1182-1192.
- [114] A. Tangerman, M.T. Meuwesearends, J. Jansen, *Lancet*, 343 (1994) 483-483.
- [115] A. Tangerman, M. Meuwese-Arends, J.M.J. Jansen, *The Lancet*, 343 (1994) 1569.
- [116] M.I. Friedman, G. Preti, R.O. Deems, L.S. Friedman, S.J. Munoz, W.C. Maddrey, *Digestive Diseases and Sciences*, 39 (1994) 1672-1676.
- [117] H. Almardini, K. Bartlett, C.O. Record, *Gut*, 25 (1984) 284-290.
- [118] A. Tangerman, *Journal of Chromatography B-Analytical Technologies in the Biomedical and Life Sciences*, 877 (2009) 3366-3377.
- [119] K. Buhr, K. Eisgruber, J. Kiefl, P. Schieberle, Garlic breath sampling and monitoring by proton transfer reaction - mass spectrometry, in: 4th International Conference on Proton Transfer Reaction Mass Spectrometry and its Applications, innsbruck university press, Universität Innsbruck, 2009.
- [120] J. Taucher, A. Hansel, A. Jordan, W. Lindinger, *Journal of Agricultural and Food Chemistry*, 44 (1996) 3778-3782.
- [121] M.E. O'Hara, S. O'Hehir, S. Green, C.A. Mayhew, *Physiological Measurement*, 29 (2008) 309-330.
- [122] M.E. O'Hara, T.H. Clutton-Brock, S. Green, S. O'Hehir, C.A. Mayhew, *International Journal of Mass Spectrometry*, 281 (2009) 92-96.
- [123] J.C. Anderson, A.L. Babb, M.P. Hlastala, *Annals of Biomedical Engineering*, 31 (2003) 1402-1422.
- [124] M.P. Hlastala, *J Appl Physiol*, 84 (1998) 401-408.
- [125] M.P. Hlastala, *J Appl Physiol*, 93 (2002) 405-406.
- [126] J. Beauchamp, A. Buettner, From pharmacokinetics to sensory science: the versatility of PTR-MS in a multidisciplinary environment, in: A. Hansel, J. Dunkl (Eds.) 5th International Conference on Proton Transfer Reaction Mass Spectrometry and its Applications, Innsbruck University Press Innsbruck, Austria, 2011.
- [127] S. O'Hehir, The development of novel techniques applicable to chemotherapy dose assessment, in: School of Physics and Astronomy, The University of Birmingham, 2010.
- [128] M. O'Hara, T.H. Clutton-Brock, S. Green, C.A. Mayhew, *Journal of Breath Research*, (2009) 027005.

- [129] M.M.L. Steeghs, S.M. Cristescu, P. Munnik, P. Zanen, F.J.M. Harren, *Physiological Measurement*, 28 (2007) 503-514.
- [130] M. O'Hara, The use of proton transfer reaction mass spectrometry for analysis of volatile organic compounds in breath and microbial headspace: Chapter 4 Measurement of acetone and isoprene in breath and blood of healthy volunteers, in: *School of Physics and Astronomy*, 2009.
- [131] J.M. Bland, D.G. Altman, *British Medical Journal*, 313 (1996) 744-744.
- [132] J. King, H. Koc, K. Unterkofler, P. Mochalski, A. Kupferthaler, G. Teschl, S. Teschl, H. Hinterhuber, A. Amann, *Journal of Theoretical Biology*, 267 (2010) 626-637.
- [133] A. Falk, E. Gullstrand, A. Lof, E. Wigaeushjelm, *British Journal of Industrial Medicine*, 47 (1990) 62-64.
- [134] M.M.L. Steeghs, C. Sikkens, E. Crespo, S.M. Cristescu, F.J.M. Harren, *International Journal of Mass spectrometry*, 262 (2007) 16-24.
- [135] P. Prazeller, P.T. Palmer, E. Boscaini, T. Jobson, M. Alexander, *Rapid Communications in Mass Spectrometry*, 17 (2003) 1593-1599.
- [136] R.S. Blake, C. Whyte, C.O. Hughes, A.M. Ellis, P.S. Monks, *Analytical Chemistry*, 76 (2004) 3841-3845.
- [137] C.J. Ennis, J.C. Reynolds, B.J. Keely, L.J. Carpenter, *International Journal of Mass spectrometry*, 247 (2005) 72-80.
- [138] A.T. Blei, J. Cordoba, G. Practice Parameters Comm Am Coll, *American Journal of Gastroenterology*, 96 (2001) 1968-1976.

Appendix A

Health status questionnaire for the study into liver disease.

Version 2 09/05/2009



Health Status Questionnaire for Liver Disease Calibration of PTR-MS Study

Participant identification number:

Date:

All the information you give in this questionnaire will be treated with confidence and will not be divulged to any third parties.

D.O.B.

Sex

Weight

Height

Nature of Liver Disease

1. Are you now, or have you in the past ever suffered from any of the following?
 - a. Asthma
 - b. Coronary Artery Disease (Angina etc.)
 - c. Diabetes
2. Have you had any of the following within the last 7 days?
 - a. A cold, 'Flu, Sore Throat etc.
 - b. A blocked nose
 - c. A nose bleed
 - d. Earache
3. Do you currently smoke

Have you ever smoked in the past?

If yes:

- a. How many cigarettes a day?
- b. For how long did you smoke? Years/months/weeks
- c. How long ago did you stop? Years/months/weeks

4. Are you taking any preparations or medications that have not been prescribed by a GP?

5. Are you taking any food supplements such as vitamin pills?

6. When did you last have something to eat or drink?

7. What did you last eat or drink?

8. Have you eaten or drunk any of the following things in the past 24 hours?

Garlic

Coffee

Alcoholic drinks

Your signature